NTIA Report 22-561

Outdoor Propagation Measurements in the 37–40 GHz Band in Boulder, Colorado

Jeffery A. Wepman
Linh P. Vu
Edward F. Drocella
John D. Ewan
Kenneth J. Brewster
Paul M. McKenna

Technical Report

NTIA Report 22-561

Outdoor Propagation Measurements in the 37–40 GHz Band in Boulder, Colorado

Jeffery A. Wepman
Linh P. Vu
Edward F. Drocella
John D. Ewan
Kenneth J. Brewster
Paul M. McKenna

U.S. DEPARTMENT OF COMMERCE

Alan Davidson
Assistant Secretary of Commerce for Communications and Information
National Telecommunications and Information Administration

August 2022

DISCLAIMER

Certain commercial equipment and materials are referenced in this report to specify adequately the technical aspects of the reported results. In no case does such reference imply recommendation or endorsement by the National Telecommunications and Information Administration, nor does it imply that the material or equipment referenced is the best available for this purpose.

CONTENTS

FIGURES

TABLES

OUTDOOR PROPAGATION MEASUREMENTS IN THE 37–40 GHZ BAND IN BOULDER, COLORADO

Jeffery A. Wepman,[1] Linh P. Vu,[1] Edward F. Drocella,[2] John D. Ewan,[1]
Kenneth J. Brewster,[1] and Paul M. McKenna[1]

Line-of-sight (LOS) and non-line-of-sight (NLOS), continuous-wave (CW), mobile outdoor propagation measurements were performed in the 37–40 GHz band in a small city downtown environment (Boulder, Colorado). The measurement system was optimized to provide measurements over the maximum practicable distance (about 3 km) between the transmitter and receiver. The transmitter was placed at a fixed location and time domain samples of in-phase and quadrature (IQ) data along with position data were collected by the mobile receiver along LOS and NLOS paths. The data were processed to provide received signal power as a function of position and basic transmission gain G_b vs. distance between the transmitter and receiver. Measured G_b as a function of distance was compared to that predicted by free space and the 3rd Generation Partnership Project (3GPP) LOS and NLOS path loss models for the urban microcell (UMi) case. In general, the measured G_b did not agree well with that predicted by the free space and 3GPP models.

Keywords: Radio propagation measurements, millimeter-wave, 5G, path loss, basic transmission gain, propagation models, continuous-wave measurements, narrowband measurements, 3GPP

1. INTRODUCTION

Current approaches to implementing emerging fifth generation (5G) wireless networks and technology incorporate the use of radio spectrum in two distinct frequency ranges: frequencies below 7.125 GHz (often called the sub-6 GHz bands) and frequencies above 24.25 GHz (the millimeter-wave bands). Due to the difficulty of accurately characterizing the radio wave propagation environment and the expense of performing propagation measurements, there is an ongoing effort to improve propagation models that help predict the behavior of radio waves in various environments. Radio propagation measurements are needed to validate existing models, provide data for enhancing existing models, and create new models. The characteristics of radio wave propagation have been studied more extensively and are better known at lower frequencies; propagation at millimeter-wave is not understood as well. Design, development, and deployment of 5G systems operating in the millimeter-wave bands are dependent on a sound understanding of the radio propagation environment in those bands. Furthermore, there is a shortage of current,

[1] The authors are with the National Telecommunications and Information Administration (NTIA), Institute for Telecommunication Sciences (ITS), U.S. Dept. of Commerce, 325 Broadway St., Boulder, Colorado 80305.

[2] The author is with the NTIA Office of Spectrum Management (OSM), U.S. Dept. of Commerce, 1401 Constitution Ave. NW, Washington, DC 20021.

publicly available, propagation measurement data at millimeter-wave frequencies, and, consequently, a lack of fully validated propagation models at these frequencies.

The objective of this effort was to perform a set of outdoor millimeter-wave propagation measurements in a small downtown environment (Boulder, Colorado) and provide measured data to the Office of Spectrum Management (OSM) of the National Telecommunications and Information Administration (NTIA). The intent is to use the data in future efforts to validate the 3rd Generation Partnership Project (3GPP) and other millimeter-wave path loss models. Downtown Boulder represents a small business district with many closely spaced commercial buildings and parking structures of varying heights including a substantial number between 10 m and 20 m (tallest is approximately 36 m) that form a set of urban canyons.

To meet this objective, the Institute for Telecommunication Sciences (ITS) conducted line-of-sight (LOS) and non-line-of-sight (NLOS) continuous-wave (CW) mobile propagation measurements in the 37–40 GHz band (3GPP Release 15 New Radio (NR) band n260) [1]. Specifically, all measurements presented in this report were taken at 37 GHz. Received signal power as a function of position (and hence distance between the transmitter and receiver) was measured. The data were processed to provide received signal power as a function of position and basic transmission gain G_b vs. distance between the transmitter and receiver. Measurements over the maximum practicable distance (about 3 km) between the transmitter and receiver were obtained by 1) constructing a custom-built preselector to obtain the best practicable receiver sensitivity, 2) utilizing a high-gain, high-power (40 Watt minimum) traveling wave tube (TWT) amplifier at the transmitter, and 3) using a carefully designed directional horn transmitter antenna to achieve maximum antenna gain while maintaining a sufficiently wide azimuthal beamwidth to accommodate all planned measurements.

The G_b vs. distance results were compared to both the free-space path loss model and the 3GPP LOS and NLOS path loss models for the urban microcell (UMi) case. The free-space model was chosen to serve as a baseline while the 3GPP models represent widely available models promulgated by the 3GPP, the preeminent organization for 5G standards. The free-space and 3GPP models represent a small subset of possible models; other path loss models exist and are being developed that could be compared with the data in the future. The primary goal of this effort is to present the measured data. A comprehensive comparison of model predictions to measured data falls outside the scope of this effort.

2. MEASUREMENT SYSTEM

The measurement system consists of both a transmitter and receiver operated by ITS. Details of the transmitter and receiver are described in the following sections of this document.

2.1 Transmitter

A simplified block diagram of the transmitter system is shown in Figure 1. The primary components of the measurement system transmitter are a microwave signal generator, high-gain power amplifier, and RF antenna. A GPS disciplined frequency reference (with associated antenna), RF power sensor and power meter, and personal computer complete the system. The transmitter was installed in the ITS modified Chevrolet Express 3500 Extended Cargo Van shown in Figure 2. This vehicle includes a 9 m (30 ft.) telescoping mast.[3]

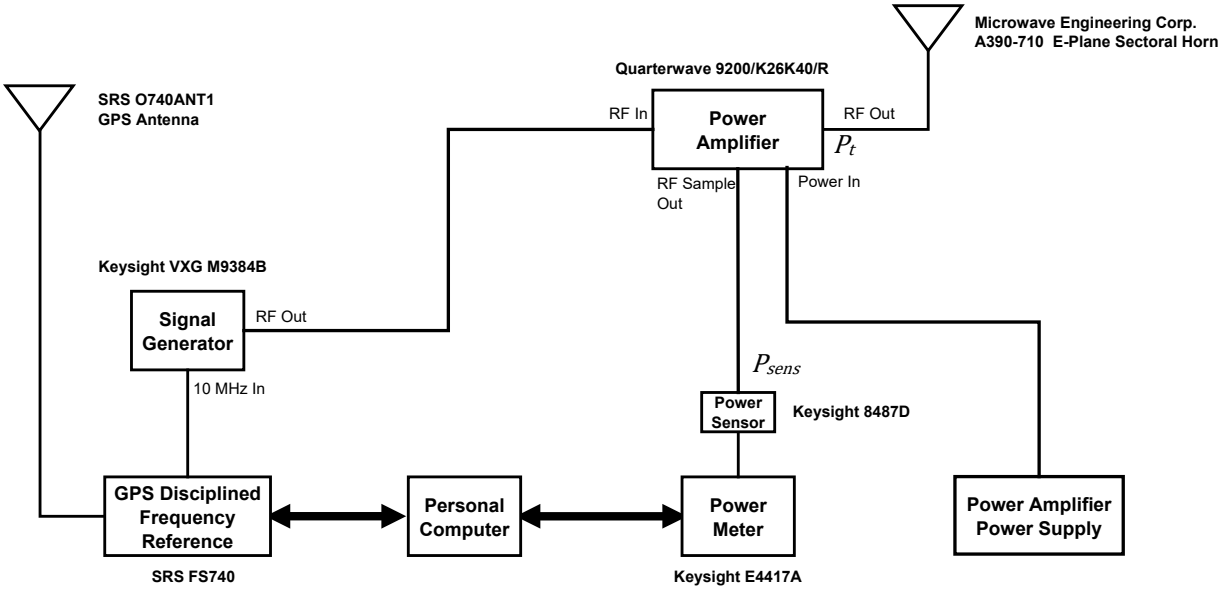

Figure 1. Block diagram of the measurement system transmitter.

[3] Note that the bottom of the 9 m mast is mounted on the floor of the measurement vehicle, allowing an antenna height of approximately 10 m above ground level (AGL).

Figure 2. Measurement system transmitter vehicle: ITS modified Chevrolet Express 3500 extended cargo van with 9 m (30 ft.) telescoping mast.

The power amplifier and RF antenna were mounted on the top of the 9 m telescoping mast. The remaining equipment was housed inside the measurement vehicle. Placing the power amplifier at

the top of the telescoping mast permitted the maximum possible transmitter power to be supplied to the RF transmitter antenna and kept RF emission exposure well below safety limits for transmitter operator personnel as well as passersby [2], [3].

A Keysight VXG M9384B microwave signal generator is locked to a Stanford Research Systems FS740 GPS disciplined 10 MHz frequency reference to provide a highly stable, CW signal up to 44 GHz. The signal generator can provide a maximum RF output power of +21 dBm (typical) in the 37–40 GHz band; sufficient power is necessary to overcome the large cable loss (approximately 40 dB) between the signal generator RF output and the high-gain power amplifier.

The high-gain power amplifier is a Traveling Wave Tube Amplifier (TWTA) built by Quarterwave Corp. It meets the requirements of weighing less than 45 pounds (significantly less than the maximum weight the mast can handle), providing a minimum of 70 dB gain, and being able to achieve a minimum 40 Watt CW output power at saturation. The minimum gain G_a is found by $G_a = P_a + L_t - P_g$ where P_a is the minimum output power of the power amplifier (+46 dBm), L_t is the cable loss between the signal generator RF output and the power amplifier RF input (40 dB), and P_g is the signal generator output power (+16 dBm, chosen to be well below its maximum). The output power of the power amplifier was continually monitored by the power sensor and power meter. The monitored output power data along with UTC time data was saved to a file on the personal computer. Knowing the output power transmitted at specific times allowed correlation with the received signal power data taken. Typically, right after the transmitter was turned on, the transmitter power would decrease somewhat linearly by 0.5 to 2.0 dB for one to one and a half hours. After this initial transient behavior, the transmitted output power became more stationary with variation typically less than ± 0.5 dB.

The choice of the RF transmitter antenna was important to the design of the millimeter-wave propagation measurement experiment. The general philosophy behind the selection was to achieve as high a gain as possible while maintaining a sufficiently wide azimuthal beamwidth to permit measurements of both LOS and NLOS paths. For propagation measurements in general, where the goal is to characterize the radio channel propagation environment, static, conventional antennas with a fixed, known, and well-characterized antenna pattern are most appropriate, not advanced antennas with dynamically adjustable antenna patterns. In a static, conventional antenna, tradeoffs between antenna gain and directionality must be made, namely higher gain is achieved with commensurately narrower beamwidths. Standard gain horn antennas are common directional antennas used at millimeter-wave frequencies and have nearly symmetrical azimuthal and elevation beamwidths. Common gains of these antennas can range from 10 to 25 dBi with 3 dB beamwidths that range roughly from 54° to 7°, respectively.

For these specific measurements, a reasonably wide azimuthal beamwidth was desired to be able to measure both LOS and NLOS paths using the same antenna. Ideally, wider azimuthal beamwidths than those achievable with standard gain horn antennas are desired. Sectoral horn antennas can achieve wider azimuthal beamwidths than standard gain horn antennas by permitting more independent control over the azimuthal and elevation beamwidths. Specifically, sectoral horn antennas can achieve a wider azimuthal beamwidth for a given gain by narrowing the elevation beamwidth. For these measurements, narrowing the elevation beamwidth was a reasonable and good tradeoff since much of the energy transmitted by an antenna with a wide

elevation beamwidth is wasted by directing that energy both into the sky and into the ground. Based on these tradeoffs and practical constraints of sectoral horn antennas, the transmitter antenna selected for the measurements was a Microwave Engineering Corporation A390-710 E-Plane Sectoral Horn. It has a 3 dB azimuthal beamwidth of roughly 98°, a 3 dB elevation beamwidth of roughly 18°, and a gain of about 11.9 dBi.[4]

2.2 Receiver

The measurement system receiver, shown diagrammatically in Figure 3, consists of an RF receiver antenna, preselector, signal analyzer, GPS disciplined frequency reference (with associated antenna), GPS receiver (with associated antennas), measurement controller, function generator, and personal computer. For these measurements, the receiver was installed in the ITS modified Chevrolet Express 3500 Passenger Van as shown in Figure 4.

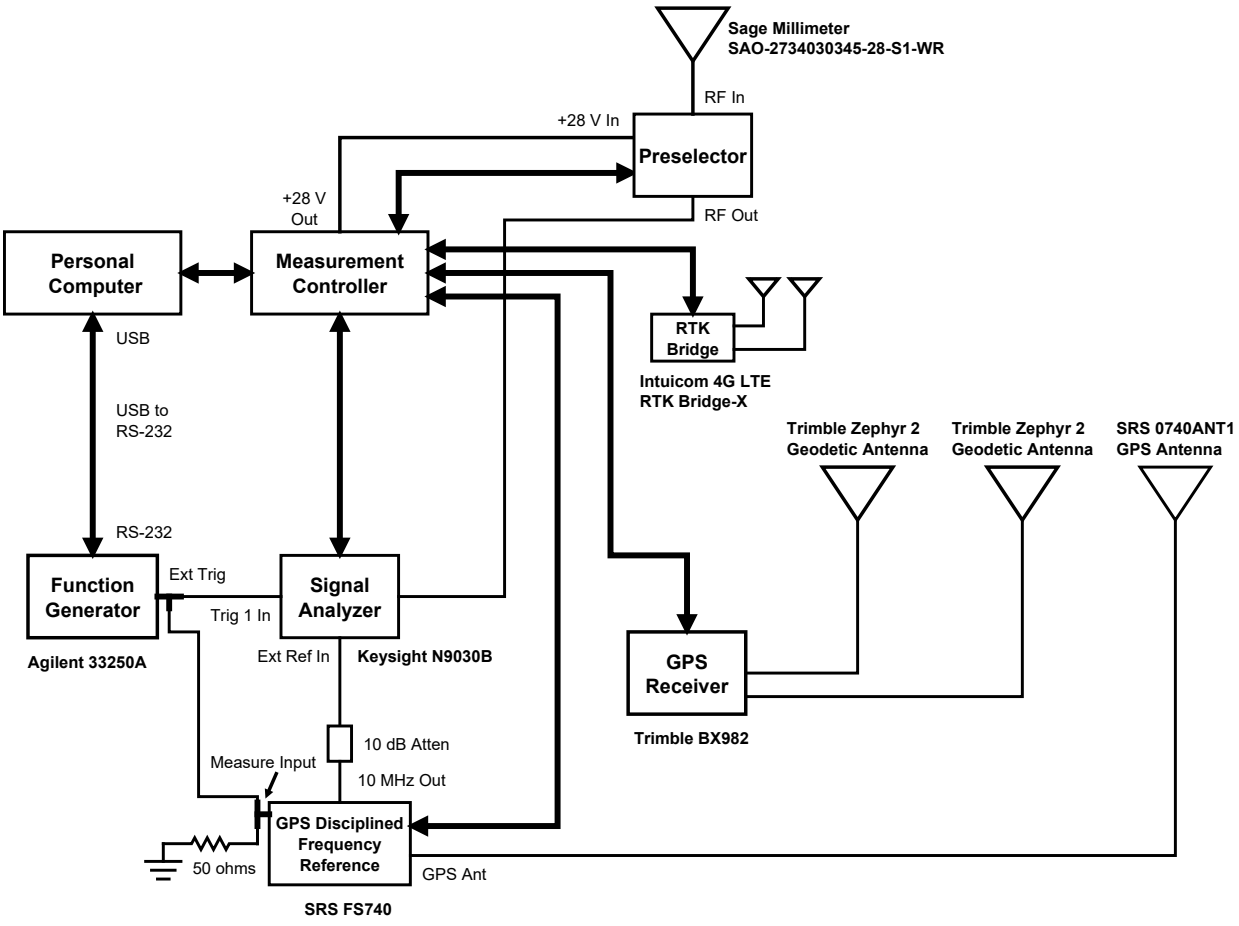

Figure 3. Block diagram of the measurement system receiver.

[4] The beamwidths were determined from antenna measurements made by the manufacturer at 40 GHz. The gain was determined by measurements made by ITS using the three-antenna method for determining antenna gain (described in Section 3.1) at 37 GHz.

Figure 4. Measurement system receiver vehicle: ITS modified Chevrolet Express 3500 passenger van.

A vertically polarized, omnidirectional RF receiver antenna was selected with as wide an elevation beamwidth as could be obtained to maximize reception of signals from all directions. This is especially beneficial for NLOS measurements when the receiver is in urban canyon environments. Given the gain/beamwidth tradeoff as discussed in the transmitter section of this document (Section 2.1), the gain of this type of antenna is significantly lower than that of more directional antennas. However, the tradeoff is seen as worthwhile. Omnidirectional antennas that operate in the 37–40 GHz band are not nearly as readily available as directional antennas in this band. Additionally, since a waveguide connector is desired to minimize loss, this constraint further limits the availability of suitable antennas. The Sage Millimeter, Inc. SAO-2734030345-28-S1-WR, available as a standard design, was selected to meet the requirements. This antenna operates over the entire Ka band (26.5–40 GHz); nominally has a 3 dBi gain at the center of the band, 45° 3 dB elevation beamwidth, and WR-28 waveguide output; and is weather resistant. While an even wider elevation beamwidth would be desirable, this antenna is nearly optimal. The gain of this antenna was measured to be 4.4 dBi at 37 GHz by ITS using the three-antenna method for determining antenna gain (described in Section 3.1).

The preselector performs several crucial functions for the measurement system. It attenuates unwanted out-of-band signals, improves the sensitivity of the system, and enables measurement system calibrations. Measurement system calibrations provide assurance that the measurement system is operating properly. They also provide measurements of the preselector gain and system noise figure (from which the system noise level in a given bandwidth can be determined).

Preselector gain is particularly important to be able to determine absolute received power at the antenna output.

A block diagram of the preselector, custom-built by ITS, is shown in Figure 5. The preselector provides a single RF path that consists of a 37–40 GHz bandpass filter with a 30 dB/3 dB shape factor of approximately 1.7 and a full Ka band (26.5–40 GHz) low-noise amplifier. The preselector includes the low-noise amplifier to be able to achieve the best practicable receiver sensitivity since measured signal levels are expected to be typically very low. The preselector also contains a noise diode that can be utilized under software control to perform measurement system calibrations.

Selection of waveguide or coaxial components was based on optimizing RF performance and the availability of commercial components. In general, if possible, waveguide components were selected since they reduce insertion loss and permit better system sensitivity. Therefore, the noise diode, single-pole double-throw (SPDT) switch, and bandpass filter are WR-28 waveguide components while the low-noise amplifier is a coaxial component.

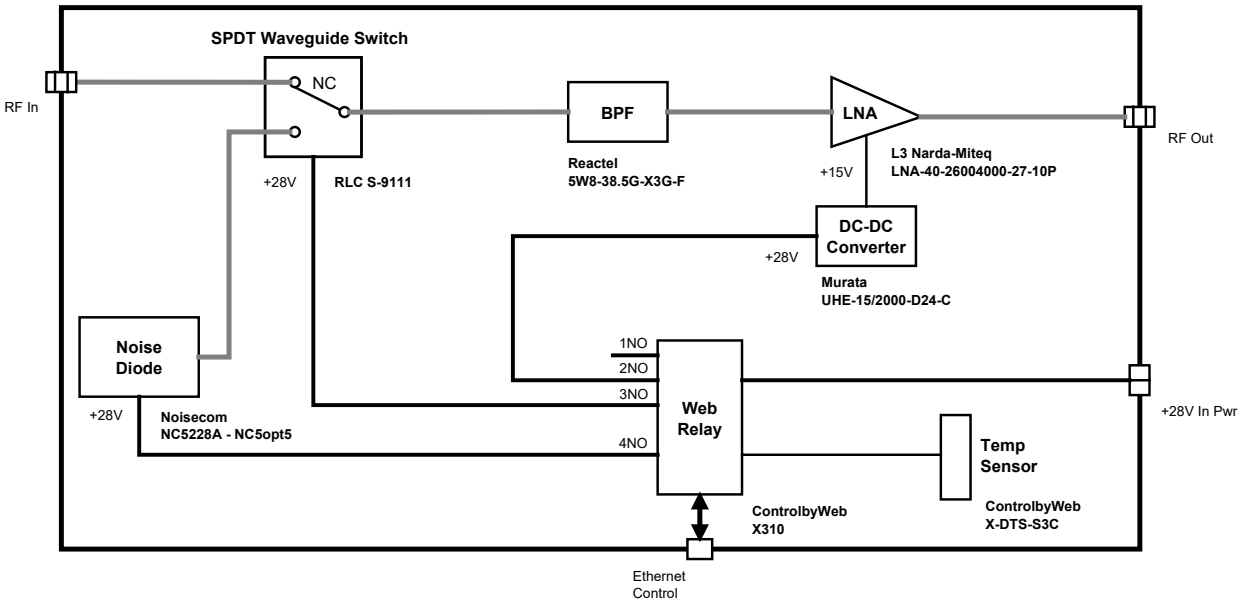

Figure 5. Block diagram of ITS custom-built Ka band millimeter-wave preselector.

The signal analyzer forms the core of the overall measurement system. It takes the RF signals received by the antenna and conditioned by the preselector and provides measurements of the received CW transmissions in a user-selected bandwidth.

A Keysight N9030B PXA millimeter-wave signal analyzer was used in the IQ Analyzer (Basic) mode. The IQ Analyzer (Basic) mode enables capture of in-phase and quadrature (IQ) data samples at precise time intervals. Note that for these measurements where the goal is obtaining G_b, IQ data is not necessary, simple power measurements would suffice. However, the IQ Analyzer (Basic) mode of the signal analyzer is used (with its inherent IQ data capture) because it provides an excellent way to collect data at precise time intervals and previously written instrument control software at ITS for propagation measurements could be leveraged. Received

signal power is easily obtained from the IQ data. Collecting IQ data also provides the opportunity to post-process the data in future efforts to obtain additional information about the radio propagation channel.

Automated control of the preselector and signal analyzer is provided by the personal computer running receiver control software developed by ITS. The receiver control software is implemented in Python running on a Linux operating system. The measurement controller consists of an Ethernet switch and a power supply for the preselector.

The function generator is used to initiate data collection by the signal analyzer by generating an external trigger pulse to the Trigger 1 Input of the signal analyzer. The trigger pulse is sent after the operator manually selects a button on the control software graphical user interface (GUI). While the generation of the trigger pulse is asynchronous, the exact UTC time (to better than 100 ns accuracy) of the rising edge of the trigger pulse is captured using the Measurement Input of the SRS FS740 GPS-disciplined frequency reference. The rising edge of the trigger pulse initiates data collection on the signal analyzer, so the exact time RF data collection occurs is also known. The GPS-disciplined frequency reference also provides a very stable signal as the frequency reference input to the signal analyzer.

The signal analyzer collects the received signal IQ measured data; the data are then saved to a local hard drive on the personal computer. Position data from the GPS receiver were collected simultaneously with the received signal RF data to be able to correlate position with received power and determine received power as a function of distance from the transmitter. This position data is saved to the hard disk on the personal computer as well.

The GPS receiver used was that from the ITS Precision Geolocation System [4]. This receiver has a significantly better position accuracy than other GPS receivers in use at ITS. Position accuracy was found to typically be better than 1 m even in downtown Boulder. In addition to having the best position accuracy, the GPS receiver provides a position update rate of up to 50 Hz. This provides a position reading up to every 20 ms.[5] At a receiver measurement vehicle speed of 25 mph (~11.18 m/sec), this corresponds to a position reading of up to approximately every 0.22 m, a resolution better than the position accuracy found during the measurements. The 50 Hz update rate was used for all the measurements in this report.

[5] Due to ease of availability, low cost, and position accuracy and update rate requirements, ITS has traditionally used consumer-grade GPS receivers in its RF measurement systems. In these consumer-grade GPS receivers, the position accuracy and update rates are not as good as those obtained using the GPS receiver from the ITS Precision Geolocation System. As an example, one commonly used consumer-grade GPS receiver has a manufacturer-specified position accuracy of 2.5 meters or better and provides a position update rate of 1 Hz (providing a position reading every second). However, position accuracies obtained during real-world mobile measurements in certain urban environments have shown even worse position accuracies than those specified by the manufacturer.

3. MEASUREMENT SYSTEM CHARACTERIZATION

To ensure accurate transmitted signal power and received signal power for the propagation measurements several measurement system characterizations were performed. Antenna gain for both the transmitter and receiver antennas was measured prior to the propagation measurement campaign. Prior to the propagation measurement campaign, the receiver dynamic range was also determined. The transmitter power supplied to the transmitter antenna was calibrated in the field as part of the measurement setup procedure. Details of the antenna characterization and the receiver characterization are provided in this section. The details of the transmitter power calibration are discussed in Section 5.1.1.

3.1 Antenna Characterization

Antenna pattern data were obtained from the respective manufacturers based on their measured data. Antenna gain for the transmitter and receiver antennas was determined by measurements at ITS. The antenna gain measurements were made using the three-antenna method for determining antenna gain [5]. This method uses three different antennas (Antennas A, B, and C) to determine the gain of all three antennas. For the antenna gain measurements, Antenna A is a 15 dBi standard gain horn antenna used for testing purposes (Penn Engineering 9030-1B15-NB), Antenna B is the E-plane sectoral horn transmitter antenna used in the propagation measurements (Microwave Engineering Corp. A390-710), and Antenna C is the omnidirectional receiver antenna used in the propagation measurements (Sage Millimeter SAO-2734030345-28-S1-WR).

Using this method, three separate transmission loss (s_{21}) measurements are made in 10 MHz steps over the 26.5–40 GHz band: one using Antenna A for transmit and Antenna B for receive, one using Antenna A for transmit and Antenna C for receive, and one using Antenna B for transmit and Antenna C for receive. The measurements were conducted in a large open-area laboratory at ITS using the Agilent N5230A Network Analyzer. The antennas were mounted on non-conductive tripods so that they were 1 meter above the floor with a 1 meter horizontal separation between antennas which ensures that the transmissions are easily in the far field. Time gating is used on the network analyzer to remove any reflections caused by the floor or other potential reflectors present in the room [6]. A time gate of 1.6 ns was chosen to remove these potential reflections and preserve the impulse response due to the direct ray. Use of this time gate captures the ringing that occurs in the antenna impulse response to more than 35 dB below the peak response. The results of the transmission loss measurements are then used to determine the gains of the three antennas as described in [5]. The resulting gain as a function of frequency for each antenna is shown in Figure 6. Note that for the propagation measurements performed for this effort at 37 GHz, the measured transmitter and receiver antenna gains were 11.9 dBi and 4.4 dBi, respectively.

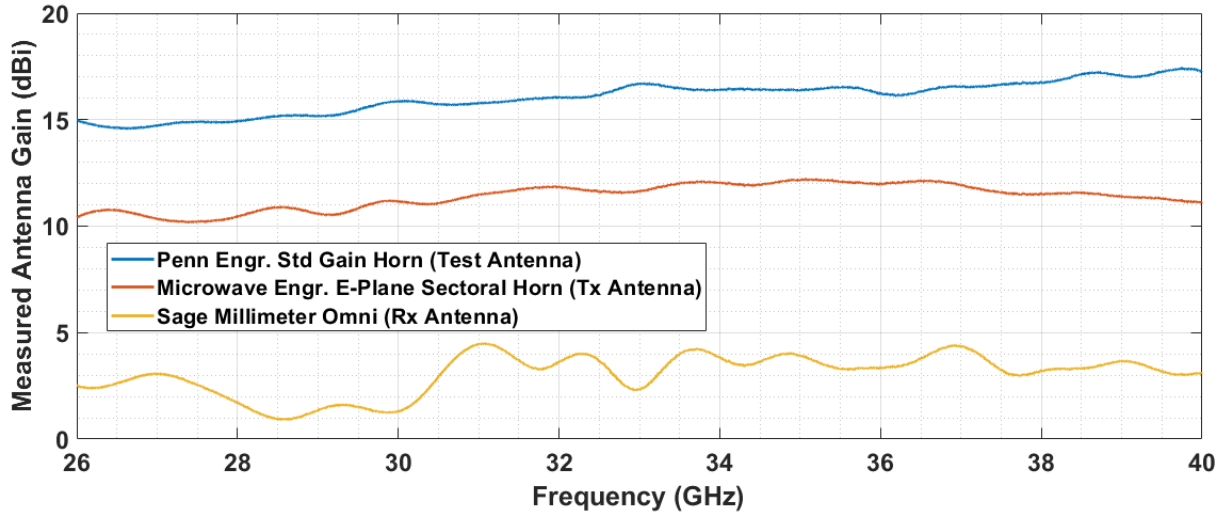

Figure 6. Measured antenna gain for the transmitter (Tx) antenna, receiver (Rx) antenna, and the antenna used for test purposes.

3.2 Receiver Characterization

The receiver characterization is a determination of the dynamic range of the receiver. It consists of determining both the mean receiver system noise power level (hereafter called mean receiver noise power) and the overload level. Knowing the mean receiver noise power provides a means of discerning the reception of our transmitted signals from noise when received signal power levels start to approach those of receiver system noise power levels. Additionally, knowing the level of received signals that cause the receiver to overload is essential; data obtained during overload conditions cannot be used since the true power level of the signal is not known when overload occurs because the signals are clipped by the signal analyzer.

The receiver characterization is dependent on the settings that are used for the signal analyzer during the propagation measurements. The following signal analyzer settings were used for all the propagation measurements conducted in this campaign.

- Center Frequency = 37.0 GHz
- Preamp = Off
- Attenuation = 0 dB
- Microwave Path = Low Noise Path (LNP)
- IF Bandwidth = 10 kHz

These settings were found to provide the maximum dynamic range for the overall measurement receiver. While an approximately 1 dB better overall system noise figure (resulting in a slightly better sensitivity) could be obtained by using the internal preamp in the signal analyzer, the preamp was not used since the signal level at which overload occurs is reduced by roughly 20 dB (resulting in a greatly reduced dynamic range).

The selection of IF Bandwidth was determined from an analysis of the required sampling rate. The sampling rate is determined by considering the maximum expected Doppler shift in the environment as the receiver traverses the measurement paths. The measurement receiver vehicle was held as closely as possible to a constant speed of 20 or 25 mph (~8.94 or 11.18 m/sec) depending on the measurement run. The maximum Doppler shift is estimated based on the possibility of other vehicles moving in the environment at up to 35 mph (~15.65 m/sec). This implies a maximum Doppler shift $f_d = \frac{\upsilon}{\lambda}$, where υ is the speed in meters per second and λ is the wavelength in meters. Assuming a maximum measurement frequency of 40 GHz and vehicle speeds of up to 35 mph (~15.65 m/sec), the maximum Doppler shift $f_d \approx 2.09$ kHz. Since the Doppler shift can be positive or negative, the maximum Doppler spread is expected to be $2f_d$. To adequately characterize Doppler spread, the sampling rate should be at least two times the maximum Doppler spread. Therefore, due to Doppler shift considerations, the sampling rate f_s is given as $f_s \geq 2 * 2f_d = \frac{\nu}{(\lambda/4)} \sim 8.35 \frac{Ksamples}{s}$.

Since a faster sampling rate implies a wider IF Bandwidth in the signal analyzer operating in the IQ Analyzer (Basic) mode, the mean receiver noise power increases with increased sampling rate. Minimization of the mean receiver noise power is desired to be able to achieve the best possible receiver sensitivity and be able to detect weak signal levels received from the transmitter. While not performed for this effort, digital filtering in post-processing may be able to be employed to reduce the mean receiver noise power and still capture the maximum Doppler spread.

A sampling rate f_s of 12.5 Ksamples/s was selected to ensure that the expected Doppler spread could be measured. This means that the time between RF samples $\Delta t = \frac{1}{f_s} = 80\ \mu s$. Since the sampling rate for the signal analyzer operating in the IQ Analyzer (Basic) mode is 1.25 times the IF Bandwidth, an IF Bandwidth of 10 kHz is used for the measurements [7].

The mean receiver noise power was determined by first performing a noise diode calibration. The noise diode calibration uses the traditional Y-factor method [8]. In this method, the calibration measurement is performed twice, once with the diode turned on and once with the diode turned off; the gain and noise figure are determined by *Y*, the difference between the measured power in decibels with the diode on and the measured power in decibels with the diode off. This calibration provides measurements of the preselector gain and system noise figure, and furthermore is used to provide assurance that the measurement system is operating properly. The preselector gain is subtracted from the received power measured at the RF input of the signal analyzer to provide calibrated power measurements referenced to the antenna output. The mean receiver noise power is found from the noise figure (NF) and IF bandwidth (BW) as

$$Mean\ receiver\ noise\ power = -174\ dBm + 10\log_{10}(BW) + NF. \quad (1)$$

Noise diode calibrations performed both in the laboratory and in the field revealed system noise figures that usually varied from about 6.5 to 7.0 dB (occasionally varying up to 7.5 dB).[6]

[6] Noise diode calibrations provide noise figure and preselector gain values that are referenced to the noise diode output of the preselector (see Figure 5, Section 2.2). However, since received signal power levels referenced to the

Variation appeared to be correlated with temperature; typically, the noise figure appeared to increase with increasing temperature. The worst-case mean receiver noise power was found to be -126.5 dBm. This mean receiver noise power can be translated into a peak value. For the purposes of this report, the peak noise power is defined as the noise power level exceeded 0.01% of the time. Since the receiver system noise is complex Gaussian noise, the peak noise power is 9.6 dB greater than the mean noise power [9]. Therefore, the worst-case peak receiver system noise power level is expected to be -116.9 dBm.

The measurement system receiver overload level was determined as the signal power at the antenna output that causes the signal analyzer to generate an ADC overload error. The receiver system was designed so that using the signal analyzer settings as listed above, the signal analyzer will overload well below (at least 6 dB below) the 1 dB compression point of the preselector low-noise amplifier. The overload level was found by injecting a CW signal into the preselector antenna input. Starting at a low signal level presumed to be well below overload (-60 dBm) the signal power level was slowly increased until ADC overload on the signal analyzer occurred. Overload occurred when the signal level increased above -35 dBm.

While one can calculate a quantitative dynamic range value based on the overload level and mean receiver noise power, dynamic range can be defined in different ways (e.g., using mean receiver noise power, peak receiver system noise power level, a threshold set above either of these levels, etc.). Therefore, the usefulness of a quantitative value for dynamic range is questionable and it is not given here. The bounds provided by overload, and mean and peak receiver system noise power level, should be adequate to determine the range of signal powers that can be considered useful.

antenna output of the measurement system receiver (see Figure 3, Section 2.2) are ultimately required, noise figure and preselector gain values are needed that are referenced to this antenna output. At 37 GHz, there is 0.5 dB more loss from the antenna output to the output of the preselector waveguide switch than from the noise diode output to the output of the preselector waveguide switch. Therefore, 0.5 dB must be subtracted from the preselector gain obtained from the noise diode calibration to reflect the true preselector gain from the antenna output to the RF input of the signal analyzer. The calibrated received power at the antenna output is then the measured received power from the signal analyzer minus the true preselector gain. Similarly, to obtain the overall system noise figure at the antenna output, 0.5 dB must be added to the overall system noise figure obtained from the noise diode calibration. Noise figure values given in this report are those referenced to the antenna output.

4. MEASUREMENT EXPERIMENT DESIGN

Mobile, CW millimeter-wave propagation measurements at 37 GHz were conducted primarily to capture the path loss characteristics of the radio propagation channel. The transmitter was placed at a fixed location and mobile measurements were taken by the receiver. Measurements were taken primarily in downtown Boulder; however, some preliminary test measurements and a reference measurement were also taken at the U.S. Department of Commerce ITS Table Mountain Field Site and Radio Quiet Zone near Boulder, Colorado (hereafter referred to as Table Mountain) [10].

4.1 Reference Measurement Path: Table Mountain

For the preliminary test measurements and the reference measurement at Table Mountain, the transmitter was located at the intersection of Center Road and the road to Building T4 at Table Mountain. The transmitter antenna height was set to approximately 10 m above ground level (AGL).

The reference measurement was made over a path with the receiver starting out near the transmitter and traveling north away from the transmitter on Center Road and then west toward building T22 as shown in Figure 7. This path provides an essentially unobstructed LOS path between the transmitter and receiver. There are just a few, very sparsely spaced, single-story buildings, and a couple of 5 to 10 m antenna towers between the transmitter and building T22 on an otherwise flat, open prairie with scarcely any trees. Figure 8 shows a photograph of the measurement environment at the transmitter site looking north along the Reference Measurement Path.

The transmitter antenna is aimed so that the center of the azimuthal beamwidth is pointed north along Center Road. The 3 dB azimuthal beamwidth for the transmitter antenna in this orientation is shown by the purple lines in Figure 7. The red arc on the map in Figure 7 shows a 3 km radius about the transmitter.

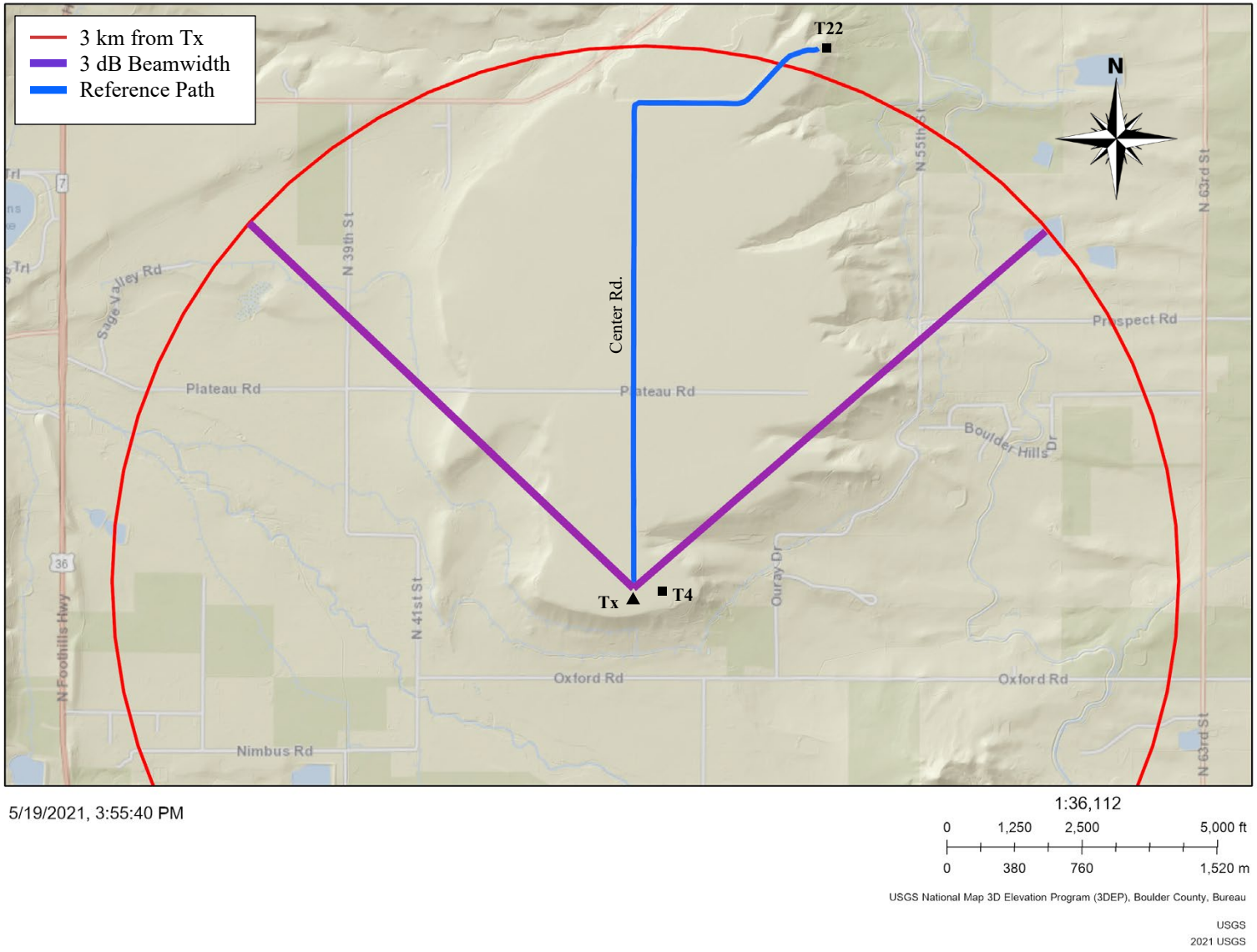

Figure 7. Map showing the Reference Measurement Path between the transmitter and receiver at Table Mountain.

Figure 8. Measurement environment at the Table Mountain transmitter site looking north along the Reference Measurement Path. (Photo courtesy of Ken Tilley)

4.2 Downtown Boulder Measurement Paths

For the measurements in downtown Boulder, the transmitter was located on the street on the north side of Walnut St. immediately east of Eighth St. The transmitter antenna height was also set to approximately 10 m AGL. Received signal power data were collected as a function of distance from the transmitter by collecting data at the mobile receiver over a set of various paths.

The first and most basic measurement was made with the receiver starting out near the transmitter and traveling east away from the transmitter on the same street that the transmitter was located on (Walnut St.) as shown in Figure 9. This path, LOS1, includes a straight path eastward along Walnut St. and after about 1850 m continues eastward on the next parallel street to the north (Pearl St.) since Walnut St. becomes discontinuous and begins to meander east of Folsom St. This semi-LOS path provides a relatively unobstructed LOS path (about the best that could be expected in downtown Boulder) for the first 1850 m and then becomes a more obstructed path, more characteristic of a NLOS path. As expected in any urban environment, partial obstructions are present along the entire path such as street signs, lamp posts, traffic lights, vehicles, trees, etc.

Downtown Boulder represents a small business district with many closely spaced commercial buildings and parking structures of varying heights including a substantial number between 10 m and 20 m (tallest is approximately 36 m) that form a set of urban canyons. This business district can be roughly delineated by a trapezoidal area from 7th to 18th St. west to east (approximately 1300 m) and from Canyon Blvd. to Spruce St. south to north (approximately 350 m). Figure 10 shows a view of this business district in downtown Boulder. Figure 11 shows a magnified view of the measurement environment at the transmitter site looking east along Walnut St.

The transmitter antenna is aimed so that the center of the azimuthal beamwidth is pointed eastward along Walnut St., i.e., along the straight path. The 3 dB azimuthal beamwidth for the transmitter antenna in this orientation is shown by the purple lines in Figure 9. The red arc on the map in Figure 9 shows a 3 km radius about the transmitter.

A second semi-LOS path, LOS2, is also shown in Figure 9. This path starts out the same way as the LOS1 Path but follows Walnut St. east of Folsom St. as it meanders through a business district east of downtown Boulder. This semi-LOS path also provides a relatively unobstructed LOS path for the first 1725 m and then becomes more obstructed.

For measurements that include NLOS paths, the general philosophy in making measurements is to start out along the LOS1 Path and then turn on a perpendicular street to continue the measurement. The intent of this routing is to be able to see degradation in signal levels as the path between the transmitter and receiver transitions from a LOS to a NLOS path. The goal was to make a series of measurement runs where each run would follow a specific path and always start at the transmitter. These measurement paths are shown as the red and black lines in Figure 12. The red lines indicate North Paths (N1–N9) that start at the transmitter, proceed east along Walnut St., and then turn north. The black lines indicate South Paths (S1–S7) that start at the transmitter, proceed east along Walnut St., and then turn south. The azimuthal orientation of the transmitter antenna remained the same as used in the measurement along the semi-LOS measurement paths. The 3 dB azimuthal beamwidth for the transmitter antenna is shown by the

purple lines in Figure 12. Additional NLOS measurement paths are shown by the blue lines (East Paths E1 and E2). These do not follow the basic philosophy (i.e., the receiver does *not* start out along the LOS1 Path and then turn on a perpendicular street). Instead, paths E1 and E2 follow a philosophy of the receiver generally starting out in a NLOS condition and then traveling East away from the transmitter while remaining in a NLOS condition. This provides the opportunity to observe the NLOS path loss behavior over the longest possible distances between the transmitter and receiver. As seen in Figure 12, the measurement paths provide a reasonably complete geographic sampling of the area defined by the 3 dB beamwidth of the transmitter antenna and a 3 km radius about the transmitter.

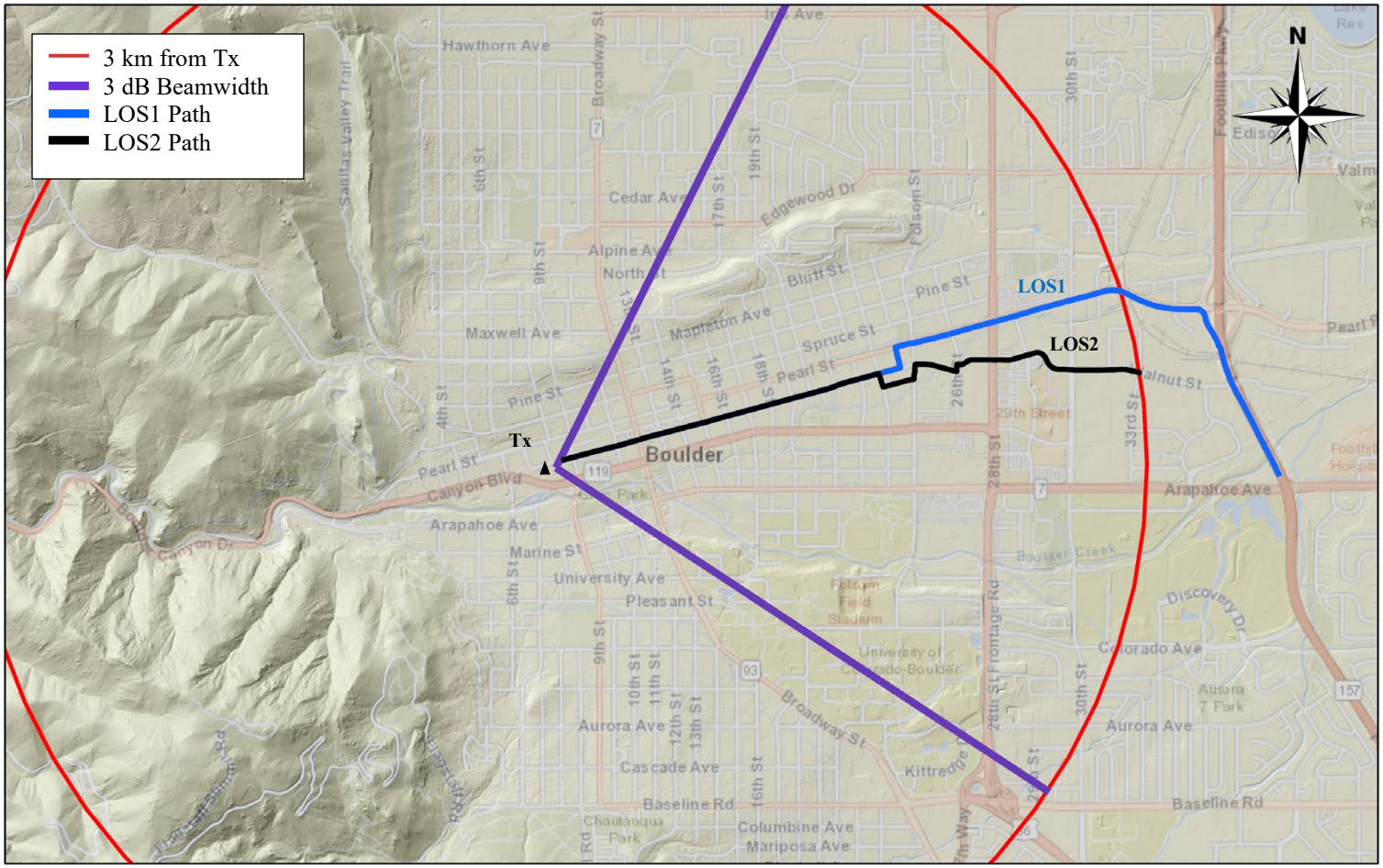

Figure 9. Map showing the semi-LOS paths between the transmitter and receiver in downtown Boulder.

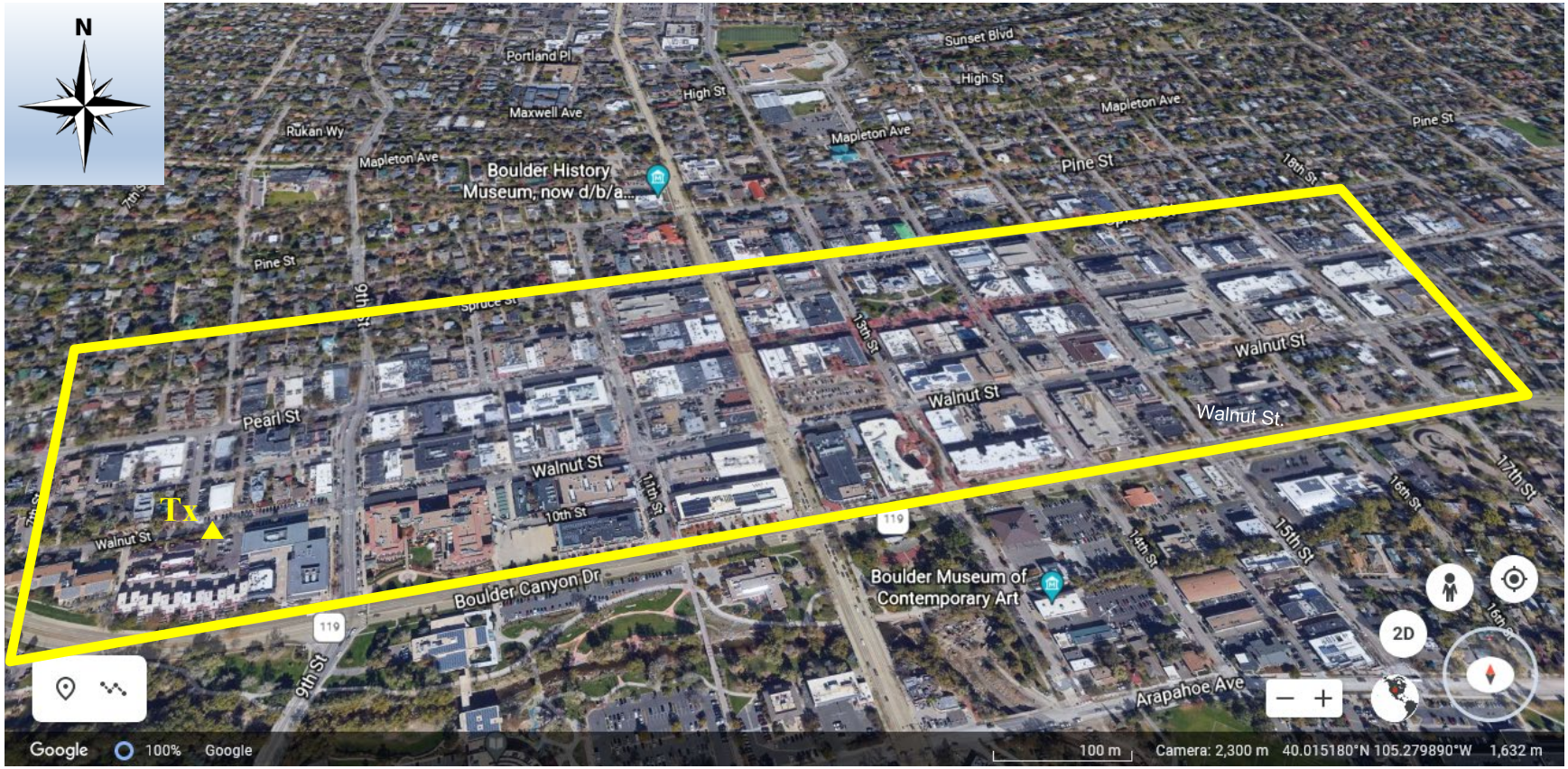

Figure 10. View of the business district (outlined in yellow) in downtown Boulder. The location of the transmitter is marked with a yellow triangle.

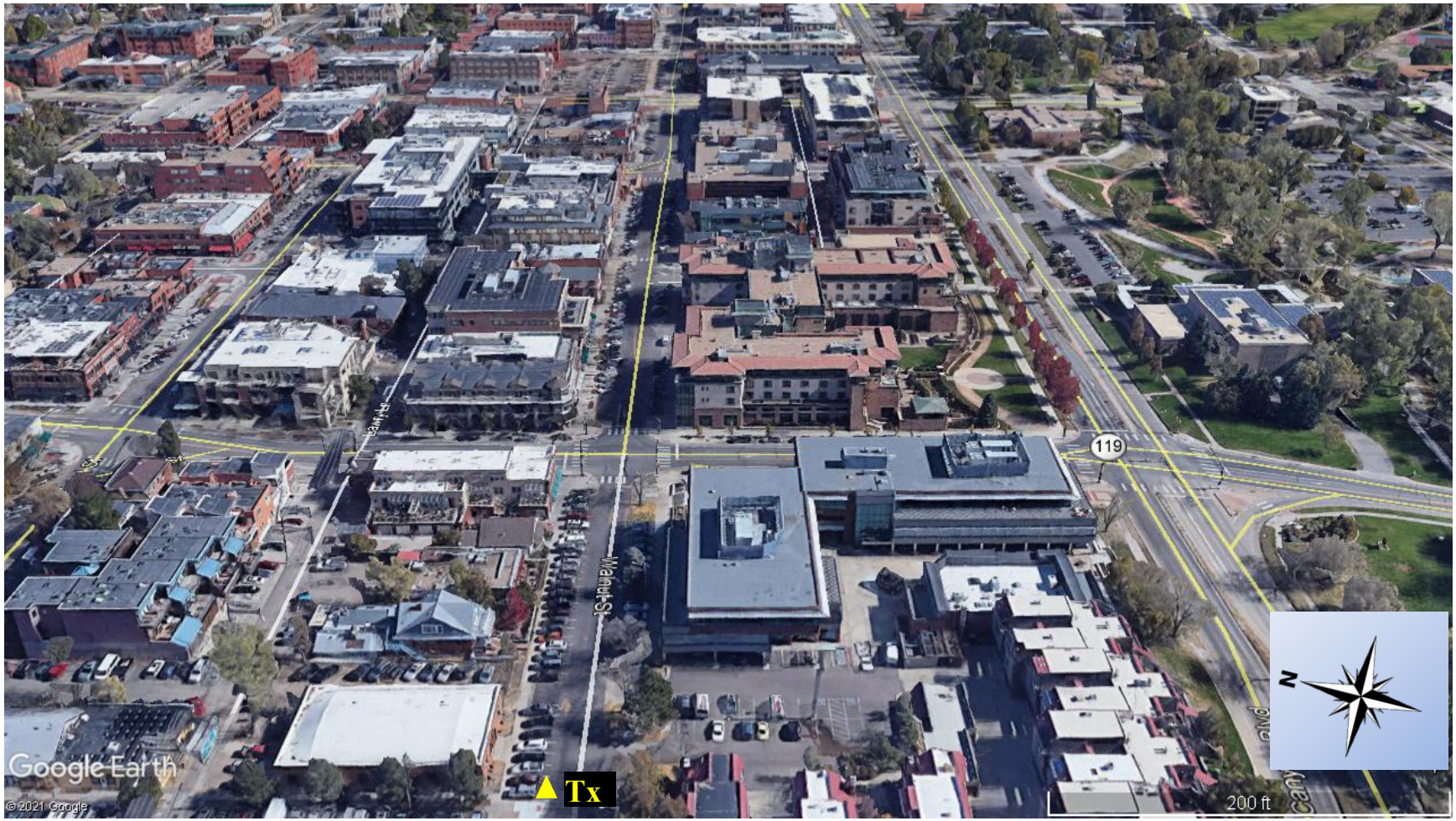

Figure 11. Magnified view of the measurement environment at the transmitter site (marked with a yellow triangle) in downtown Boulder looking east along Walnut St.

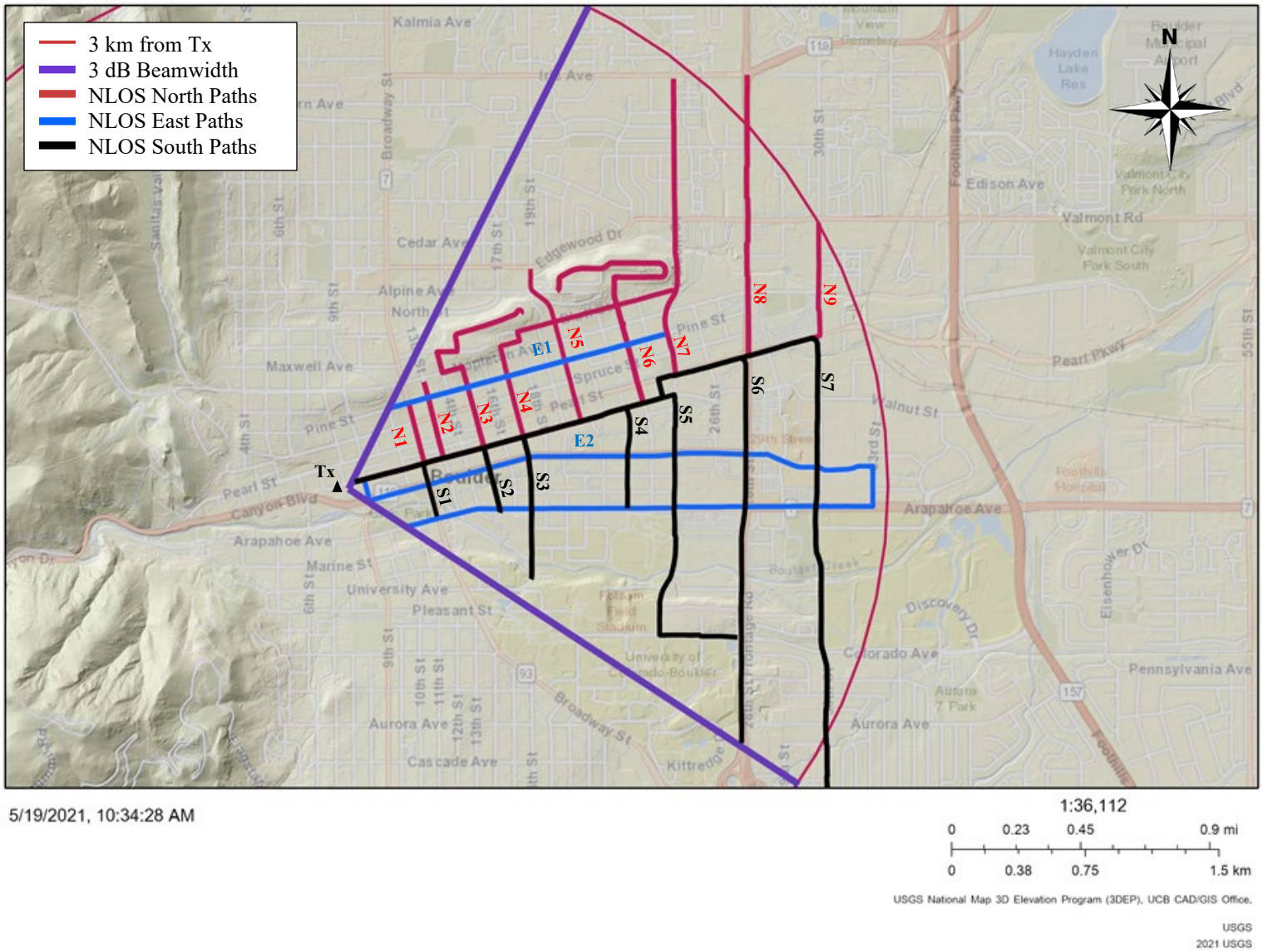

Figure 12. Map showing the NLOS paths between the transmitter and receiver in downtown Boulder.

5. MEASUREMENT SETUP, OPERATING, AND DATA COLLECTION PROCEDURE

For each set of mobile measurements, the following general setup, operating, and data collection procedure, was followed.

5.1 Transmitter

The transmitter was set up in the measurement vehicle shown in Figure 2 (Section 2.1) of this report and placed at a fixed location. As described in Section 4.2 of this report, the transmitter was located at Walnut St. and 8th St. for the measurements conducted in downtown Boulder. For the reference measurements conducted at Table Mountain, the transmitter was located at the intersection of Center Road and the road to building T4. The internal AC generator in the measurement vehicle was started and the transmitter equipment was powered on and allowed to warm up for at least 30 minutes. On each measurement day, the following general transmitting procedure was followed.

5.1.1 Power Calibration

At the start of each measurement day, a power calibration was conducted to set the output power level at the RF output of the power amplifier (i.e., the transmitter power P_t) to the 1 dB compression point of the power amplifier. Additionally, the power calibration is used to determine the coupling factor CF which is the difference in power between the transmitter power P_t and the power at the input to the power sensor for the power meter P_{sens} (see Figure 1 in Section 2.1). Knowing the coupling factor allowed the transmitter operator to determine the output power of the power amplifier based on the power measured by the power meter. Therefore, the transmitter power is found from

$$P_t = P_{sens} + CF. \quad (2)$$

The procedure for performing the power calibration follows. The Coupler Test Assembly, shown in Figure 13, is used for the calibration. This test assembly consists of a high-power 10 dB attenuator and a 40 dB bidirectional coupler with the output and reverse power ports terminated. First, the loss through the Coupler Test Assembly from the RF In to RF Out port $L_c$was measured at the transmitter frequency (37 GHz) using a Keysight N9952A FieldFox Handheld Microwave Analyzer in the network analyzer mode. Next, referring to Figure 1, the transmitter antenna is removed and replaced by the Coupler Test Assembly.

The 1 dB compression point of the transmitter was determined by first setting the signal generator output power to a low level (-40 dBm) to ensure operation in the linear region. The power at the RF Out port of the test assembly, P_{test}, is then measured with the handheld microwave signal analyzer in spectrum analyzer mode. The difference between P_{test} and the signal generator output power, power gain G_p, was then calculated. The output power of the signal generator was then increased by 10 dB, P_{test} was measured, and G_p was computed again. G_p remained the same confirming that the transmitter was operating in the linear region. The process of increasing the output power of the signal generator by 10 dB, measuring P_{test}, and

calculating G_p was repeated up to a signal generator power of -10 dBm. Thereafter, this process was continued with increases in the signal generator output power in 1 dB steps until a 1 dB reduction in G_p occurs. The signal generator output power level where this occurs signifies the 1 dB compression point of the transmitter.

Next, the coupling factor CF is found from

$$CF = P_{test} + L_c - P_{sens} \quad (3)$$

where P_{sens} and P_{test} were measured at the transmitter 1 dB compression point. The transmitter power P_t at the 1 dB compression point was then found by applying (2). This was the power level used for transmission for the propagation measurements.

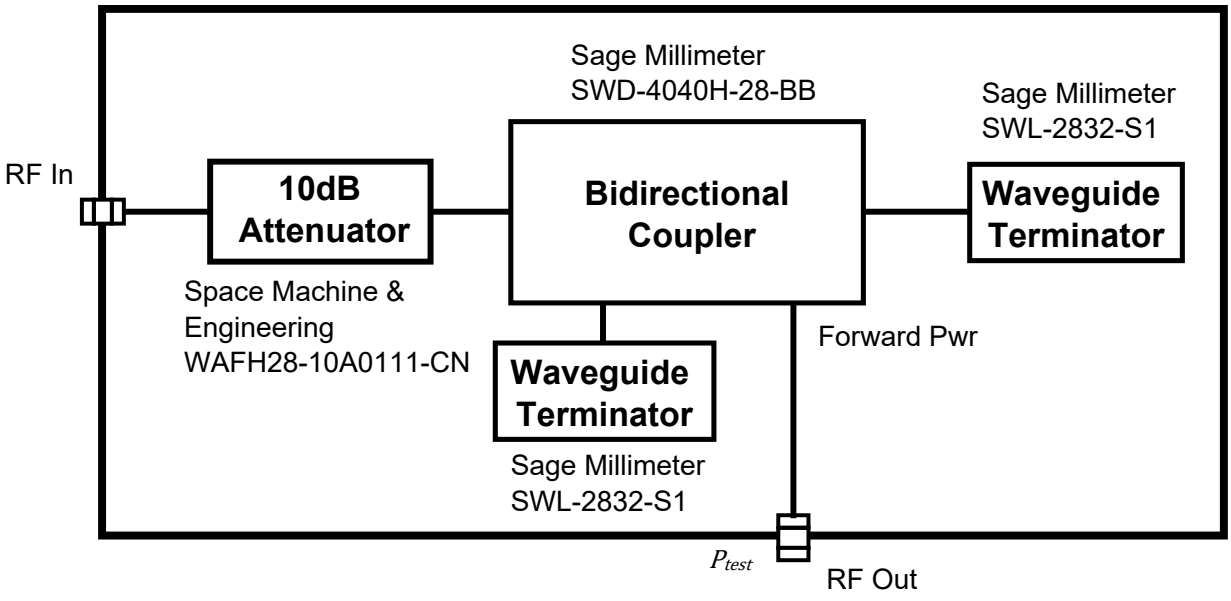

Figure 13. Block diagram of the Coupler Test Assembly.

5.1.2 Transmitter Operation

After the power calibration was completed, the Coupler Test Assembly was removed, and the transmitter system was set up as shown in Figure 1. The power amplifier and the transmitter antenna, mounted on the telescoping mast, were raised 10 meters AGL. The transmitter antenna was rotated azimuthally so that its boresight pointed east along Walnut St. The signal generator was set up to produce a 37 GHz CW signal with its output power set to produce the transmitter power P_t obtained from the power calibration. Output power of the transmitted signal P_t was automatically monitored by the power meter, using transmitter power monitoring software developed by ITS. The software added the coupling factor CF to the power meter's power level reading to get the actual transmitter power P_t at the RF output of the high-power amplifier. The transmitter power P_t was then displayed in a plot on the personal computer monitor to provide real-time monitoring and recorded along with time stamps to provide an opportunity for correlation with the received signal data. An example plot showing the transmitter power P_t

taken during the measurements conducted in downtown Boulder on March 25, 2021 is shown in Figure 14. Note that for a brief period around 22:00 the transmitter was not operating at full power and no measurements were conducted.

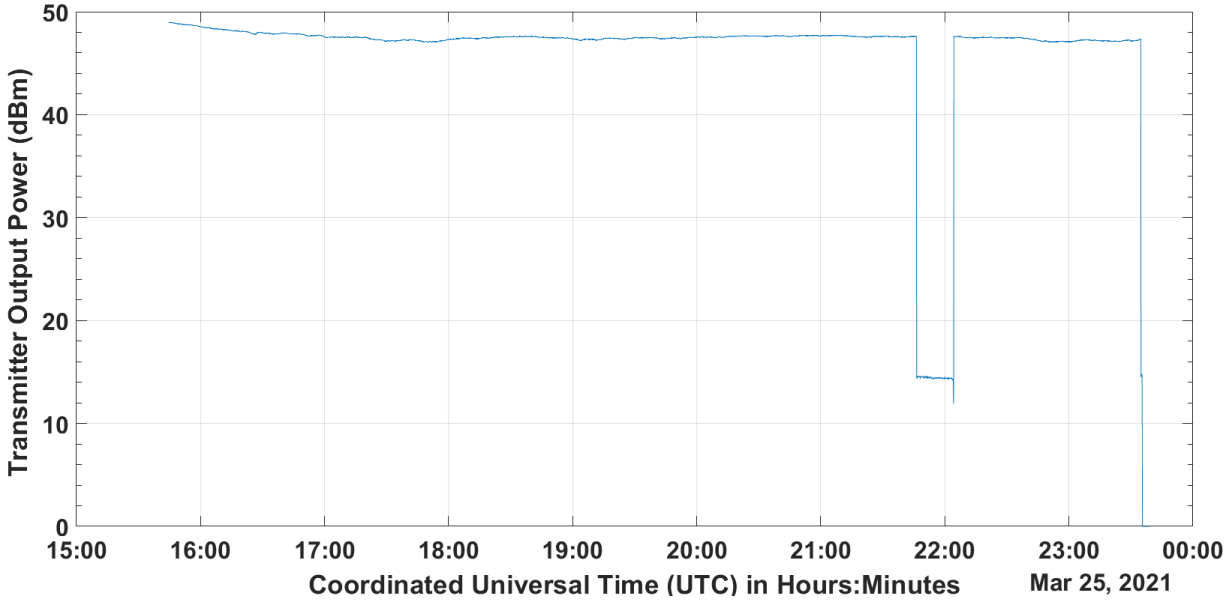

Figure 14. Example plot of transmitter power P_t taken during the measurements conducted in downtown Boulder on March 25, 2021.

5.2 Receiver

5.2.1 Initial Setup Procedure

The receiver was set up in the mobile measurement vehicle shown in Figure 4 (Section 2.2) of this report and driven to the starting point for the measurement runs which was located near the transmitter. The equipment was powered on and allowed to warm up for at least 30 minutes.

An initial noise diode calibration using the procedure described in Section 3.2 was performed. This calibration provided a measurement of the preselector gain and system noise figure at the measurement operating frequency. These results were used to check that the measurement system was operating properly.

Next, a spectrum measurement was performed from 35 to 40 GHz to look for any potential interfering signals. As expected, no interfering signals were encountered in this range of frequencies at any time during the measurement campaign. The spectrum measurement was also used to verify the reception of the signal from the transmitter. After this, the signal analyzer was set up in the Vector Signal Analyzer mode to observe the transmitted signal. The transmitted signal was observed on both an IQ plot and a spectrum plot with a narrow span (1 kHz) and resolution bandwidth (8 Hz) to ensure that the transmitter and receiver system reference frequencies were as close as possible. When the transmitter and receiver system reference frequencies differ, the spectrum shows that the received signal is not on the center frequency.

The IQ plot shows a rotating circular pattern. As the difference in the two frequencies becomes smaller, the rotation of the circular pattern slows down; when the two frequencies are nearly identical, the circular pattern becomes nearly stationary. The GPS disciplined frequency references in both the transmitter and the receiver are set to automatically tune their reference frequencies to received GPS signals resulting in continual synchronization of the reference signals every second. A difference of typically 2.5 Hz or less (at 37 GHz) was seen between the transmitter and receiver frequencies.

The next step entailed starting the actual receiver measurement control software. This software presents the user with a GUI to enter the desired measurement parameters. The signal analyzer parameters are entered as listed in Section 3.2. Additionally, the user enters the recording duration for the IQ data capture (the duration varied depending on the length of the measurement run) and the filename and path for storing the output data.

5.2.2 Procedure for Each Measurement Run

Before the beginning of each measurement run, another noise diode calibration was performed to verify the proper operation of the measurement system and to obtain the preselector gain and system noise figure. The preselector gain is used to provide calibrated power measurements referenced to the antenna output. Knowing the antenna gain then completes the receiver information required to calculate G_b.

The signal analyzer was set up to alert the user when it required an internal alignment. The user was notified of this on the GUI. Whenever this alert was received, the alignment procedure was initiated via a push button control on the GUI. It was discovered that performing this alignment procedure was very important in maintaining the accuracy of the measured received signal power. Laboratory testing showed measured received power accuracies of better than 1 dB when an alignment was performed.

Once calibration and signal analyzer alignment, if needed, was completed at the start of each measurement run, the measurement system was set up to collect semi-automated measurements. The signal analyzer was set up in the IQ Analyzer (Basic) Mode using the settings given in Section 3.2.

After measurement system set up, at the start of each measurement run, data collection was initiated, and data were taken as the receiver traveled along the measurement paths defined in Section 4.[7] While the receiver traveled along a given measurement path, time domain samples of

[7] Data were actually collected with the receiver traveling in a loop starting at a location roughly 120 m west of the transmitter for the downtown Boulder measurements and 215 m east of the transmitter for the Table Mountain measurements. Data collection proceeded with the receiver following the specified measurement paths given in Section 4 and continued as the receiver traveled back to the starting location. This resulted in extra data collected that needed to be disregarded. There were several reasons why the data were collected in this manner. First, the signal analyzer has a limitation in collection of IQ data where a fixed recording duration must be chosen before data collection is initiated; there is no means to terminate this data collection earlier upon user request without jeopardizing the integrity of the data. Second, it was beneficial to have the receiver sufficiently separated from the transmitter both from a standpoint of vehicle parking constraints and for ease of performing noise diode calibrations

IQ data were collected by the signal analyzer. Position data were collected simultaneously along with the received signal data to enable analyzing how received signal power (and ultimately G_b) varies with distance from the transmitter and the relative position of the transmitter and receiver.

Calibration, RF measurement, and position data were stored in separate files on the hard drive in the personal computer for each measurement run. After each measurement run, both the RF measurement data and the position data were reviewed to ensure validity and data backup was performed. This measurement procedure was repeated for each measurement run performed for the day.

All measurements were taken on four separate days (non-consecutive days due to delays caused by inclement weather and necessary vehicle and measurement equipment repairs) in March 2021, a time when the deciduous trees are still dormant and thus have no foliage in the areas where the measurements were taken. This is a factor that must be considered for the downtown Boulder measurements as there are many deciduous trees in downtown Boulder. This is a non-issue for the Table Mountain measurements as there are scarcely any trees between the transmitter and receiver over the Reference Measurement Path. Measurements were generally taken on days that were partly sunny with no precipitation. Measurements for all downtown Boulder South Paths (S1–S7) and East Paths (E1–E2) were taken on an overcast day with no precipitation except for the South S7 Path when light rain was experienced during data collection.

without experiencing very high signal levels from the transmitter. Third, starting and ending the data collection at the same location provided an additional way to check on the health of the measurement system. Received signal levels from both the start and end of the measurement route were compared to ensure the proper operation of the measurement system during the route.

6. DATA PROCESSING AND ANALYSIS

The data were processed using ITS custom software written in MATLAB®. The goal of the data processing was to create a comprehensive MATLAB® data table that associates the RF captured data with the GPS data collected from the GPS receiver, the transmitter power data from the transmitter power log, and various other calculated parameters. The primary types of data that are included in this MATLAB® table are shown in Table 1 and are discussed in more detail in this section.

Table 1. Data included in processed MATLAB® data table.

Origin of Data	Type of Data
Data from GPS receiver	GPS UTC timestamp
	Rx Latitude (degrees)
	Rx Longitude (degrees)
	Rx Altitude (meters)
	Rx RMS Latitude Error (meters)
	Rx RMS Longitude Error (meters)
	Rx RMS Altitude Error (meters)
	Rx Speed (meters/second)
	Track Made Good (degrees from True North)
Data from RF data capture	RF UTC timestamp
	Power at Rx Antenna Output (mW)
	Power at Rx Antenna Output P_r (dBm)
Data from transmitter power log	Transmitter Power P_t (dBm)
Calculated data	Azimuthal Angle between Tx and Rx (degrees)
	Elevation Angle between Tx and Rx (degrees)
	Tx Antenna Gain G_t (dBi)
	Distance from Tx to Rx (meters)
	Mean Power at Rx Antenna Output (dBm)
	Basic Transmission Gain G_b (dB)

The first step in the data processing was to correlate the position data (and other associated data) from the GPS receiver with the received signal RF data recorded from the signal analyzer. Aside from position data (Latitude and Longitude) from the GPS receiver, the other associated data from the GPS receiver include (see Table 1) GPS UTC timestamp, Altitude, root-mean-squared (RMS) Latitude Error, Longitude Error, and Altitude Error, Rx Vehicle Speed, and Track Made Good (showing the direction the Rx vehicle is traveling).

To accomplish the correlation, the UTC timestamp from the GPS data that is closest to the UTC timestamp of the first RF data sample is found. The corresponding GPS position (and the other associated GPS data) are then assigned to this first RF data sample. These same GPS data are assigned to the next 249 RF data samples. (Recall that an RF sample is obtained every 80 μs

while GPS position and the other associated GPS data are obtained only every 20 ms).[8] This means that a single GPS position (and other associated GPS data) sample is assigned to 250 RF data samples. Each subsequent single GPS position (and other associated GPS data) sample is assigned to the next 250 RF data samples and so on.

Both the distance and azimuthal angle between the transmitter and receiver are determined for each RF sample by using the `geoddistance` function in the MATLAB® Central™ Geographiclib toolbox [11], [12]. The elevation angle between the transmitter and receiver antennas for each RF sample is found from the transmitter and receiver coordinates, the transmitter and receiver altitudes, and the transmitter and receiver antenna heights AGL. Both the azimuthal and elevation angles between the transmitter and receiver were used with the transmitter antenna gain and pattern data to determine the transmitter antenna gain in the direction of the receiver for each RF sample. For each RF data sample, the mean received signal power in decibels (referred to as the local mean) is found by taking the moving average of the received signal power in milliwatts. The local mean is used to smooth out the fluctuations in instantaneous signal power seen in the mobile radio channel due to fast fading [13]. The moving average is computed with a window starting at the current RF sample and with a length of 700 RF samples. The window length of 700 RF samples was chosen to average over roughly 62–77 wavelengths as the receiver traveled at nominal speeds of 20–25 mph (~8.94 or 11.18 m/sec). This is based on the 37 GHz transmitter frequency and sampling the IQ data at a 12.5 kHz sample rate.

The transmitter power associated with each RF data sample is found from the transmitter power log and finally, G_b is determined for each RF data sample from

$$G_b = -L_b = -(P_t + G_t + G_r - P_r), \tag{4}$$

where P_t is the transmitter power in dBm, G_t is the transmitter antenna gain in the direction of the receiver in dBi, G_r is the receiver antenna gain in dBi, and P_r is the received signal power in dBm. G_b is used in this report instead of basic transmission loss L_b to show the relationship more easily to the mean receiver noise power. Note that G_b is simply the L_b expressed as a negative number.

[8] It was noticed sometimes in the downtown Boulder data (less than 0.1% of the time), that the GPS data would drop out for short periods of time (the maximum GPS data dropout seen in all measurement data was 120 ms). Note that the receiver only travels a very short distance over this dropout time. Assuming a maximum Rx vehicle speed of 25 mph (11.18 m/s), the Rx vehicle travels 0.22 m in the normal 20 ms between GPS data samples. For the maximum dropout of 120 ms, the vehicle travels 1.34 m. The method used to compensate for the dropouts in the GPS data was to use the GPS data from right before and right after the dropout in place of the missing GPS data during the dropout. This has the effect of making the resulting GPS data never more than one half of the dropout duration away from a valid GPS data sample. Therefore, the vehicle only travels a maximum of one half of the distance traveled over the dropout (0.67 m) between the resulting valid GPS data samples. Note that this is on the order of the accuracy of the GPS position data (typically less than 1 m in downtown Boulder) and therefore does not present any problems. Dropouts in the GPS data were only seen in the downtown Boulder data, not for any of the Table Mountain data.

7. PROCESSED DATA: RESULTS AND ANALYSIS

The data presented in the plots in this section are limited to the data collected that meet the criteria where the receiver was inside the transmitter antenna 3 dB azimuthal beamwidth, the receiver was far enough from the transmitter so that the receiver was inside the transmitter antenna 3 dB elevation beamwidth, and the transmitted signal did not overload the receiver. The resulting processed measured data are presented in two ways: mean received signal power as a function of receiver location (heat map) and G_b as a function of distance between the transmitter and receiver.[9] Both types of plots are shown adjacent to each other for each measurement path since it can be insightful to compare the results from each type of plot.

7.1 Reference Measurement Path: Table Mountain

Figure 15 shows the heat map for the Reference Measurement Path at Table Mountain. This plot (and all heat maps provided in this report) shows the transmitter location as a black triangle. The dashed light purple lines show the transmitter antenna 3 dB azimuthal beamwidth while the dashed blue purple semicircle shows the 3 km radius around the transmitter. The colored path shows the mean received signal power as the receiver traveled along the path. The mean receiver noise power (worst case) was -126.5 dBm as described in Section 3.2. Therefore, black regions of the path represent mean received signal powers that are less than 10 dB above the mean receiver noise power. Any color other than black on the path represents mean received signal powers greater than 10 dB above the mean receiver noise power. The mean received signal power becomes less accurate as it approaches the mean receiver noise power and becomes increasingly influenced by noise. The accuracy of mean received signal powers less than 10 dB above the mean receiver noise power is questionable. Figure 15 specifically shows that relatively strong signals were seen all along the path. The minimum mean received signal power was at least -85 dBm (more than 40 dB above the mean receiver noise power) even at distances beyond 3 km from the transmitter.

Figure 16 shows the G_b for this same path. This plot (and all the G_b plots in this report) shows the measured G_b in blue, the theoretical free space G_b as a red dashed line, and the mean receiver noise power expressed in terms of G_b as a black dashed line. The theoretical free space G_b is given as

$$G_{bfs}(dB) = -\{20\log_{10} f(GHz) + 20\log_{10} d_{3D}(m) + 32.4\}, \quad (5)$$

[9] The distance between the transmitter and receiver d_{3D} used in all the G_b plots for both measured data and predictions from path loss models should ideally be the three-dimensional distance between the transmitter antenna and the receiver antenna taking into consideration the antenna heights AGL and elevations of the transmitter and receiver [15]. In this report, however, the distance used in the G_b plots, for both the measured data and the models, is the distance between the transmitter and receiver coordinates as determined by the `geoddistance` function in the MATLAB® Central™ Geographiclib toolbox [11], [12] which does not take into consideration the antenna heights AGL and the elevations of the transmitter and receiver. For the measurement geometries described in this report, this results in only a negligible error (maximum error in distance is approximately 0.5 m for the downtown Boulder paths and 1.0 m for the Reference Path at Table Mountain). As an example, the difference in the free space G_b due to a 1.0 m error for the worst case (50m) distance between the transmitter and receiver at Table Mountain is 0.17 dB.

where G_{bfs} is given in terms of decibels, f is the frequency in GHz, and d_{3D} is the three-dimensional distance between the transmitter and receiver antennas in meters [14].[9] The G_b plots for the downtown Boulder paths also include the 3GPP LOS and NLOS path loss models for the UMi case [15]. This will be discussed in more detail when the downtown Boulder paths are presented in Section 7.2.

Note that while the worst-case mean receiver noise power is a constant (-126.5 dBm), when expressed in terms of G_b, it is not necessarily constant. This occurs because, from (4), G_b is a function of the transmitted power P_t, transmitter antenna gain G_t, and receiver antenna gain G_r in addition to P_r (the mean receiver noise power in this case). The transmitted power P_t does vary slightly with time, and the transmitter antenna gain G_t varies with both the azimuthal and elevation angles between the transmitter and receiver antennas.

The data in Figure 16 are plotted starting at 50 m, which is slightly beyond the distance at which the receiver starts to enter the 3 dB elevation beamwidth of the transmitter antenna and receiver overload does not occur. Figure 16 specifically shows that measured G_b is far above the mean receiver noise power and that it generally follows the free space G_b quite well. Also evident in Figure 16 is the effect of the ground reflection seen as the fluctuation in G_b vs. distance. Looking at a magnified version of Figure 16, Figure 17 shows a region of measured G_b where the effects of ground reflection are minimal (distances of 50 m to 60 m). This region provides a good comparison of the measured G_b to the free space G_b. This shows measured results to within roughly 1 dB of the free space prediction and thus provides an over-the-air calibration as verification of the proper operation of the entire measurement system.

7.2 Downtown Boulder Semi-LOS Paths

Figure 18 shows the heat map for the LOS1 Path in downtown Boulder. Except for a very small region around Walnut and 23rd St., this plot shows received signal levels along the straight path down Walnut St. to be greater than -85 dBm. Even after the receiver turned off Walnut St. and continued on the next parallel street (Pearl St.), the received signal levels are still generally more than 10 dB above the mean receiver noise power out to about 3 km from the transmitter. As the receiver traveled beyond 3 km from the transmitter, the signal levels drop below 10 dB above the mean receiver noise power. Note that there is a region where the receiver is more than 3 km from the transmitter where the signal levels are more than 10 dB above the mean receiver power. This is understandable since it is an area where the receiver elevation increased as it traveled up a small hill onto Highway 157 (Foothills Parkway).

The G_b plot for this path, shown in Figure 19, provides further insight. As mentioned in Section 7.1, the G_b plots for this and all the downtown Boulder paths include the basic transmission gains G_{bLOS}, G_{bNLOS}, and $Optional\ G_{bNLOS}$ for the 3GPP UMi LOS, NLOS, and Optional NLOS path loss models, respectively. The G_b for these models is given as [15]

$$G_{bLOS}(dB) = -\{20\log_{10} f(GHz) + 21\log_{10} d_{3D}(m) + 32.4\}, \quad (6)$$

$$G_{bNLOS}(dB) = -\{21.3\log_{10} f(GHz) + 35.3\log_{10} d_{3D}(m) + 22.4 - 0.3\,(h_{UT} - 1.5)\}, \quad (7)$$

$$Optional\ G_{bNLOS}(dB) = -\{20\log_{10} f(GHz) + 31.9\log_{10} d_{3D}(m) + 32.4\}, \quad (8)$$

where f is the frequency in GHz, h_{UT} is the height of the receiver antenna AGL in meters, and d_{3D} is the three-dimensional distance between the transmitter and receiver antennas in meters.[10]

G_b for free space is shown as a red dashed line while that of the 3GPP LOS model is shown as a cyan dashed line. Note that there is just a small difference in G_b between the free space model and the 3GPP LOS model for the antenna heights and measurement distances particular to this measurement campaign. The G_b for the 3GPP NLOS and Optional NLOS models are shown as a green dashed line and a light purple dashed line, respectively.

The measured G_b is shown starting at 100 m from the transmitter where the receiver was far enough from the transmitter that the receiver was inside the transmitter antenna 3 dB elevation beamwidth and the transmitted signal did not overload the receiver. Note that measured G_b, even though derived from the measured mean received signal power (where the moving average was applied to obtain a local mean as described in Section 6), does still fluctuate with small changes in distance. There is a small region (from 100 m to 150 m) where the overall trend of the measured G_b does not change much with distance. It is not clear why this occurs. From about 150 m to 1850 m, the overall trend of the G_b decreases. The measured G_b somewhat follows that predicted by the free space model and the 3GPP LOS UMi model for distances from 100 m to 400 m. However, for distances between 400 and 1850 m, the measured G_b is less than and decreases with a greater slope than that predicted by the free space model. At about 1850 m, there is a sharp decrease in measured G_b of about 20 dB. This corresponds to the receiver turning north onto 24th Pl. from Walnut St. and deviating from the straight, more strictly LOS path (see Figure 18). The trend in G_b decreases with distance until slightly over 2 km. From this distance to 3 km the G_b does not appear to decrease with distance. It is not known why this occurs; however, it is repeatable. This same behavior was observed on an additional measurement run on this same path (the LOS1 Path) later in the day using a different transmitter antenna (a standard gain horn) in place of the E-plane sectoral horn.

Further, detailed analysis of the received signals in this region including, but not limited to, analysis of the fading characteristics and analysis of the Doppler spread, is warranted to attempt to better understand the reason for this behavior. Wideband channel measurements may also provide more insight into the behavior of the received signals in this (and other) regions. Also note that in this region the mean received signal power, on average appears to be roughly 10 dB above the mean receiver noise power. While this level of signal power permits one to clearly identify that a signal was received as differentiated from noise, it is not clear that it is sufficiently high above the mean receiver noise power to determine accurate G_b values without being unduly influenced by noise. Determining how far received signals experiencing different types of fading

[10] The 3GPP UMi LOS path loss model is based on the determination of the breakpoint $d'_{BP} = 4\,h'_{BS}\,h'_{UT}\,\frac{f_c}{c}$ where f_c is the center frequency in Hz and c is the speed of light ($3 \times 10^8\ m/s$). The effective transmitter (base station) antenna height $h'_{BS} = h_{BS} - h_E$, and the effective receiver (user terminal) antenna height $h'_{UT} = h_{UT} - h_E$, where h_{BS} and h_{UT} are the transmitter and receiver antenna heights AGL, respectively and h_E = 1 m. For the measurements in downtown Boulder, $d'_{BP} = 6600\ m$.

need to be above the mean receiver noise power to obtain accurate G_b information, while outside the scope of this effort, is worthy of future study.

Beyond 3 km, the trend in G_b decreases with distance, then increases with distance (corresponding to the receiver traveling up a small hill), and then decreases with distance again as the receiver travels down the hill. While the G_b in this region beyond 3 km is less than 10 dB above that due to the mean receiver noise power and is therefore not accurate from a quantitative standpoint, it does provide further confidence in the capability of the measurement system to detect signals below the 10 dB threshold above the mean receiver noise power.

Figures 20 and 21 show the heat map and G_b for the LOS2 Path. As would be expected, the G_b is very similar to that for the LOS1 Path until about 1725 m since the two paths are the same up until this point. This also serves as confirmation of the repeatability of the measurements. The G_b characteristics for the LOS1 and LOS2 Paths differ for distances greater than 1725 m. For the LOS2 Path, at about 1725 m, there is a sharp decrease in G_b of just less than about 20 dB. This corresponds to the receiver turning south onto 23rd St. from Walnut St. and deviating from the straight, more strictly LOS portion of the path (see Figure 20). This decrease in G_b when turning off the more strictly LOS portion of the path is very similar to that seen for the LOS1 Path. At distances just beyond this turn, the trend of the G_b does not decrease and remains relatively constant for a short distance (approximately 1725 to 1900 m). The trend of G_b then increases briefly (presumably as the receiver experiences less clutter). The trend of the G_b then decreases for distances between 1900 and 2200 m from the transmitter, slightly increases for distances between 2200 and 2550 m, and abruptly decreases by nearly 10 dB at around 2550 m. This last, abrupt decrease occurs because the receiver goes down a hill and between buildings on Walnut St. between 29th and 30th St (buildings part of, and adjacent to, the 29th St. Mall). This location is clearly seen on the heat map as the transition from blue to black. The trend of the G_b then remains roughly constant for farther distances. While the G_b in this region is just slightly above that due to the mean receiver noise power and is therefore not accurate from a quantitative standpoint, it does provide further confidence in the capability of the measurement system to detect signals below the 10 dB threshold above the mean receiver noise power.

7.3 Downtown Boulder NLOS Paths

In this section, heat maps and G_b plots from a couple of notable and illustrative NLOS paths in downtown Boulder are presented. These plots represent the most notable trends and observations seen over all the NLOS paths. The remaining set of heat maps and G_b plots for all the other NLOS paths is given in Appendix A. Additionally, a G_b plot from an aggregate of the North and South NLOS paths is provided.

Figures 22 and 23 show the heat map and G_b for the NLOS S3 Path. This path is an example of the typical NLOS path in downtown Boulder in which the general philosophy in making measurements was to start out along the LOS1 Path and then turn onto a perpendicular street to continue the measurement. The intent was to be able to see degradation in signal levels as the path between the transmitter and receiver transitions from a LOS to a NLOS path. Figure 23 shows that the G_b is very similar to that of the LOS1 Path up to just over 1000 m since the NLOS S3 and LOS1 Paths are the same up to this point. At just over 1000 m, the G_b decreases abruptly

by roughly 45 dB. This corresponds to the receiver turning south onto 17th St. from Walnut St. and traveling in a direction roughly perpendicular to the straight, more strictly LOS path along Walnut St. as seen in Figure 22.

The reason for this dramatic decrease in G_b is the presence of relatively tall buildings along Walnut St. (part of the main downtown area in Boulder) that are present between the transmitter and receiver. The general trend of the G_b decreasing abruptly as the receiver turned in a direction roughly perpendicular to the more strictly LOS path along Walnut St. was seen for all the North and South NLOS paths; however, the NLOS S3 Path represents the largest decrease in G_b observed. Smaller, abrupt decreases were seen for the other North and South NLOS paths and typically ranged from roughly 15 dB (NLOS N9 Path) to 35 dB (NLOS Paths N4, S1, S2, and S4). Note that the smaller decreases were usually, but not always, seen for paths where the receiver turn occurred at farther distances from the transmitter and may be somewhat influenced by the lower signal levels approaching the mean receiver noise power experienced at the time of the turn. These phenomena can be examined in more detail from the G_b plots shown in Appendix A.

Figures 24 and 25 show the heat map and G_b for the first section of the NLOS E2 Path.[11] The NLOS E2 Path, out of all the downtown Boulder paths, contains the longest section of a strictly NLOS path extending eastward away from the transmitter.

From Figure 25, the trend of the G_b decreases steadily with distance out to around 1575 m when it ceases to decrease much with distance. Like the LOS1 Path discussed in Section 7.2, this occurs when the mean received signal level reaches around 10 dB above the mean receiver noise power.

Comparing the measured G_b to that predicted from the models, Figure 25 shows that while the 3GPP NLOS path loss models certainly are significantly better at predicting the measured G_b than the free space model or the 3GPP LOS model, there is still a significant difference between measured and predicted values.

Consider the G_b plots for all the downtown Boulder North and South paths (see Figure 23 and the even numbered Figures A-2–A-30 in Appendix A) at distances between 100 m and 150 m (at these distances the receiver traveled over the same section of Walnut St. for each path). For some paths, over these distances, the trend of the G_b decreases slightly with distance (e.g., North Paths N1–N4 and South Paths S1, S2, and S7) and for the others the trend remained somewhat constant with distance. While the cause of this is not known, the measurements were taken on different dates and at different times. There is a significant and varying amount of vehicular traffic in the area including some large trucks and buses that may affect the dynamics of the propagation channel.

[11] For analysis purposes the NLOS E2 path was divided into two sections. The first section of the path consists of the receiver starting from the transmitter traveling east on Walnut St., turning south on 9th St., going east on Canyon Blvd. until turning south on 33rd St. and ending at the intersection of Arapahoe Ave. and 33rd St. The second section consists of the receiver starting at the intersection of Arapahoe Ave. and 33rd St., traveling west on Arapahoe Ave., and ending when the receiver goes outside of the transmitter antenna 3 dB azimuthal beamwidth. The heat map and G_b for the second section of the path are shown in Appendix A.

Figure 26 shows the G_b for the aggregate of the North and South NLOS paths. For this plot, only data from the segments of the paths that are north or south of Walnut St. and north or south of Pearl St. are included, i.e., data from the portion of the paths that include Walnut St., Pearl St, and 24th Pl. (the segment of the path between Walnut St. and Pearl St.) are removed. Detailed heat maps and G_b for each individual path in this plot are found in Figures Figure 22 and Figure 23 and in Figures A-1–A-30 in Appendix A.

The intent of this plot is to show the overall NLOS G_b over a reasonable representation of the entire area in downtown Boulder bounded by the transmitter antenna 3 dB beamwidth and a 3 km radius about the transmitter. The segments of these paths that are shown in the plot begin at discrete distances from the transmitter. The beginning of these segments is generally seen as rapidly decreasing peaks in the plot indicative of the transition from the LOS region to the NLOS region of each path.[12]

Several observations can be made from this plot. The relatively high levels of G_b seen for the NLOS N3 and NLOS N6 Paths correspond to the receiver being on hills with an inherently less obstructed transmission path. Aside from the peaks representing the transition from the LOS to NLOS regions of the paths, and the portions of the NLOS N3 and NLOS N6 Paths where the receiver was on a hill, at distances out to just over 1000 m, the measured G_b generally decreases with distance. At distances beyond this, also disregarding the transition and hill regions, the measured G_b was generally less than 10 dB above the typical G_b due to mean receiver noise power.[13]

Even in regions when the measured G_b is close to or less than 10 dB above the typical G_b due to mean receiver noise power, there are portions of some paths where the trend in G_b does not change much with distance (e.g., NLOS Paths N4, N6, S5, and S7) while portions of other paths show a decrease in the trend in G_b with distance (e.g., NLOS Paths N5, N7, N8, and N9). The measured G_b is generally less than what is predicted by the 3GPP NLOS path loss models, except for regions where the receiver was on a hill. Another exception to this is over a very small range of distances from about 450 to 550 m where the predicted and measured G_b values agree.

As seen in the aggregate plot, but more clearly in the plots of the individual paths in Appendix A, the G_b appears as two separate traces for the same distance, in varying degrees, over certain sections of NLOS Paths S4, S5, S7, N3, and N6. This is caused by signals being received at the same distance from the transmitter but in different geographical areas along the path resulting in different G_b values for the same distance.

Finally, the NLOS S7 Path represents an anomalous case where the G_b was significantly higher than that seen for other paths over the same distances. This path is discussed in more detail in Appendix A.

[12] While removing the data from the portion of the paths that include Walnut St., Pearl St., and 24th Pl. removes the more strictly LOS data, it does not remove the data from the LOS to NLOS transition region.

[13] Typical G_b due to mean receiver noise power is used here since the G_b due to mean receiver noise power will vary depending on the distance between the transmitter and receiver and the particular path. This variation is due to varying transmitter power and transmitter antenna gain in the direction of the receiver as discussed in Section 7.1.

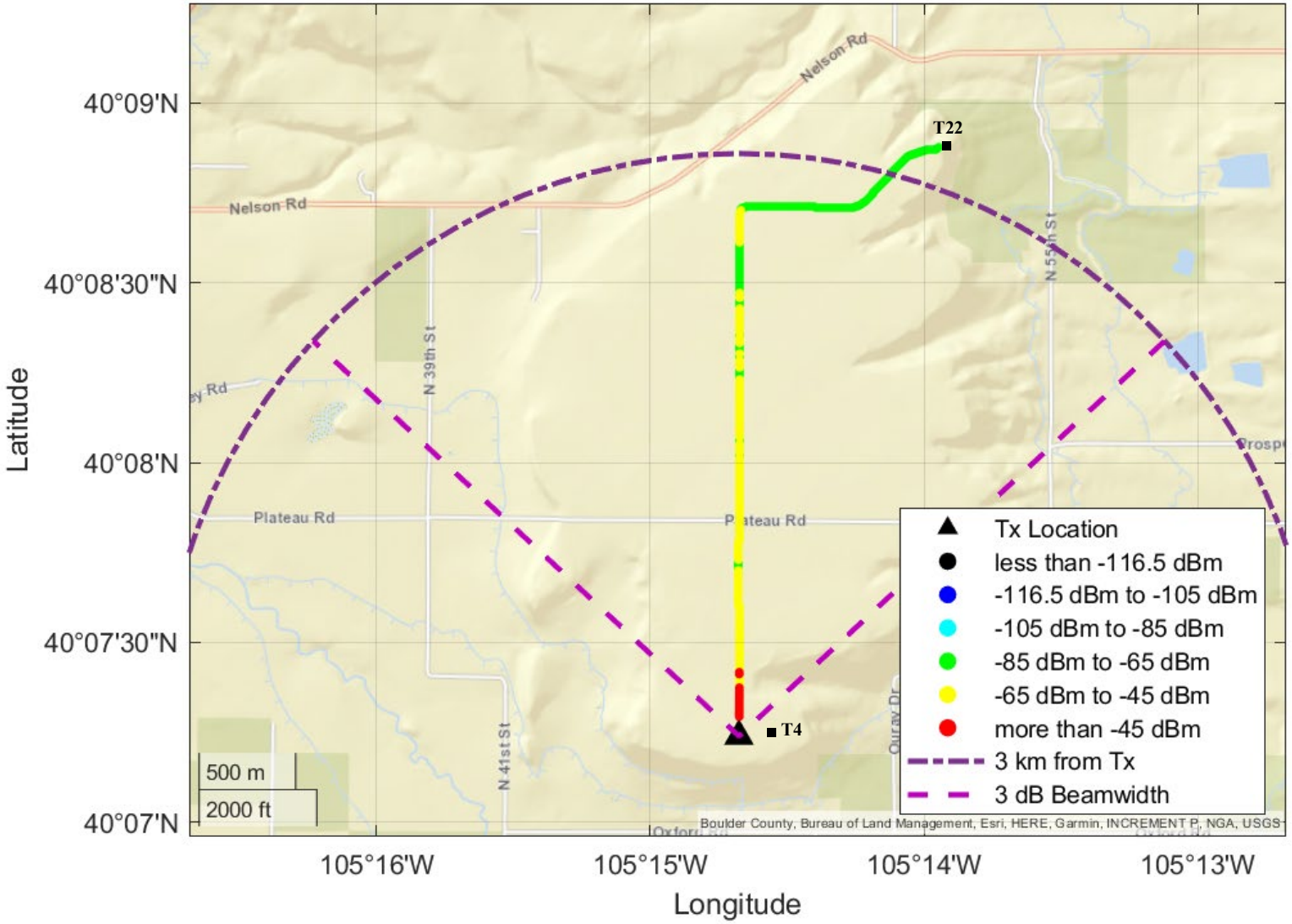

Figure 15. Mean received signal power as a function of receiver location for the Reference Path at Table Mountain (mean receiver noise power = -126.5 dBm).

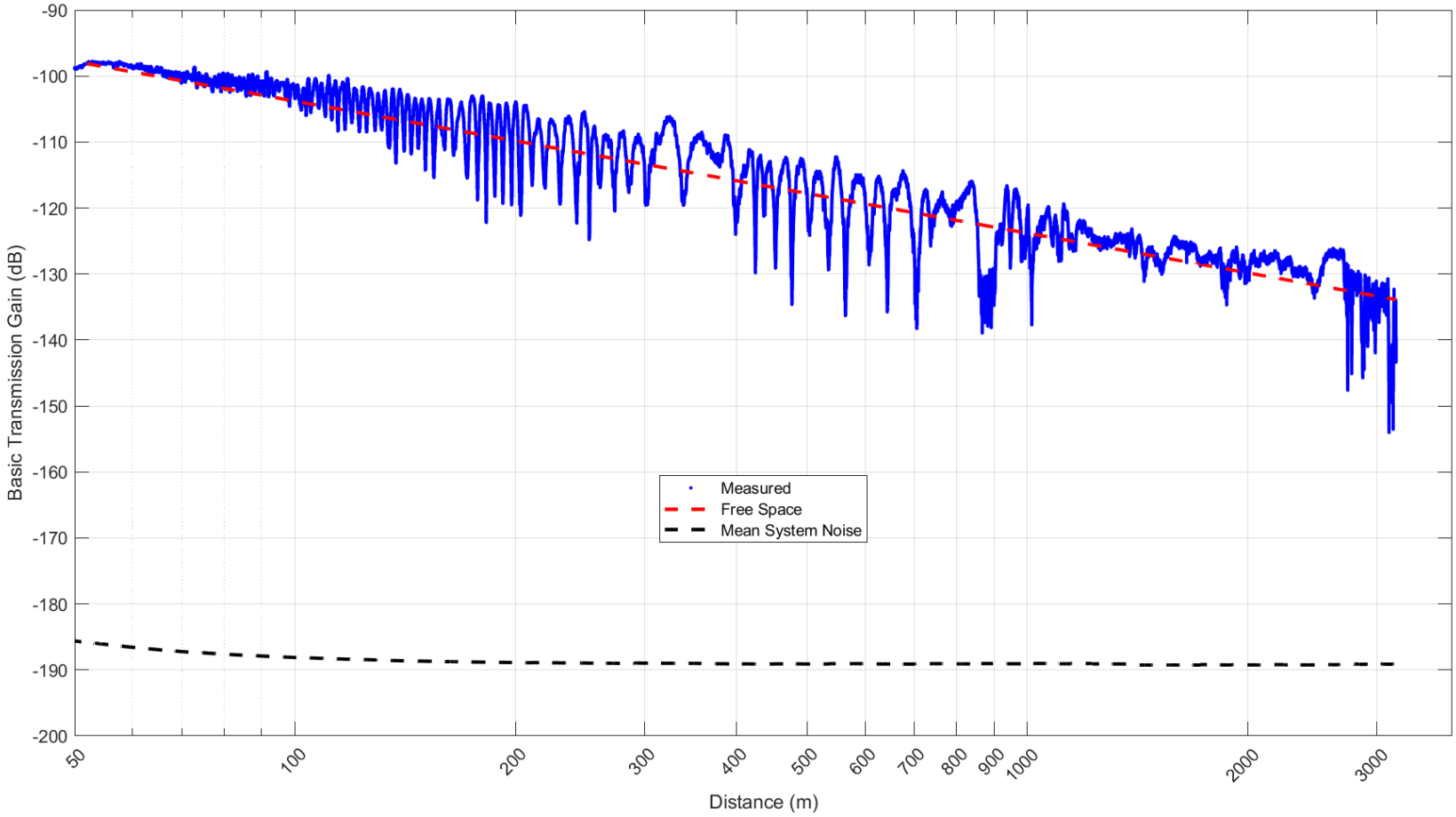

Figure 16. G_b as a function of distance between the transmitter and receiver for the Reference Path at Table Mountain.

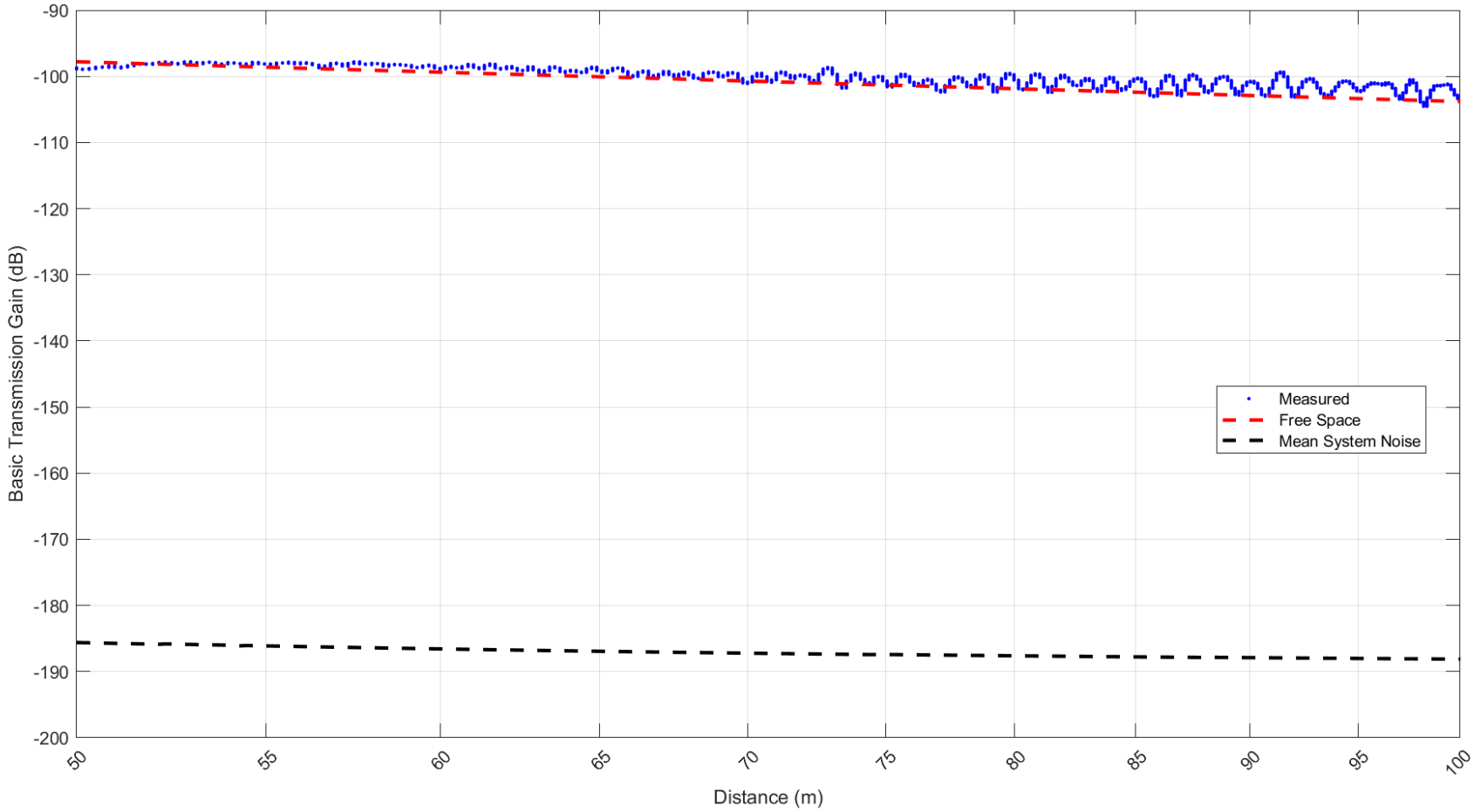

Figure 17. Magnified view of G_b as a function of distance between the transmitter and receiver for the Reference Path at Table Mountain.

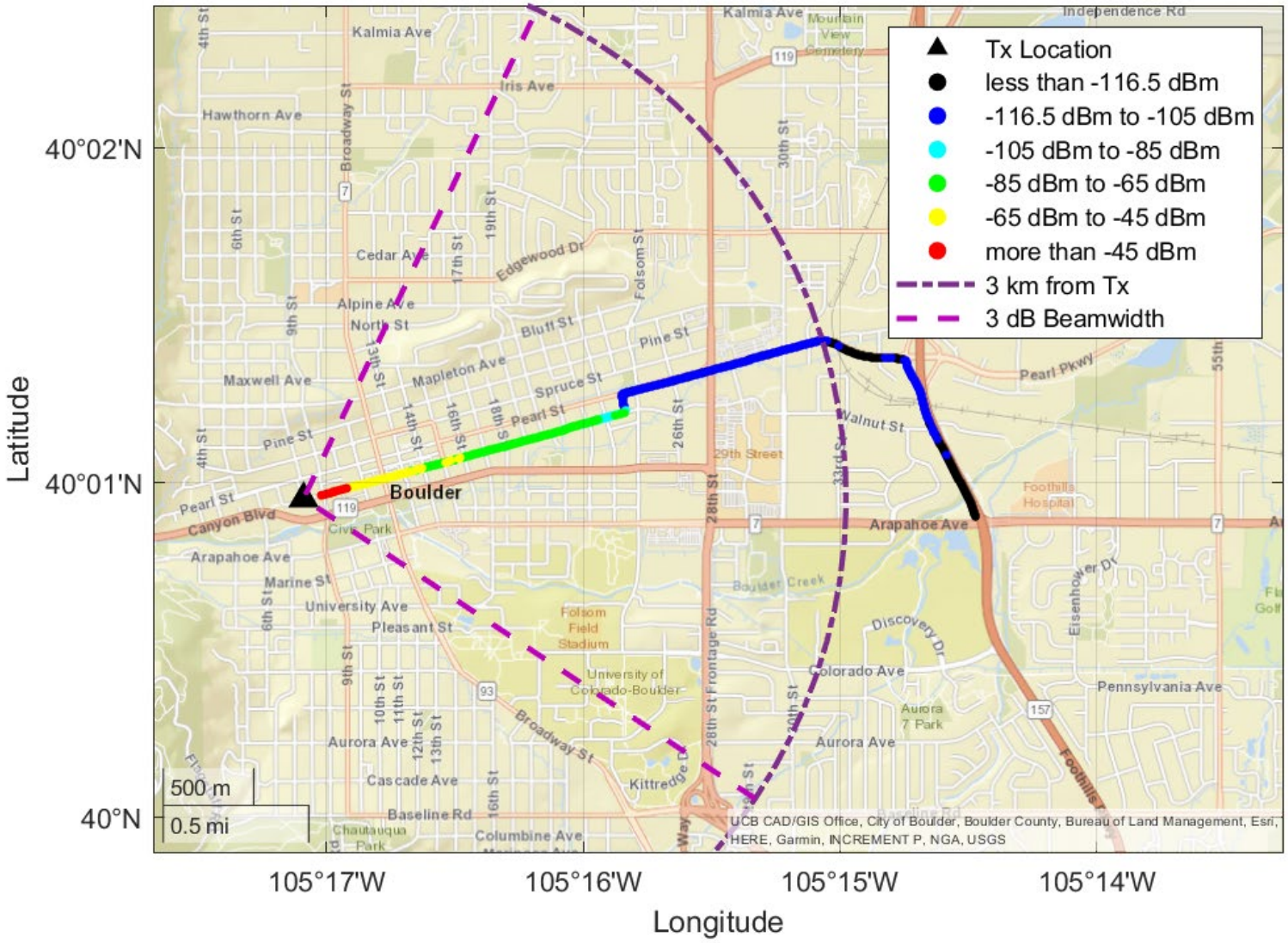

Figure 18. Mean received signal power as a function of receiver location for the LOS1 Path in downtown Boulder (mean receiver noise power = -126.5 dBm).

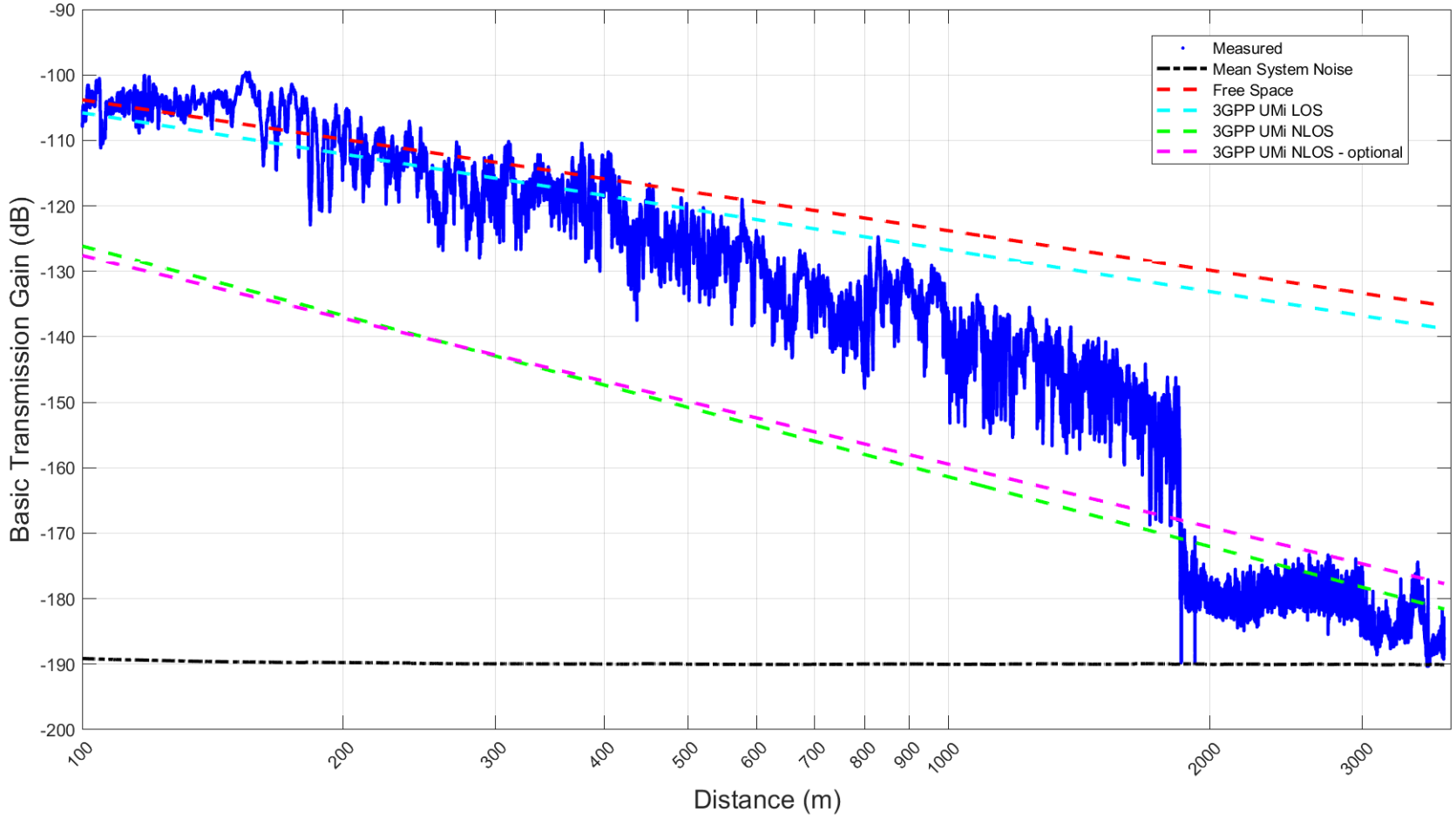

Figure 19. G_b as a function of distance between the transmitter and receiver for the LOS1 Path in downtown Boulder.

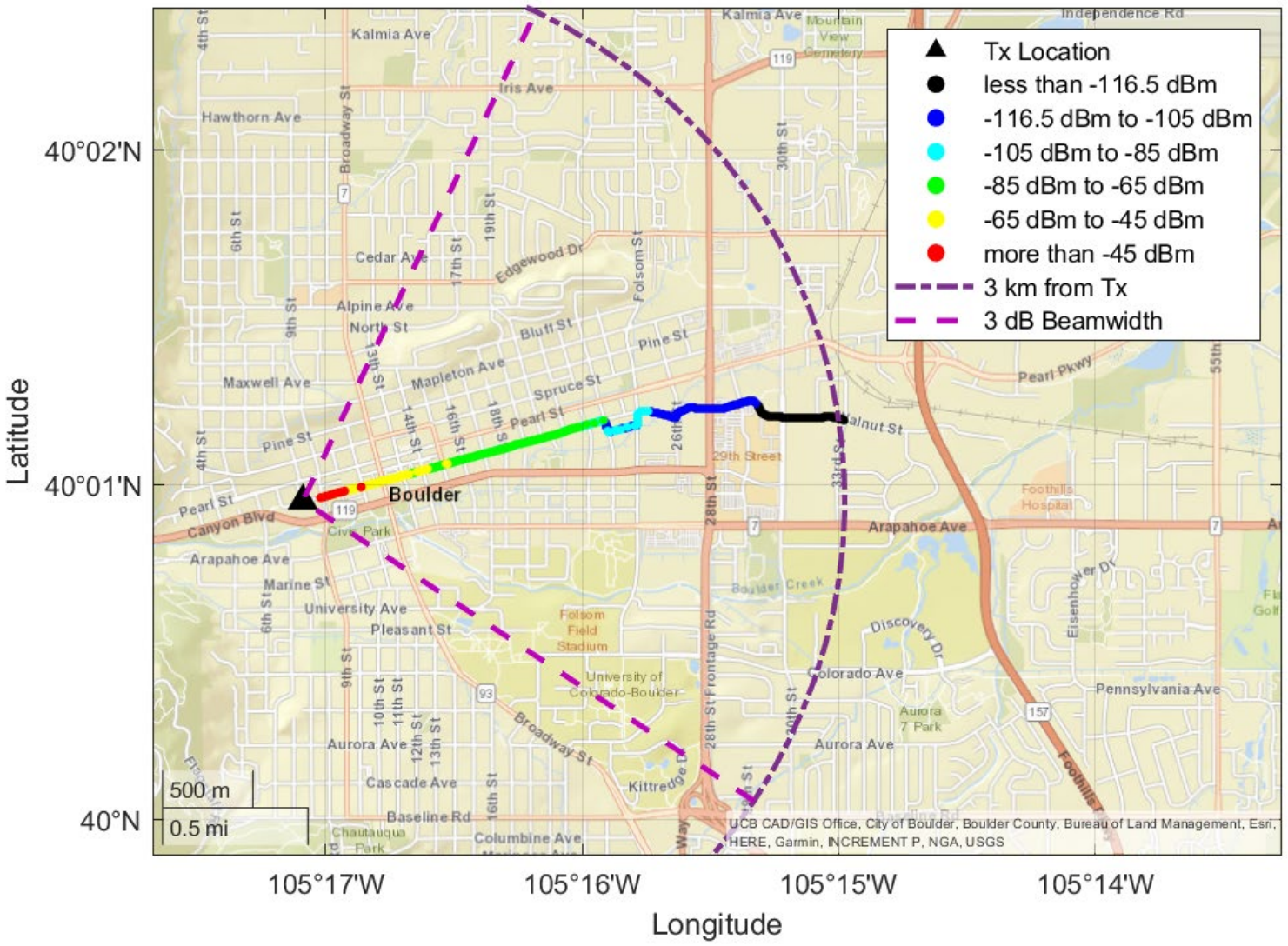

Figure 20. Mean received signal power as a function of receiver location for the LOS2 Path in downtown Boulder (mean receiver noise power = -126.5 dBm).

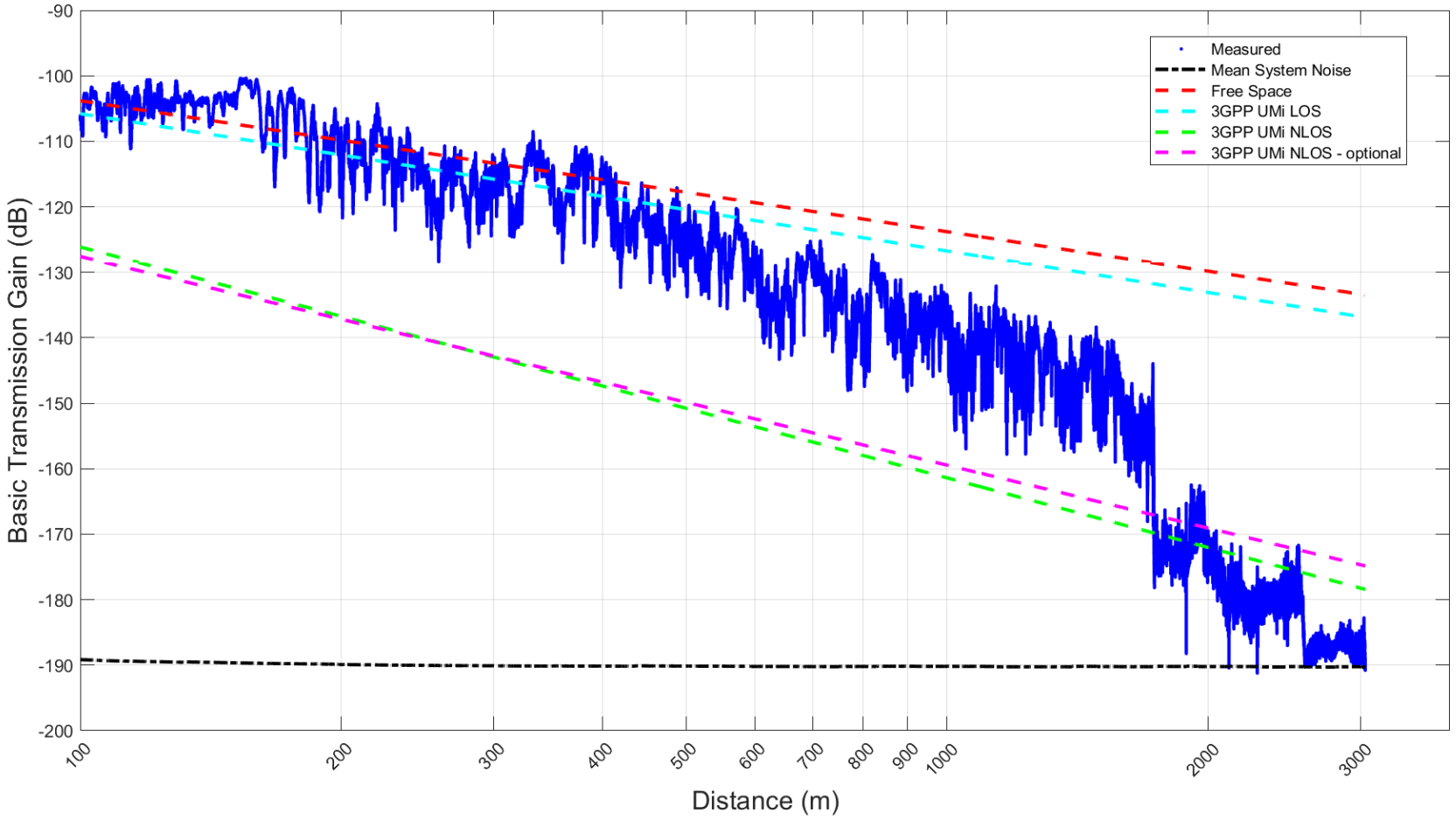

Figure 21. G_b as a function of distance between the transmitter and receiver for the LOS2 Path in downtown Boulder.

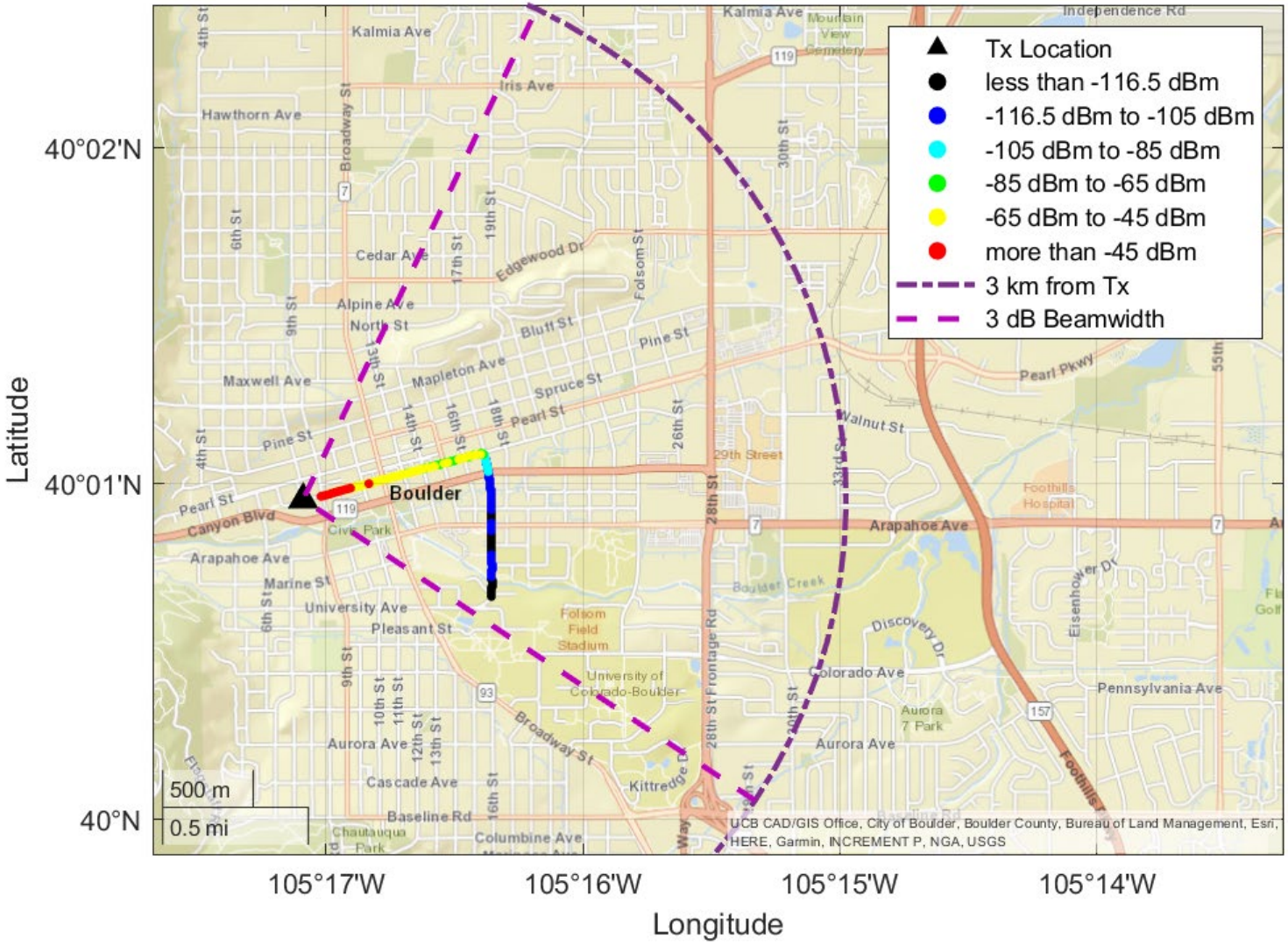

Figure 22. Mean received signal power as a function of receiver location for the NLOS S3 Path in downtown Boulder (mean receiver noise power = -126.5 dBm).

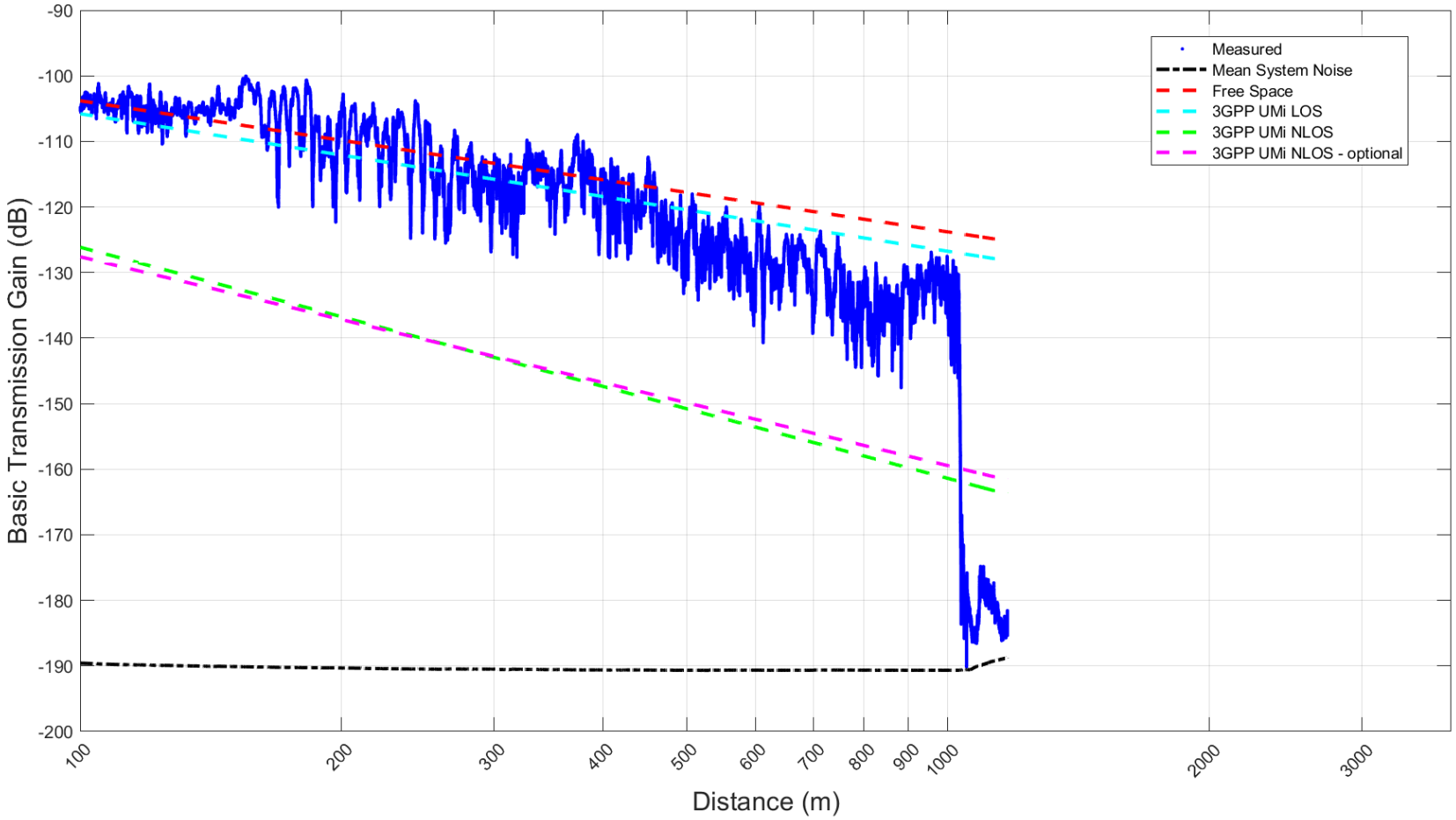

Figure 23. G_b as a function of distance between the transmitter and receiver for the NLOS S3 Path in downtown Boulder.

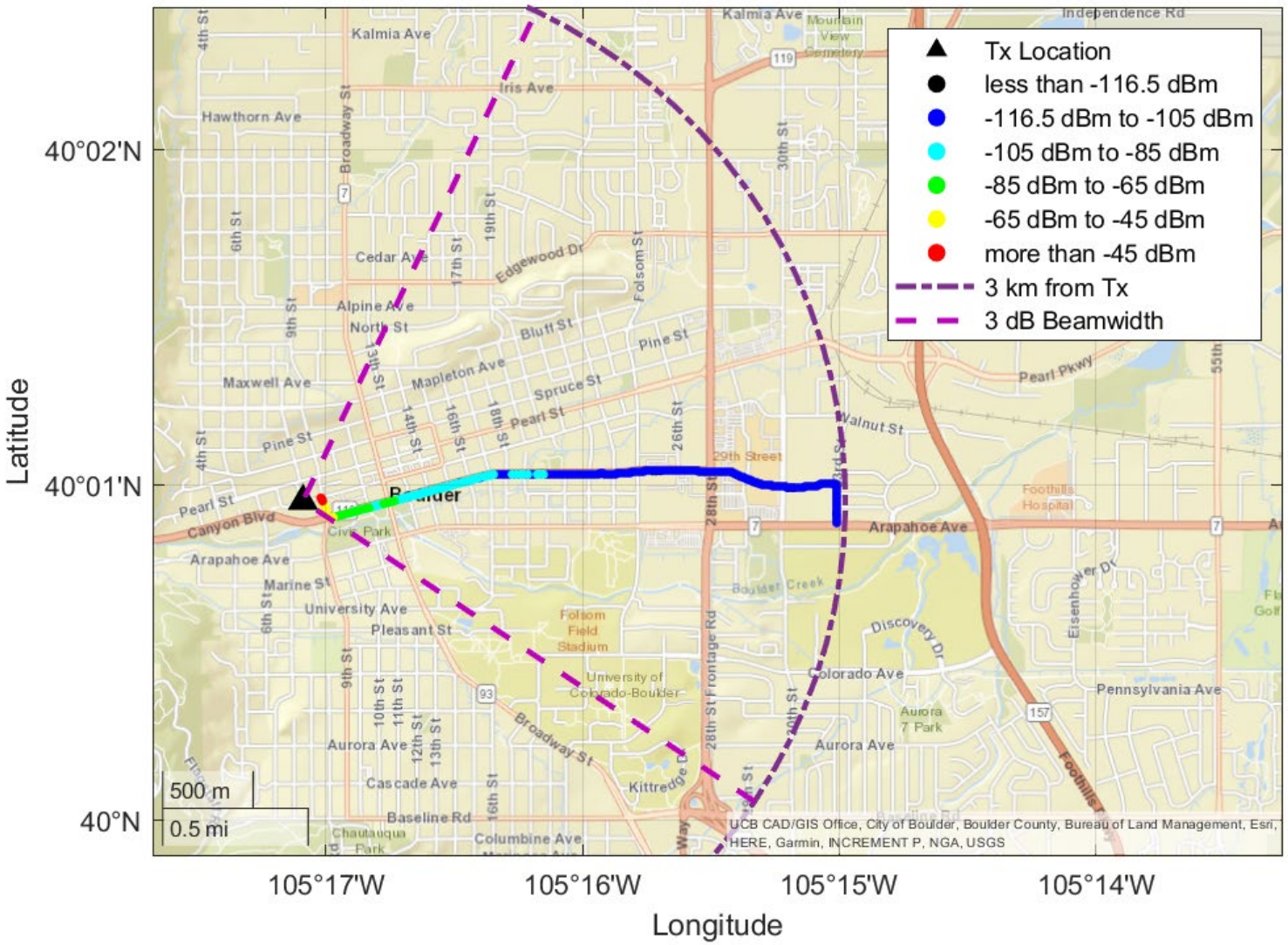

Figure 24. Mean received signal power as a function of receiver location for the first section of the NLOS E2 Path in downtown Boulder (mean receiver noise power = -126.5 dBm).

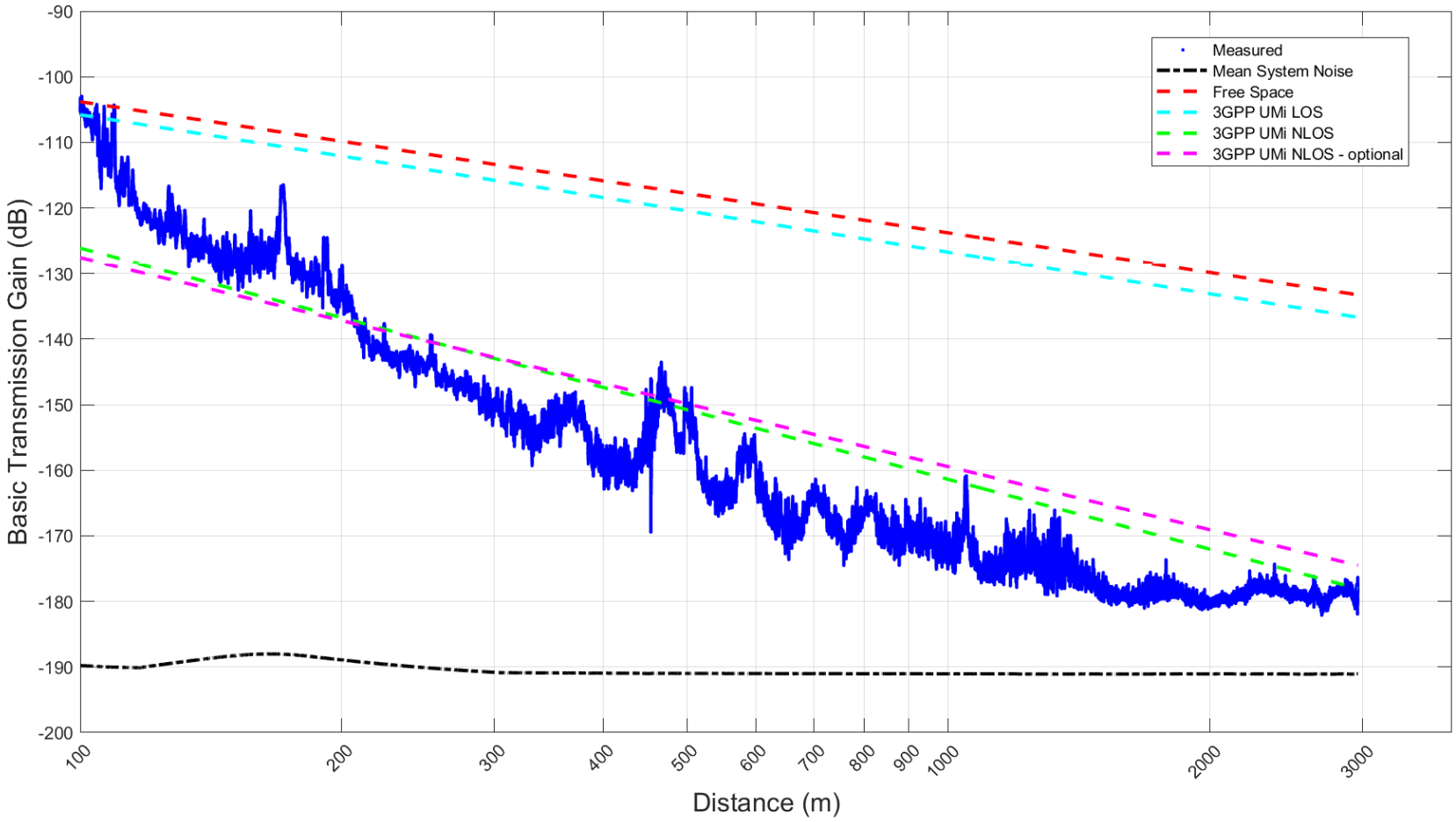

Figure 25. G_b as a function of distance between the transmitter and receiver for the first section of the NLOS E2 Path in downtown Boulder.

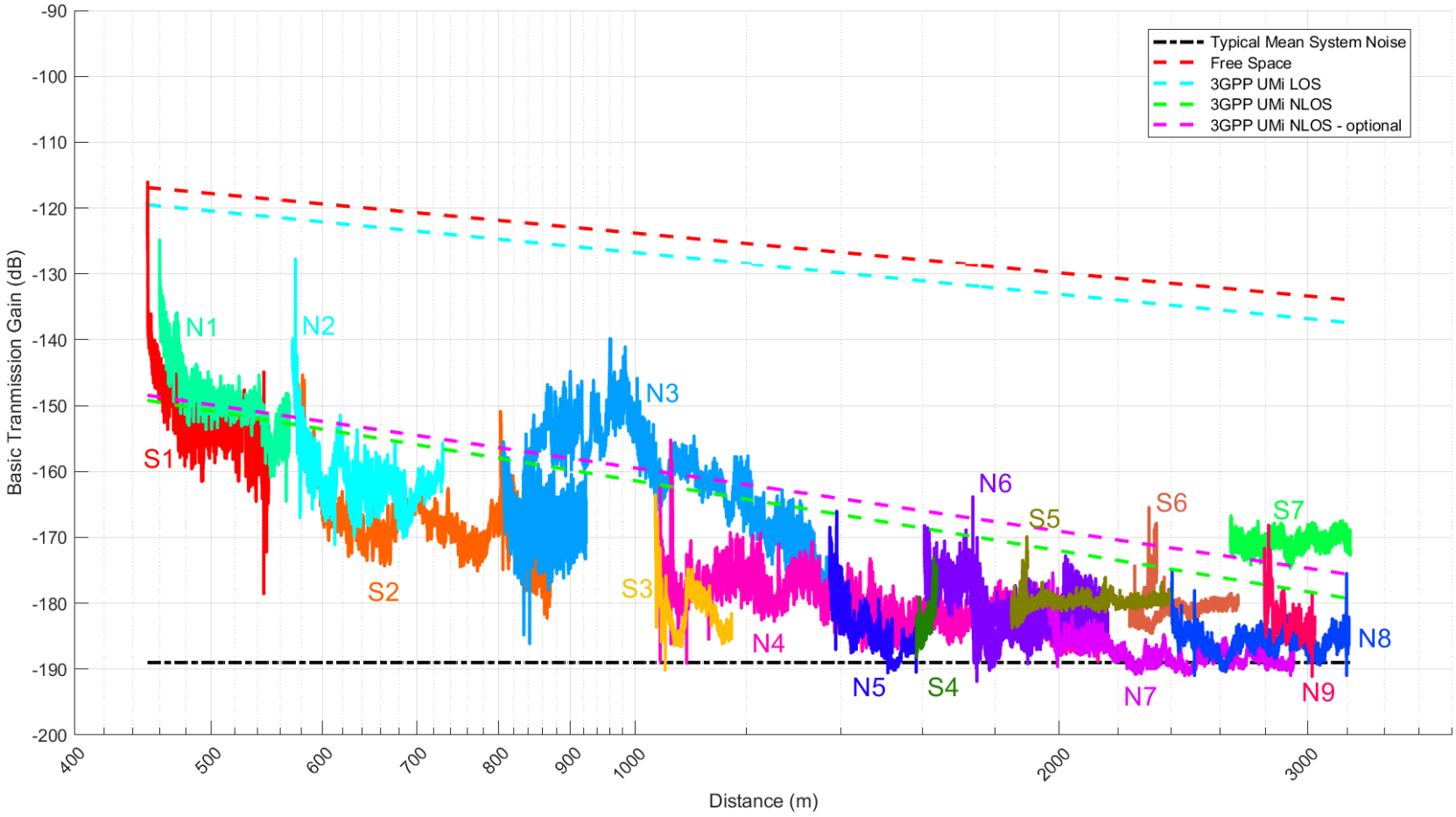

Figure 26. G_b as a function of distance between the transmitter and receiver for the aggregate of the North and South NLOS paths in downtown Boulder.

8. SUMMARY AND CONCLUSIONS

The objective of this work was to perform a set of outdoor, CW, mobile, millimeter-wave propagation measurements in the 37–40 GHz band in a small city downtown environment (Boulder, Colorado) and provide measured data that can be used to help future efforts by OSM to validate 3GPP and other millimeter-wave path loss models.

The measurement system consists of both a transmitter and receiver operated by ITS. The primary components of the measurement system transmitter consist of a microwave signal generator, high-gain power amplifier, and an E-plane sectoral horn RF antenna. Additionally, a GPS disciplined frequency reference (with associated antenna), RF power sensor and power meter, and personal computer complete the system. For these measurements, the transmitter was installed in the ITS modified Chevrolet Express 3500 Extended Cargo Van.

The measurement system receiver consists of a vertically polarized, omnidirectional RF antenna, ITS custom-built preselector, signal analyzer, GPS disciplined frequency reference (with associated antenna), GPS receiver (with associated antennas), function generator, measurement controller, and personal computer. For these measurements, the receiver was installed in the ITS modified Chevrolet Express 3500 Passenger Van.

To ensure accurate transmitted signal power and received signal power for the propagation measurements, several measurement system characterizations were performed: transmitter and receiver antenna gain measurements, receiver dynamic range measurements, and transmitter power calibration.

Measurements were taken primarily in downtown Boulder; however, some preliminary test measurements and a reference measurement were also taken at Table Mountain. The transmitter was placed at a separate, fixed location for each measurement area and mobile measurements were taken by the receiver. The transmitter and receiver antenna heights were set to approximately 10 m and 2.5 m AGL, respectively.

The Reference Measurement Path at Table Mountain provided an essentially unobstructed LOS path between the transmitter and receiver of more than 3 km. The measurement paths in downtown Boulder consisted of two semi-LOS and a set of NLOS paths providing a reasonably complete geographic sampling of the area defined by the 3 dB beamwidth of the transmitter antenna and a 3 km radius about the transmitter. The semi-LOS paths provide a straight, relatively unobstructed LOS path (about the best that could be expected in downtown Boulder) for the first segment of the path (up to 1850 m). The semi-LOS paths then become more obstructed, more characteristic of a NLOS path since they no longer follow a straight path down the street from the transmitter.

Most of the NLOS paths in downtown Boulder are defined by following the general philosophy of the receiver starting out along the LOS1 Path and then turning south (NLOS South Paths S1–S7) or north (NLOS North Paths N1–N9) onto a perpendicular street. The intent is to be able to see degradation in signal levels as the path between the transmitter and receiver transitions from a LOS to a NLOS path. Additional NLOS measurement paths (East Paths E1 and E2) do not follow this general philosophy; the receiver travels roughly along radials away from or towards the transmitter on streets that are not on the same street as the transmitter.

For each set of mobile measurements, a systematic setup, operating, and data collection procedure was followed. The transmitter was set up in the measurement vehicle and placed at a fixed location. After equipment power-on and warm-up, the signal generator was set up to produce a 37 GHz CW signal and a power calibration was conducted to set the output power level at the RF output of the power amplifier to its 1 dB compression point. The transmitter antenna was rotated azimuthally so that its boresight pointed straight down the street defining the LOS path. Output power of the transmitted signal was displayed in real time and saved to hard disk using the power meter under computer control with software developed by ITS.

The receiver was set up in the mobile measurement vehicle and driven to the starting point for the measurement runs located near the transmitter. After equipment power-on and warm-up, an initial noise diode calibration was performed to provide measurements of the preselector gain and system noise figure and check that the measurement system was operating properly. A spectrum measurement was performed from 35–40 GHz to look for any potential interfering signals. As expected, no interfering signals were encountered in this range of frequencies at any time during the measurement campaign. The transmitted signal was observed on the signal analyzer to verify reception and to ensure that the difference in transmitter and receiver system frequencies was as small as possible (typically 2.5 Hz or less).

After measurement system set up, at the start of each measurement run, data collection was initiated, and data were taken as the receiver traveled along the measurement paths. While the receiver traveled along a given measurement path, time domain samples of IQ data were collected by the signal analyzer. Position data were collected simultaneously along with the received signal data. After each measurement run, both the RF measurement data and the position data were reviewed to ensure validity and data backup was performed. This measurement procedure was repeated for each measurement run performed for the day.

All measurements were taken in March 2021, a time when the deciduous trees are still dormant and thus have no foliage in the areas where the measurements were taken. While the Table Mountain area has scarcely any trees, downtown Boulder has many deciduous trees. Measurements taken in downtown Boulder during other times when full foliage exists may experience more path loss.

The data were processed using ITS custom software written in MATLAB® to provide mean received signal power, distance between the transmitter and receiver, transmitter antenna gain, transmitter power, and G_b for each RF data sample collected. The resulting processed measured data are presented in two ways; mean received signal power as a function of receiver location (heat map) and G_b as a function of distance between the transmitter and receiver.

The mean received signal power for the Reference Path at Table Mountain showed relatively strong signals all along the path. The minimum mean received signal power was at least -85 dBm (more than 40 dB above the mean receiver noise power) even at distances more than 3 km from the transmitter.

The measured G_b for this path generally follows that predicted by the free space model. Also evident is the effect of the ground reflection seen as the fluctuation in G_b vs. distance. In the

region where the effects of ground reflection are minimal (distances of 50 m to 60 m from the transmitter), measured G_b was found to be within roughly 1 dB of the free space prediction.

For the LOS1 Path in downtown Boulder, received signal levels along the straight, strictly LOS portion of the path down Walnut St. were generally greater than -85 dBm. Even after the receiver turned off Walnut St. and continued on the next parallel street (Pearl St.), the received signal levels were still generally more than 10 dB above the mean receiver noise power out to about 3 km from the transmitter.

Measured G_b values below the 10 dB threshold above the G_b due to mean receiver noise power were seen for regions of the semi-LOS and some of the NLOS paths. While the accuracy of these values is questionable, it does provide confidence in the capability of the measurement system to detect signals below the 10 dB threshold above the mean receiver system noise power and to be able to observe trends in G_b as a function of distance.

The measured G_b of the first section of the NLOS E2 Path (a NLOS path where the receiver travels roughly along a radial eastward away from the transmitter) was compared to that predicted from the models. While the 3GPP NLOS path loss models certainly are significantly better at predicting the measured G_b than the free space model or the 3GPP LOS model, there is still a significant difference between the measured and predicted values.

The G_b plots for all the downtown Boulder North and South NLOS paths and the semi-LOS paths at distances between 100 m and 150 m (at these distances the receiver traveled over the same section of Walnut St. for each path) revealed that for some paths the trend of the G_b decreased slightly with distance (e.g., North Paths N1–N4 and South Paths S1, S2, and S7) and for the others the trend remained somewhat constant with distance. While the cause of this is not known, the measurements were taken on different dates and at different times. There is a significant amount of vehicular traffic in the area including some large trucks and buses that may affect the dynamics of the propagation channel.

Additionally, there were some other regions along some of the downtown Boulder paths where the trend of the G_b remained somewhat constant with distance. The cause of this is also not known. However, for at least the one case where a measurement run was repeated along the same path at another time (the LOS1 Path), this behavior was repeatable. Further, detailed analysis of the received signals for these situations including, but not limited to, analysis of the fading characteristics and analysis of the Doppler spread, is warranted to attempt to better understand the reason for this behavior. Wideband channel measurements may also provide more insight into the behavior of the received signals in these (and other) regions.

The measured G_b along the strictly LOS portion of all the downtown Boulder North and South NLOS paths and the semi-LOS paths (along Walnut St.) reasonably followed that predicted by the free space model and the 3GPP LOS UMi model for relatively short distances (100 m to 400 m) from the transmitter. (Note that there is only a small difference in G_b between the free space model and the 3GPP LOS model for the antenna heights and measurement distances particular to this measurement campaign). For farther distances, the measured G_b was less than and decreased with a greater slope than that predicted by these models.

For all the downtown Boulder North and South NLOS paths and the semi-LOS paths, a rapid and sharp decrease in G_b (typically varying between 15 and 45 dB depending on the specific path) was seen as the receiver turned onto a perpendicular street transitioning from the more strictly LOS path along Walnut St. to a NLOS region.

The measured G_b as seen for the aggregate of the North and South NLOS paths was generally less than what is predicted by the 3GPP NLOS path loss models, except for regions where the receiver was on a hill. Another exception was over a very small range of distances (450 to 550 m) where the predicted and measured G_b values agree.

Determining how far received signals experiencing different types of fading need to be above the mean receiver noise power to obtain accurate G_b information, while outside the scope of this effort, is worthy of future study. Further CW measurements in a different urban environment with a longer, true LOS path than what was available in downtown Boulder would be beneficial for observing the trend of G_b over LOS paths out to farther distances. While the free space model predicted the measured G_b for the Reference Path at Table Mountain, the free space and 3GPP models did not predict the measured G_b very well for the downtown Boulder semi-LOS and NLOS paths. The free-space and 3GPP models represent a small subset of possible models; other path loss models exist and are being developed that could be used in the future to compare with the data. A multi-slope model would be better suited to predict the data observed from this measurement campaign.

9. ACKNOWLEDGEMENTS

The authors would like to thank the following individuals for their efforts in helping complete this work. Robert Johnk and Chriss Hammerschmidt provided invaluable advice and guidance on CW propagation measurement system design and calibration, performing measurements, and data analysis. Additional thanks go to Robert Johnk for his advice and assistance in performing antenna gain measurements using a vector network analyzer with time gating to remove reflections. Finally, special thanks go to Michael Cotton for his guidance and support during all phases of this effort. Without the assistance of these individuals, this work would not have been possible.

10. REFERENCES

[1] 3GPP TS 38.101-1 V16.9.0 (2021-09), 3rd Generation Partnership Project; Technical Specification Group Radio Access Network; NR; User Equipment (UE) radio transmission and reception; Part 1: Range 1 Standalone (Release 16).

[2] Frank H. Sanders, "Derivations of relationships among field strength, power in transmitter-receiver circuits and radiation hazard limits," NTIA Technical Memorandum TM-10-469, Jun. 2010, pp. 14-18. <https://www.its.ntia.gov/publications/2507.aspx>

[3] International Commission on Non-Ionizing Radio Protection (ICNIRP), "Guidelines for limiting exposure to electromagnetic fields (100 kHz to 300 GHz)", Health Physics, vol. 118, no. 5, pp. 483–524, May 2020.

[4] A.E. Paulson, "Precision Geolocation of Propagation Data Using GPS and Data Fusion," *Proceedings of the 2019 IEEE International Symposium on Electromagnetic Compatibility, Signal & Power Integrity (EMC+SIPI)*, New Orleans, LA, July 2019, pp. 469-474. <https://www.its.ntia.gov/publications/3229.aspx>

[5] E.B. Larsen, R.L. Ehret, D.G. Camell, and G.H. Koepke, "Calibration of antenna factor at a ground screen field site using an automatic network analyzer," in *Proc. of the 1989 IEEE National Symposium on EMC*, Denver, CO, May 23-25, 1989, pp. 19-24.

[6] D. Camell, R. T. Johnk, D. Novotny, and C. Grosvenor, "Free-space antenna factors through the use of time-domain signal processing," in *Proc. of the 2007 IEEE International Symposium on Electromagnetic Compatibility*, Honolulu, HI, Jul 9–13, 2007, pp. 1-5.

[7] Keysight Technologies, "PXA specifications guide (comprehensive reference data)," Keysight Technologies Manual Part Number N9030-90089, Edition 1, Jun. 2021, p.134.

[8] Keysight Technologies, "Noise figure measurement accuracy: the Y-factor method," Application Note 5952-3706E, Jan. 25, 2021.

[9] J.A. Wepman and G.A. Sanders, "Wideband man-made radio noise measurements in the VHF and low UHF bands," NTIA Report TR-11-478, Jul. 2011. <https://www.its.ntia.gov/publications/2553.aspx>

[10] U.S. Department of Commerce ITS Table Mountain Field Site and Radio Quiet Zone. <https://its.ntia.gov/research-topics/table-mountain/tm-home.aspx>

[11] Charles Karney (2021). geographiclib, MATLAB® Central™ File Exchange. <https://www.mathworks.com/matlabcentral/fileexchange/50605-geographiclib>, retrieved May 21, 2021.

[12] C.F.F. Karney, "Algorithms for geodesics," Journal of Geodesy, vol. 87, no. 1, Springer Science and Business Media LLC, June 2012, pp. 43-55. <https://doi.org/10.1007/s00190-012-0578-z>.

[13] R.T. Johnk, C.A. Hammerschmidt, and I. Stange, "A high-performance CW mobile channel sounder," *Proceedings of the 2017 IEEE International Symposium on Electromagnetic Compatibility and Signal/Power Integrity (EMCSI)*, Washington DC, 7-11 Aug. 2017, pp. 698–703. <https://www.its.ntia.gov/publications/3186.aspx>

[14] ITU-R Recommendation P.525-4 (08/2019), "Calculation of free-space attenuation," Recommendations of the ITU, Radiocommunication Sector. <https://www.itu.int/rec/R-REC-P.525/en>

[15] 3GPP TR 38.901 V16.1.0 (2019-12), 3rd Generation Partnership Project; Technical Specification Group Radio Access Network; Study on channel model for frequencies from 0.5 to 100 GHz (Release 16).

APPENDIX A: PROCESSED DATA FOR ADDITIONAL DOWNTOWN BOULDER NLOS PATHS

This Appendix includes the heat maps and the basic transmission gain G_b plots for the downtown Boulder NLOS paths that were not presented in the main body of the report (i.e., all downtown Boulder NLOS paths except the S3 Path and the first section of the E2 Path). Comments provided in the discussion of the NLOS paths presented in the main body of the report are generally applicable here. A few of the plots shown in this Appendix are deserving of some additional commentary. The heat map for the S2 Path shown in Figure A-3, shows an extra, unintended rectangular closed loop. This was caused by an erroneous turn made by the receiver during data collection that was corrected to complete the originally intended path. The corresponding G_b plot shown in Figure A-4 appears as if it splits into two separate traces at distances greater than 600m. This is caused by signals being received at the same distance from the transmitter but in different geographical areas along the path (one LOS and the other NLOS) resulting in different G_b values for the same distance.

This same behavior, of the G_b appearing as two separate traces for the same distance, is seen in varying degrees in NLOS Paths S4, S5, S7, N3, and N6 as shown in Figures A-6, A-8, A-12, A-18, and A-24, respectively.

The NLOS S7 Path represents an anomalous case. Figures A-11 and A-12 show the heat map and G_b for the NLOS S7 Path, respectively. Comparing Figure A-11 to Figure 18 (the heat map for the LOS1 Path) shows that the NLOS S7 Path is the same as the LOS1 Path out to a distance of about 2775 m when the receiver turns south off Pearl St. onto 30th St.[14] It is also clear comparing these figures that the received signal power was greater for the NLOS S7 Path than the LOS1 Path after the turn off Walnut St. Figure A-12 shows that the G_b is very similar to that of the LOS1 Path up to a distance of just over 1850 m. However, at about 1850 m, when the receiver turns north off Walnut St., to about 2925 m, the G_b does not appear to decrease noticeably with distance.

Of note is that the received signal power is roughly 15 dB greater than what was seen along the same path over these same distances for the LOS1 Path. While it is not known exactly why this occurred, recall that the NLOS S7 Path was the only path where light rain was experienced. While it is counter-intuitive that the received signal power would increase when measuring in light rain conditions as compared to dry conditions, it is the only difference between the two measurement scenarios that could be identified. It is also possible, although highly unlikely, that an interfering signal was present that could be detected by the receiver at the time the measurement was taken. At distances farther than 2925 m, the G_b becomes a little harder to interpret since it appears as if it splits into two separate traces. Again, this is caused by signals being received at the same distance from the transmitter but in different geographical areas along the path, resulting in different G_b values for the same distance.

[14] Note that Figure A-11 shows that the receiver path actually extended east of 30th St. along Pearl St. This occurred due to an unintended, missed turn from Pearl St. south onto 30th St. during data collection. A U-turn was made by the receiver to complete the intended path.

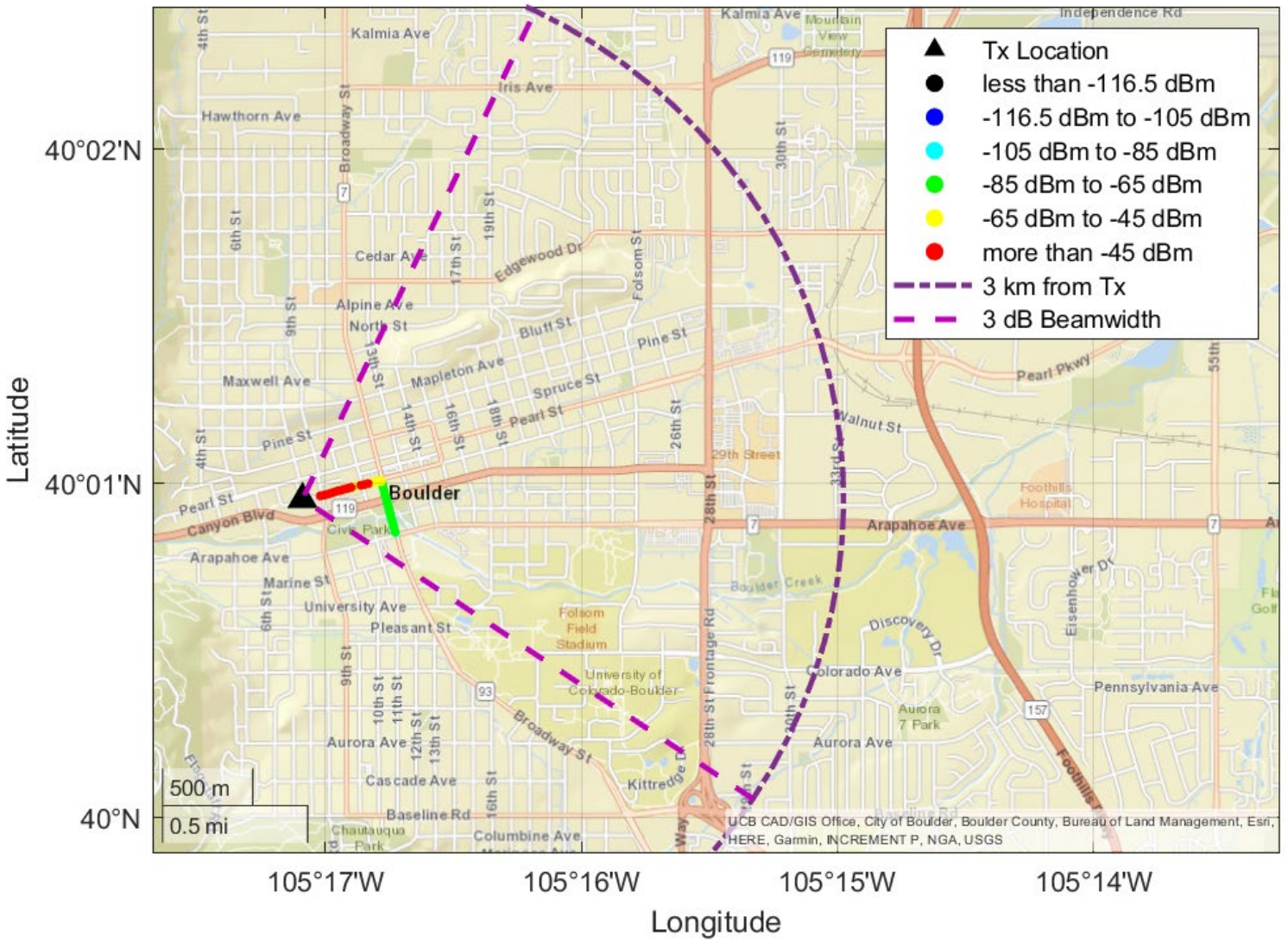

Figure A-1. Mean received signal power as a function of receiver location for the NLOS S1 Path in downtown Boulder (mean receiver noise power = -126.5 dBm).

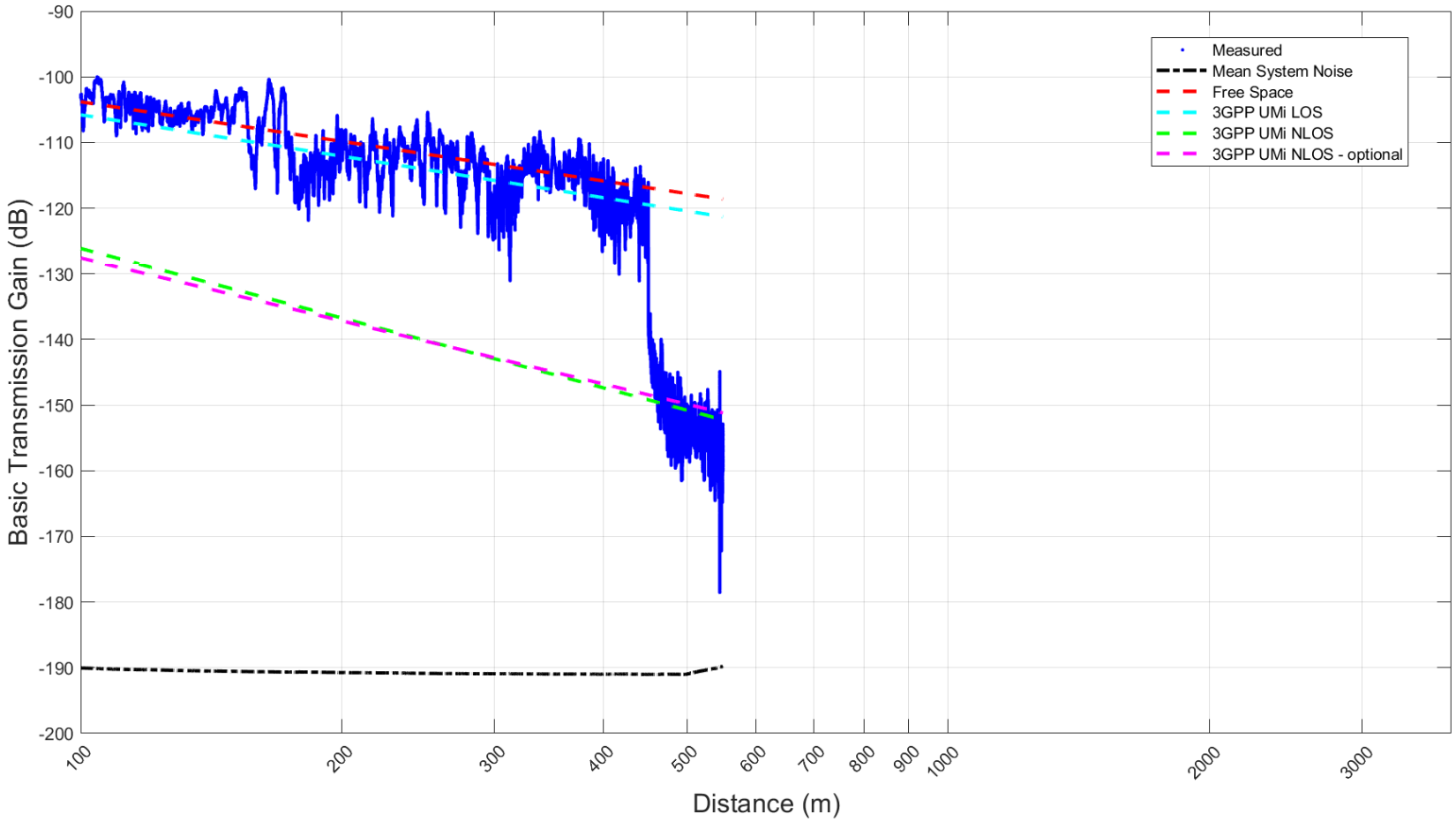

Figure A-2. G_b as a function of distance between the transmitter and receiver for the NLOS S1 Path in downtown Boulder.

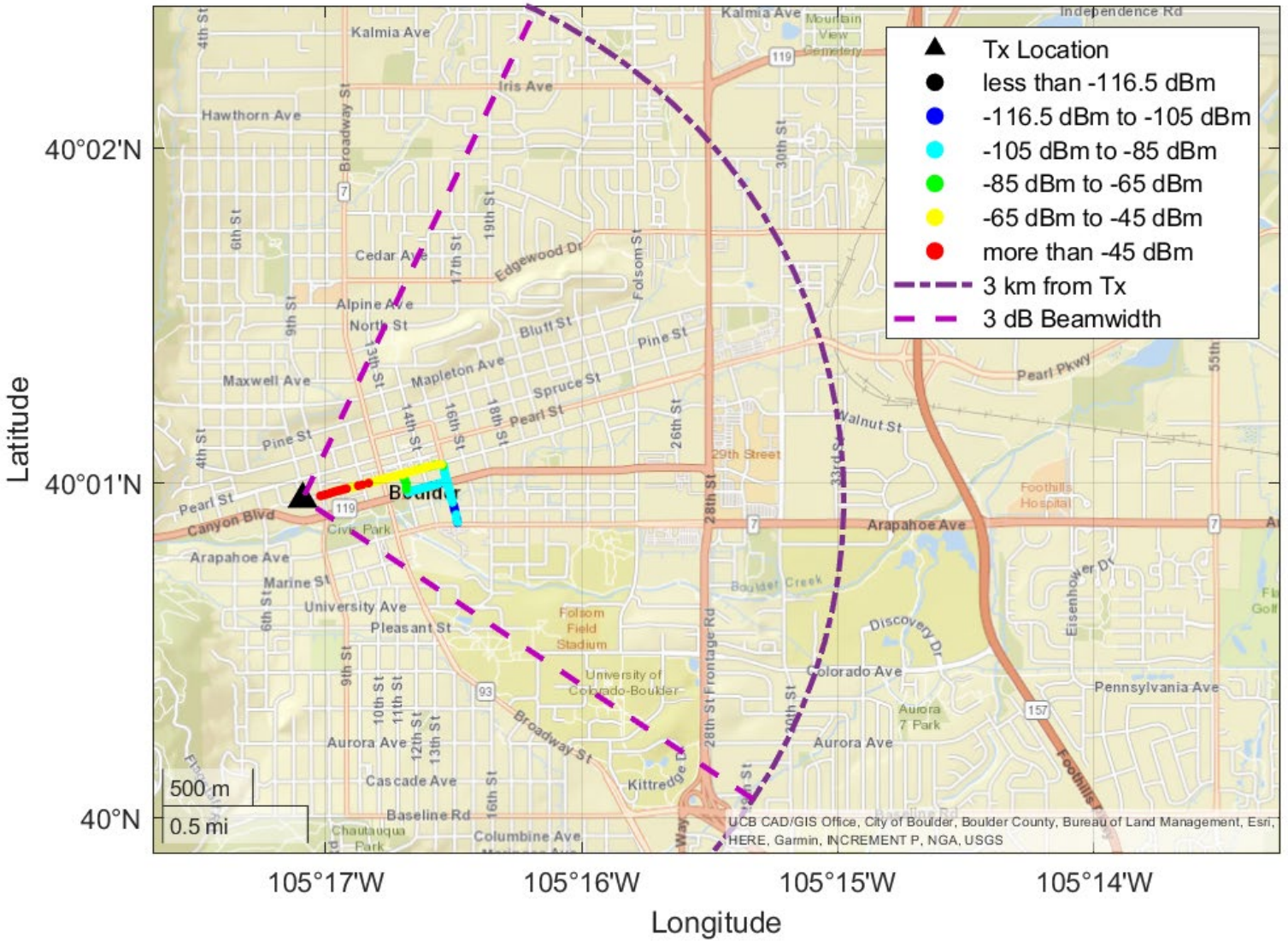

Figure A-3. Mean received signal power as a function of receiver location for the NLOS S2 Path in downtown Boulder (mean receiver noise power = -126.5 dBm).

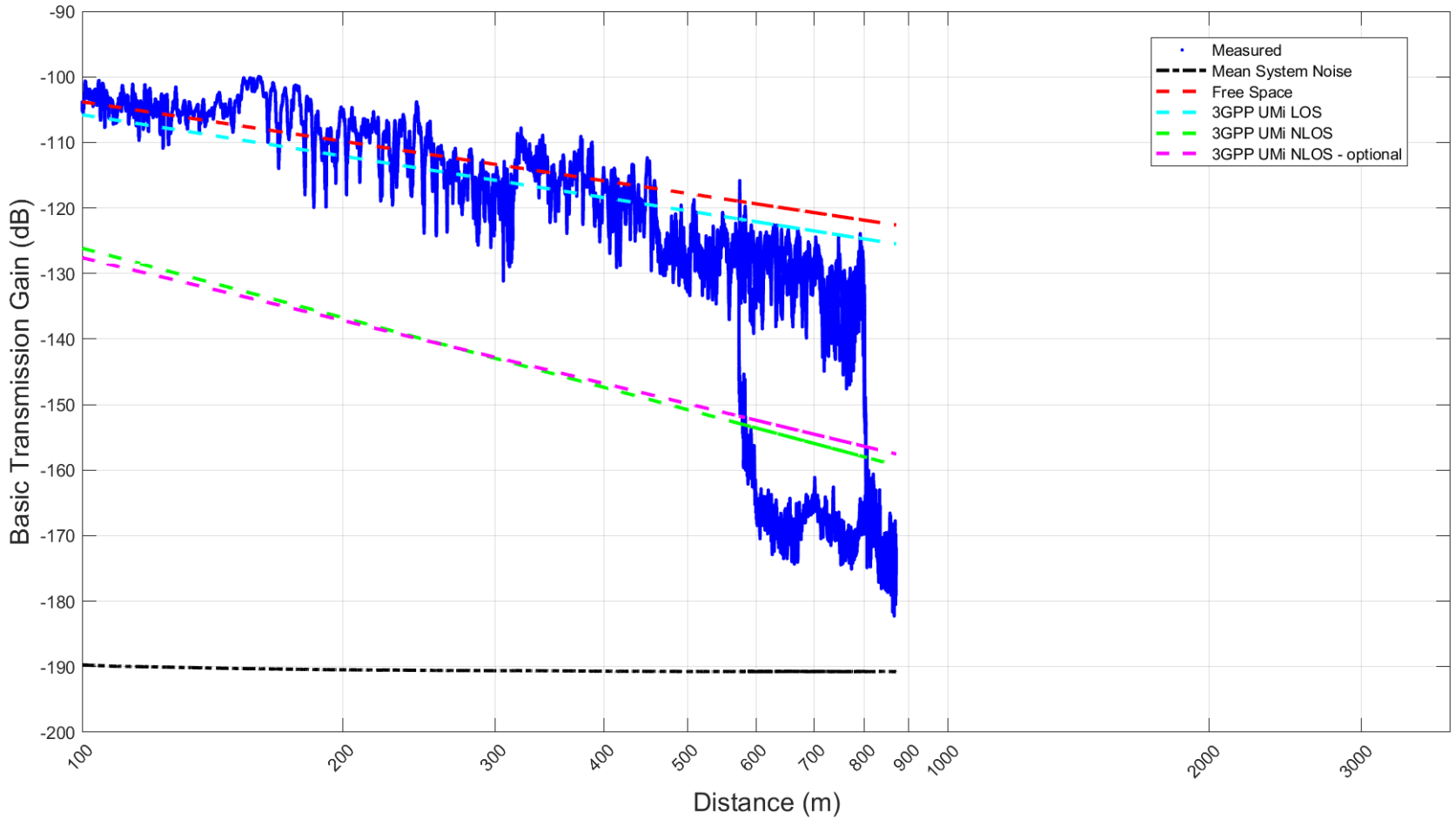

Figure A-4. G_b as a function of distance between the transmitter and receiver for the NLOS S2 Path in downtown Boulder.

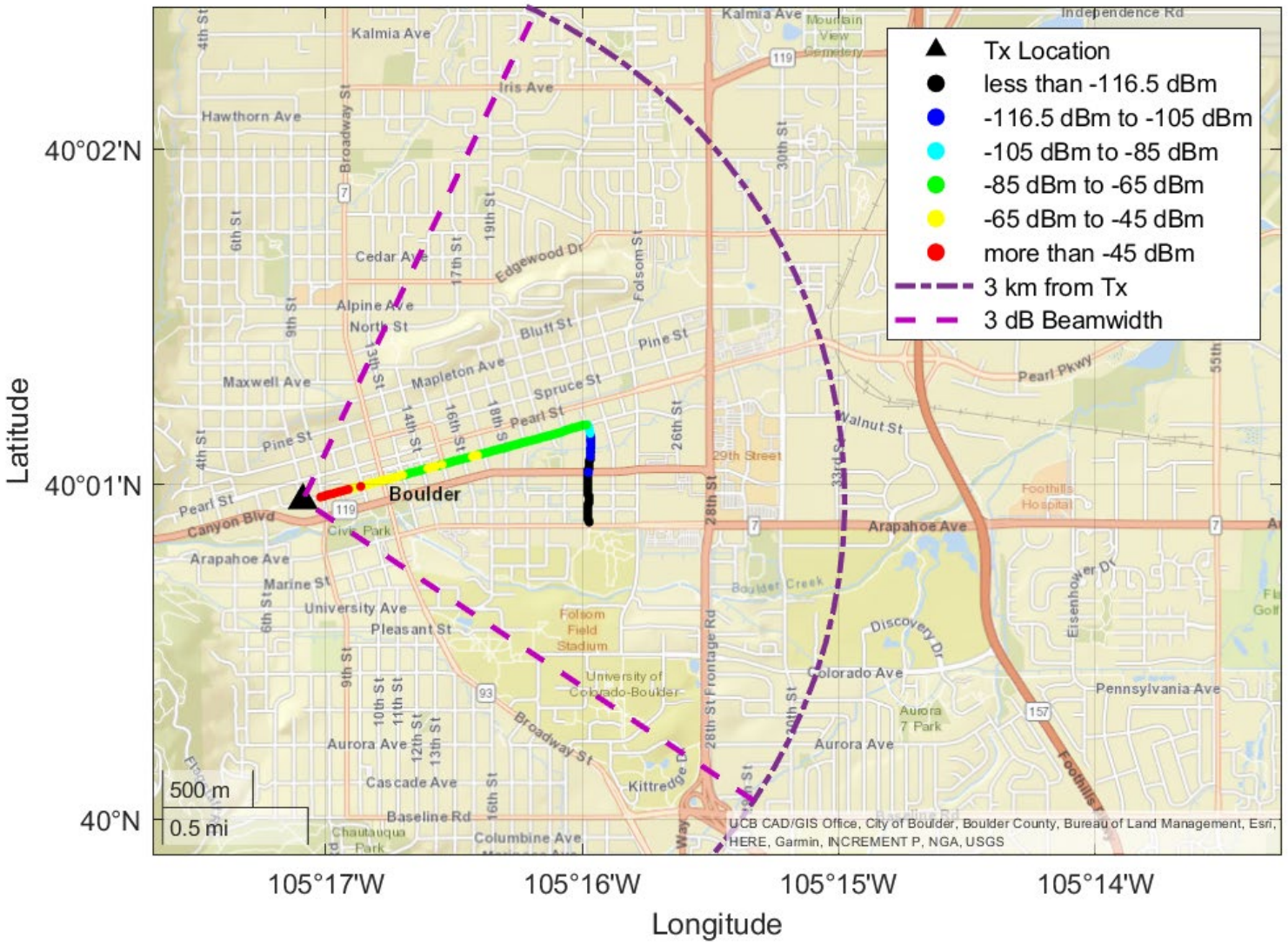

Figure A-5. Mean received signal power as a function of receiver location for the NLOS S4 Path in downtown Boulder (mean receiver noise power = -126.5 dBm).

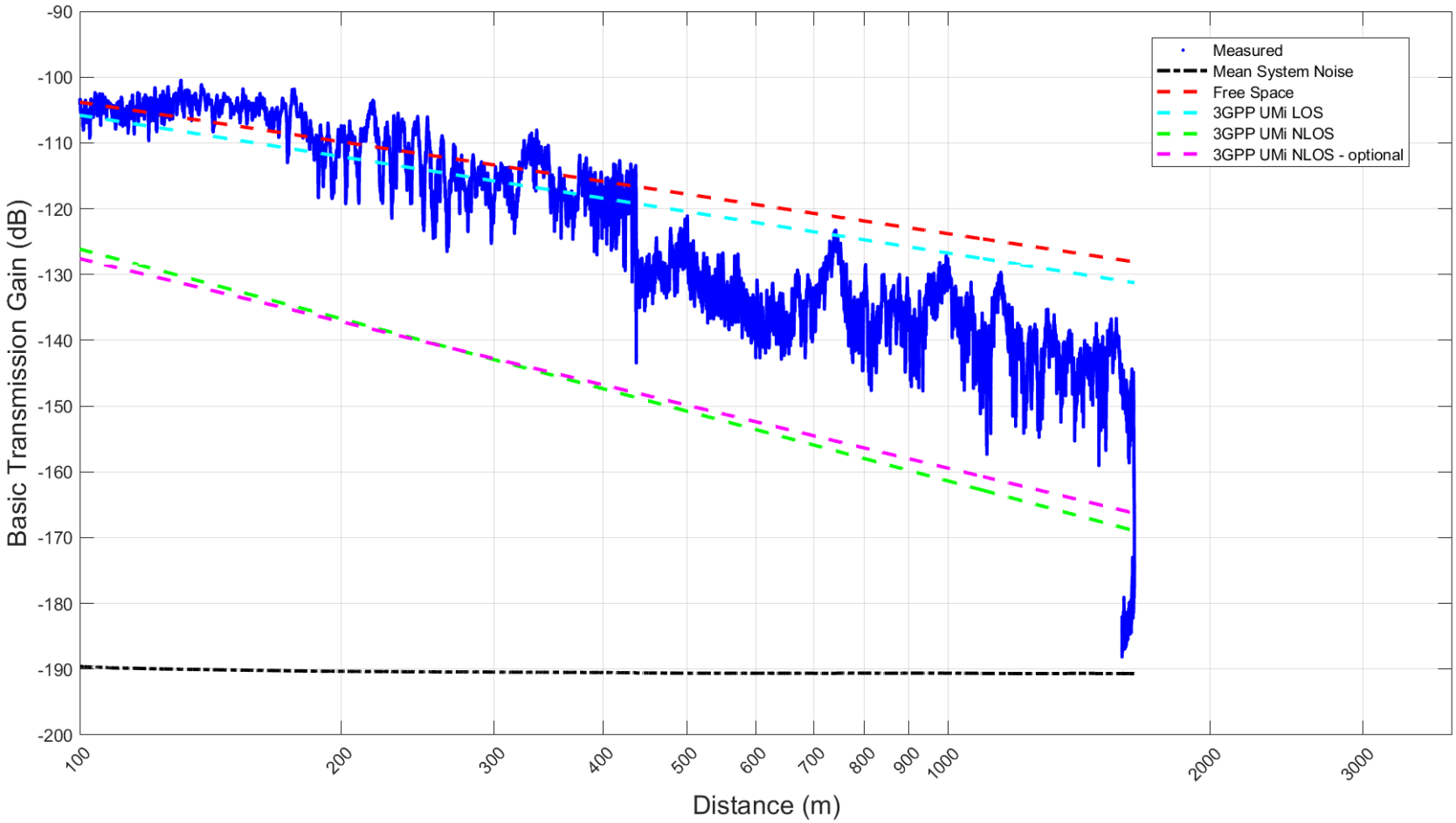

Figure A-6. G_b as a function of distance between the transmitter and receiver for the NLOS S4 Path in downtown Boulder.

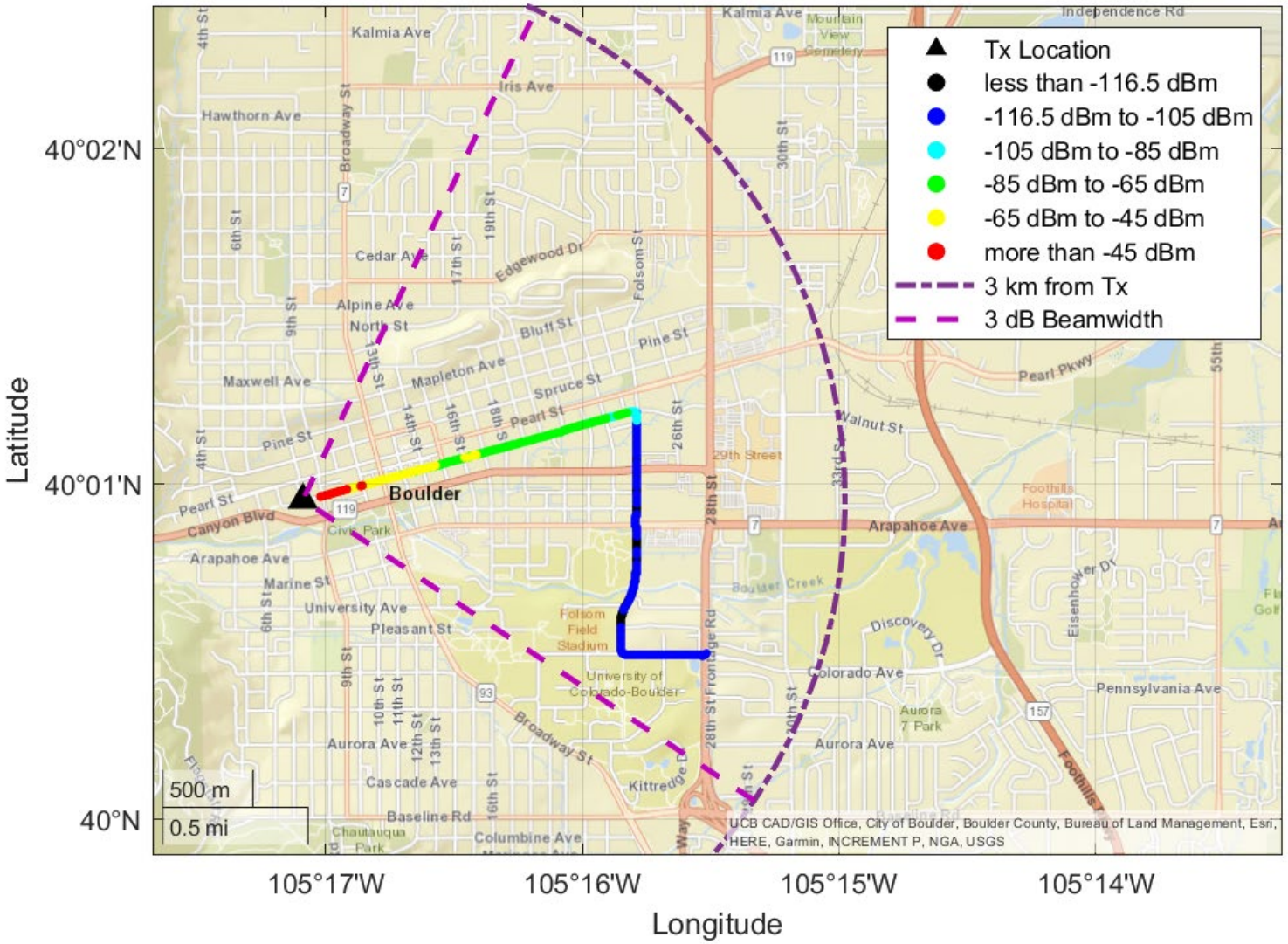

Figure A-7. Mean received signal power as a function of receiver location for the NLOS S5 Path in downtown Boulder (mean receiver noise power = -126.5 dBm).

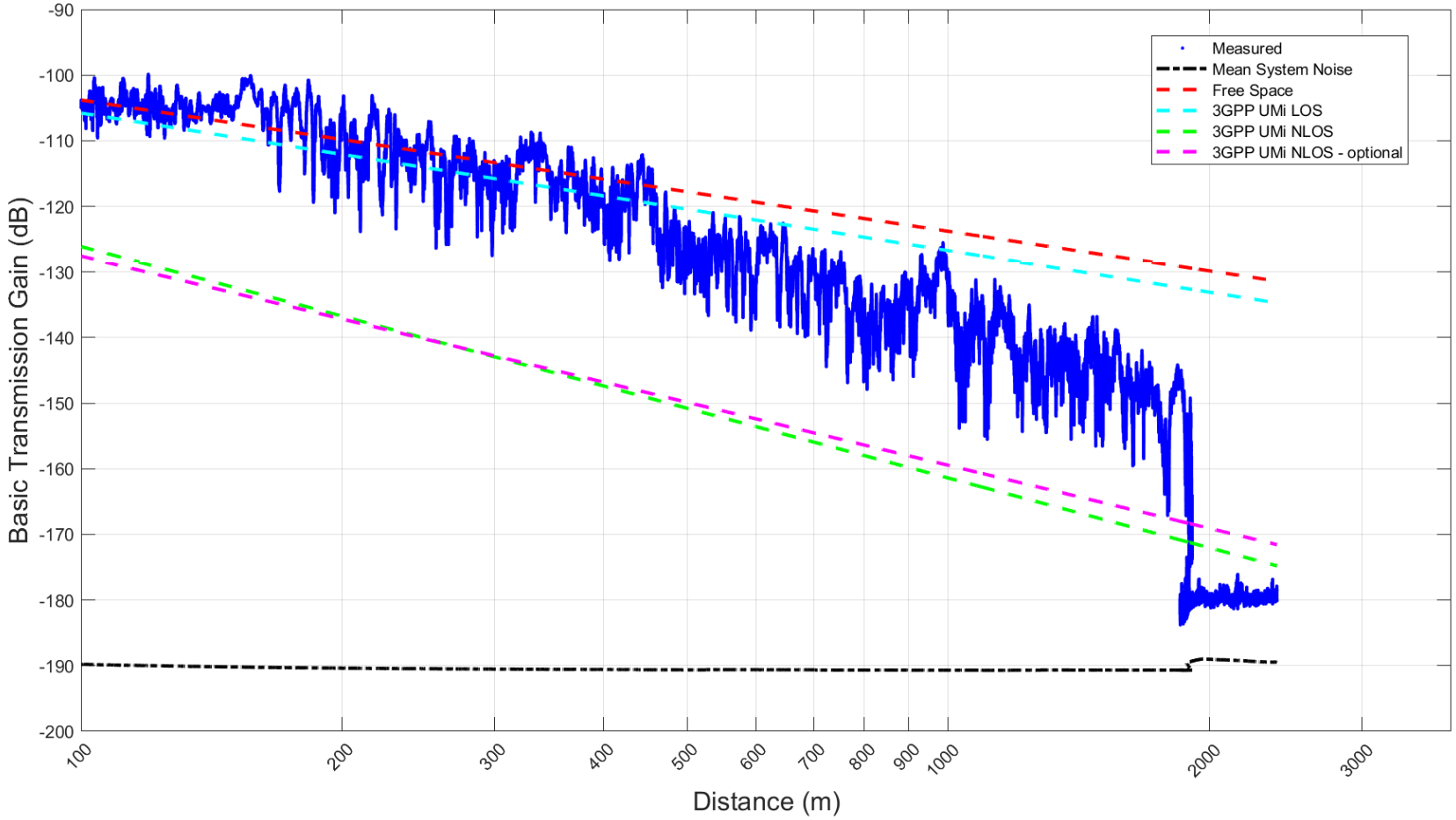

Figure A-8. G_b as a function of distance between the transmitter and receiver for the NLOS S5 Path in downtown Boulder.

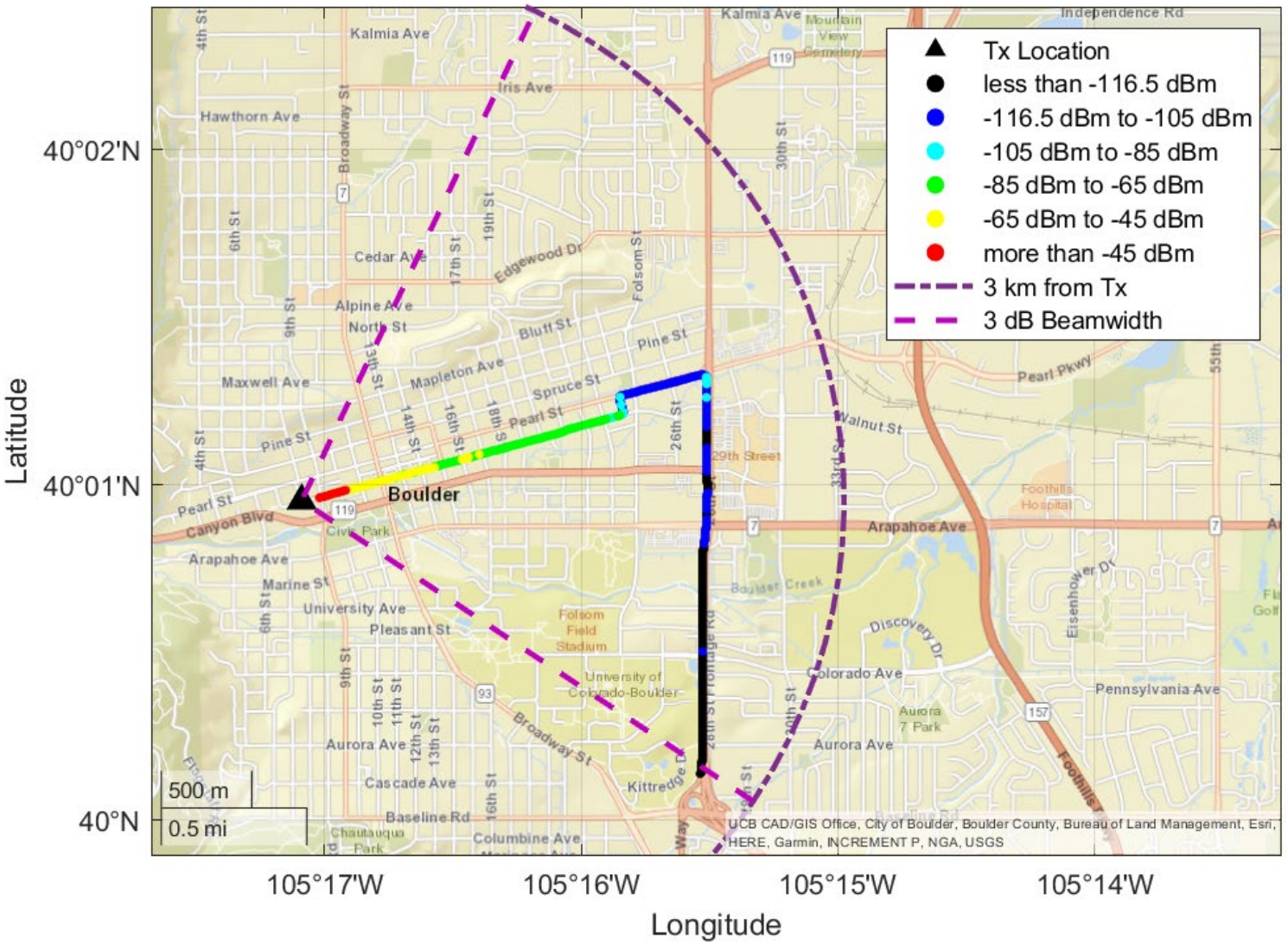

Figure A-9. Mean received signal power as a function of receiver location for the NLOS S6 Path in downtown Boulder (mean receiver noise power = -126.5 dBm).

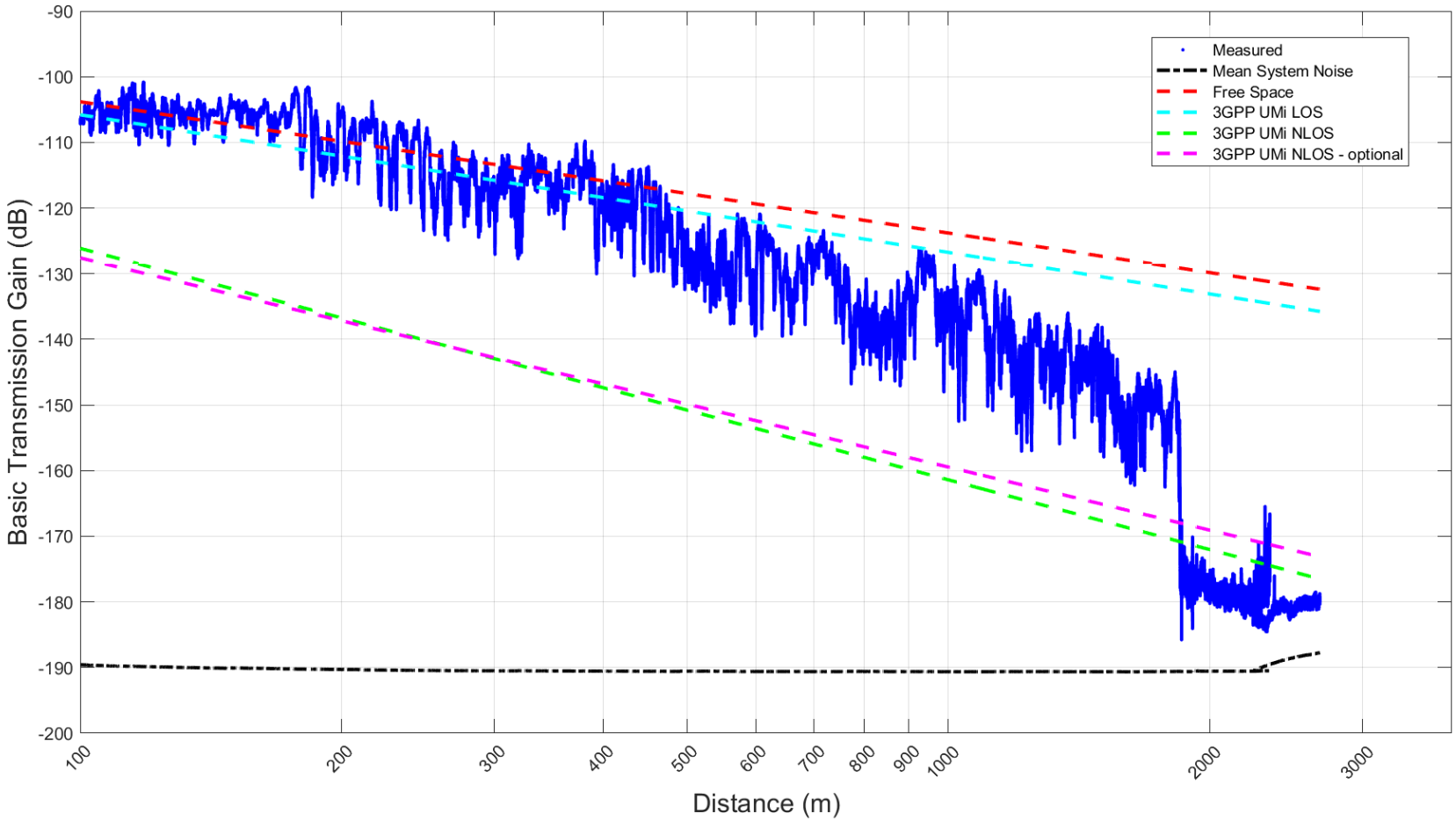

Figure A-10. G_b as a function of distance between the transmitter and receiver for the NLOS S6 Path in downtown Boulder.

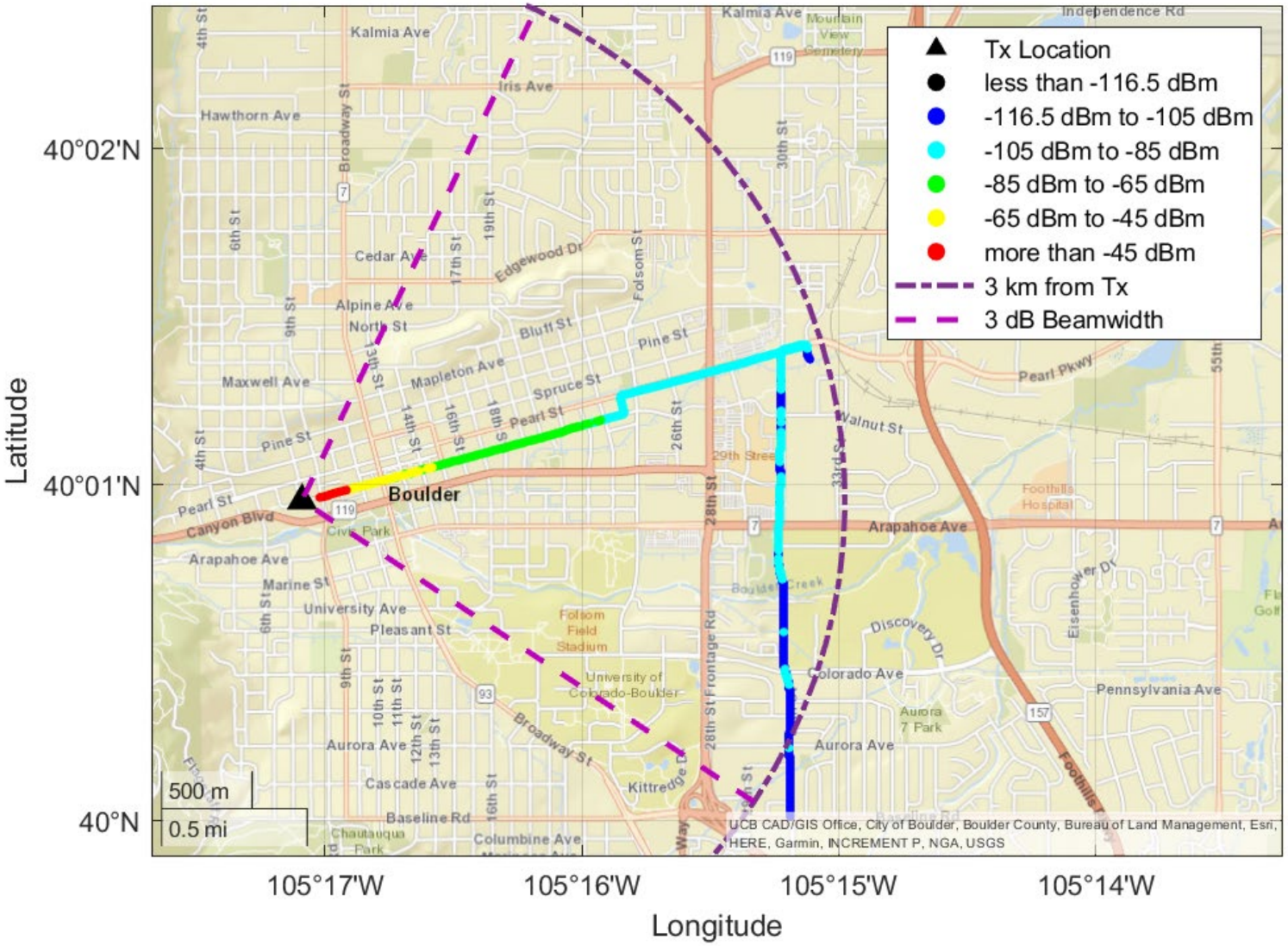

Figure A-11. Mean received signal power as a function of receiver location for the NLOS S7 Path in downtown Boulder (mean receiver noise power = -126.5 dBm).

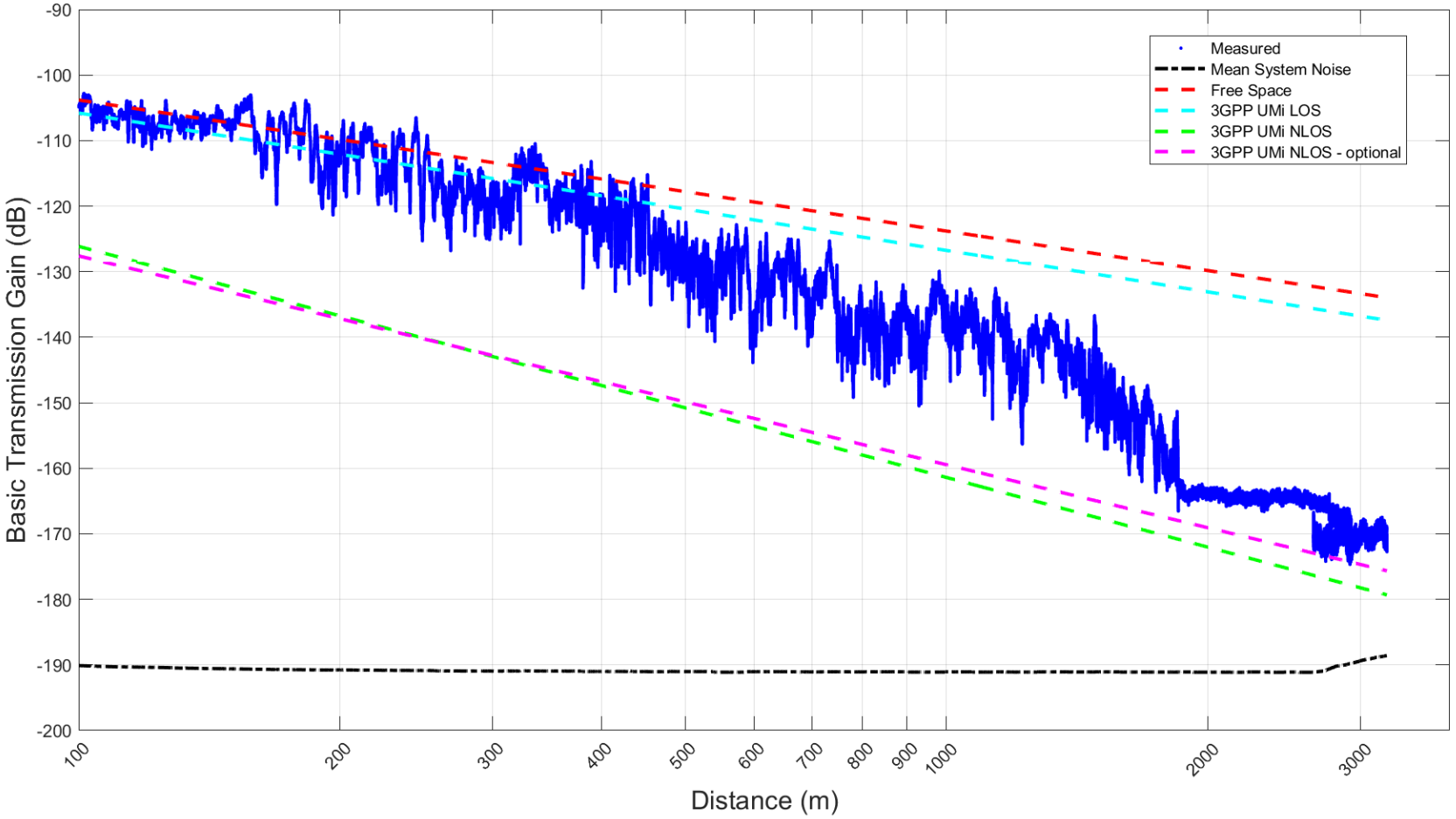

Figure A-12. G_b as a function of distance between the transmitter and receiver for the NLOS S7 Path in downtown Boulder.

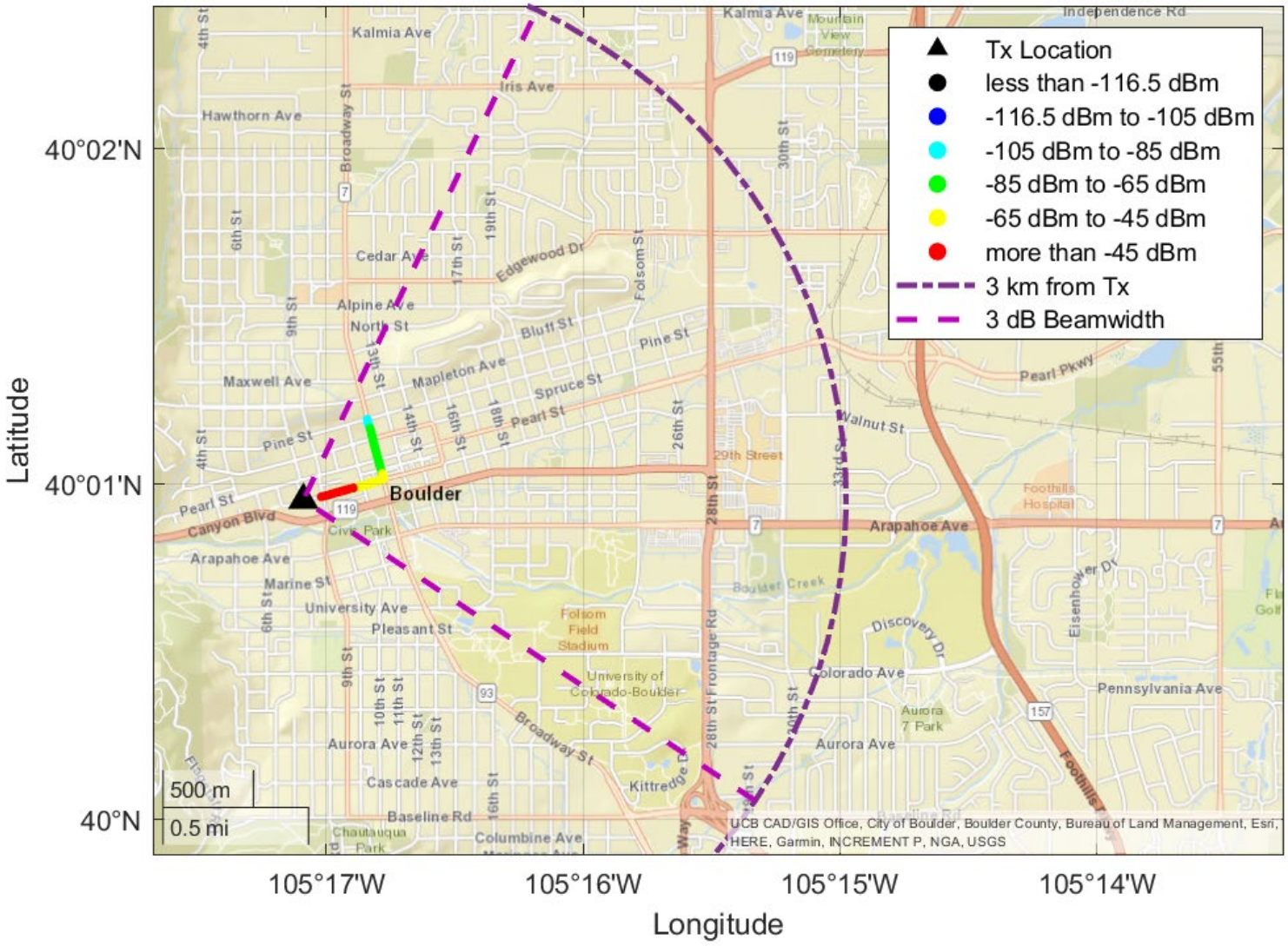

Figure A-13. Mean received signal power as a function of receiver location for the NLOS N1 Path in downtown Boulder (mean receiver noise power = -126.5 dBm).

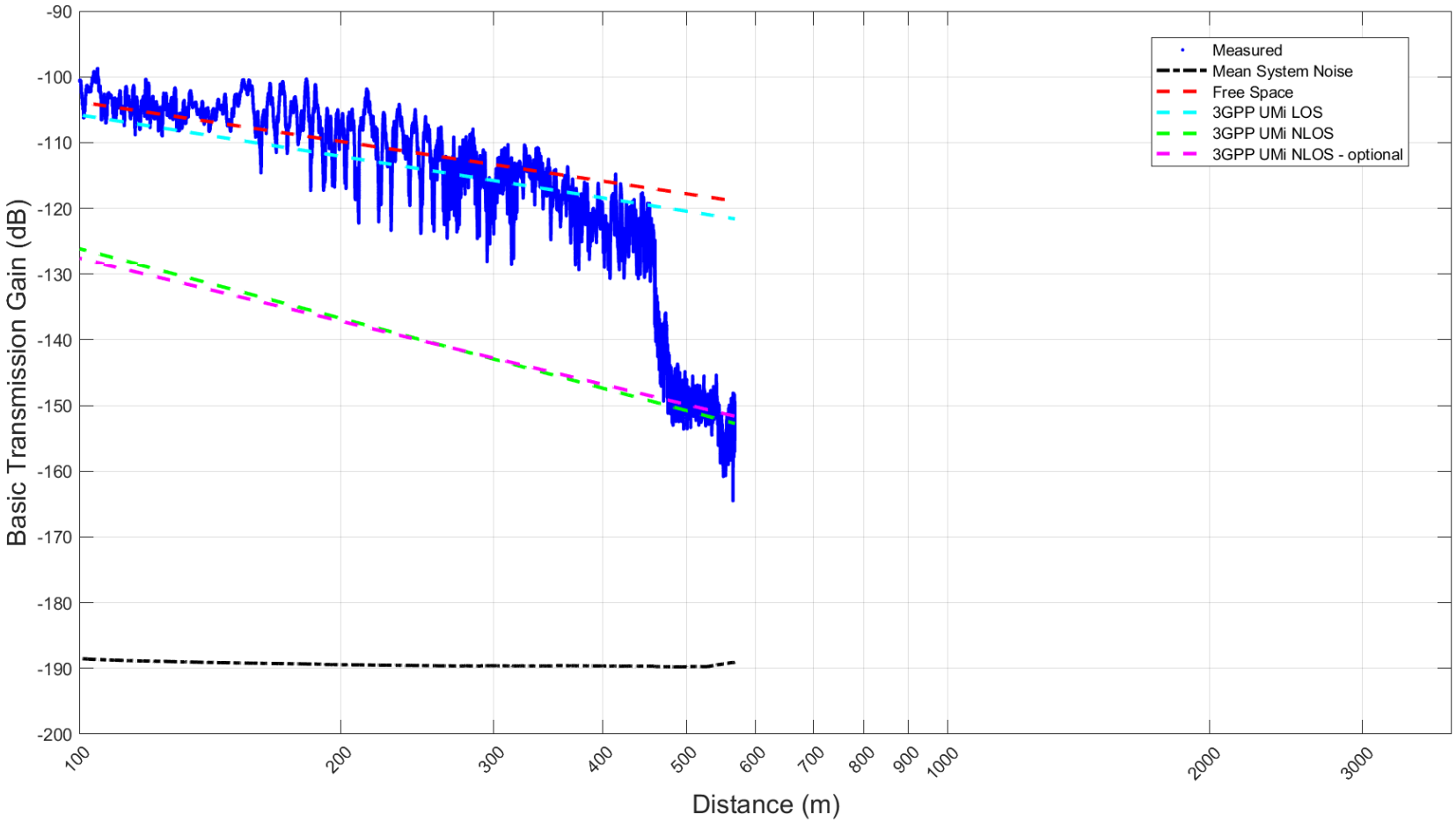

Figure A-14. G_b as a function of distance between the transmitter and receiver for the NLOS N1 Path in downtown Boulder.

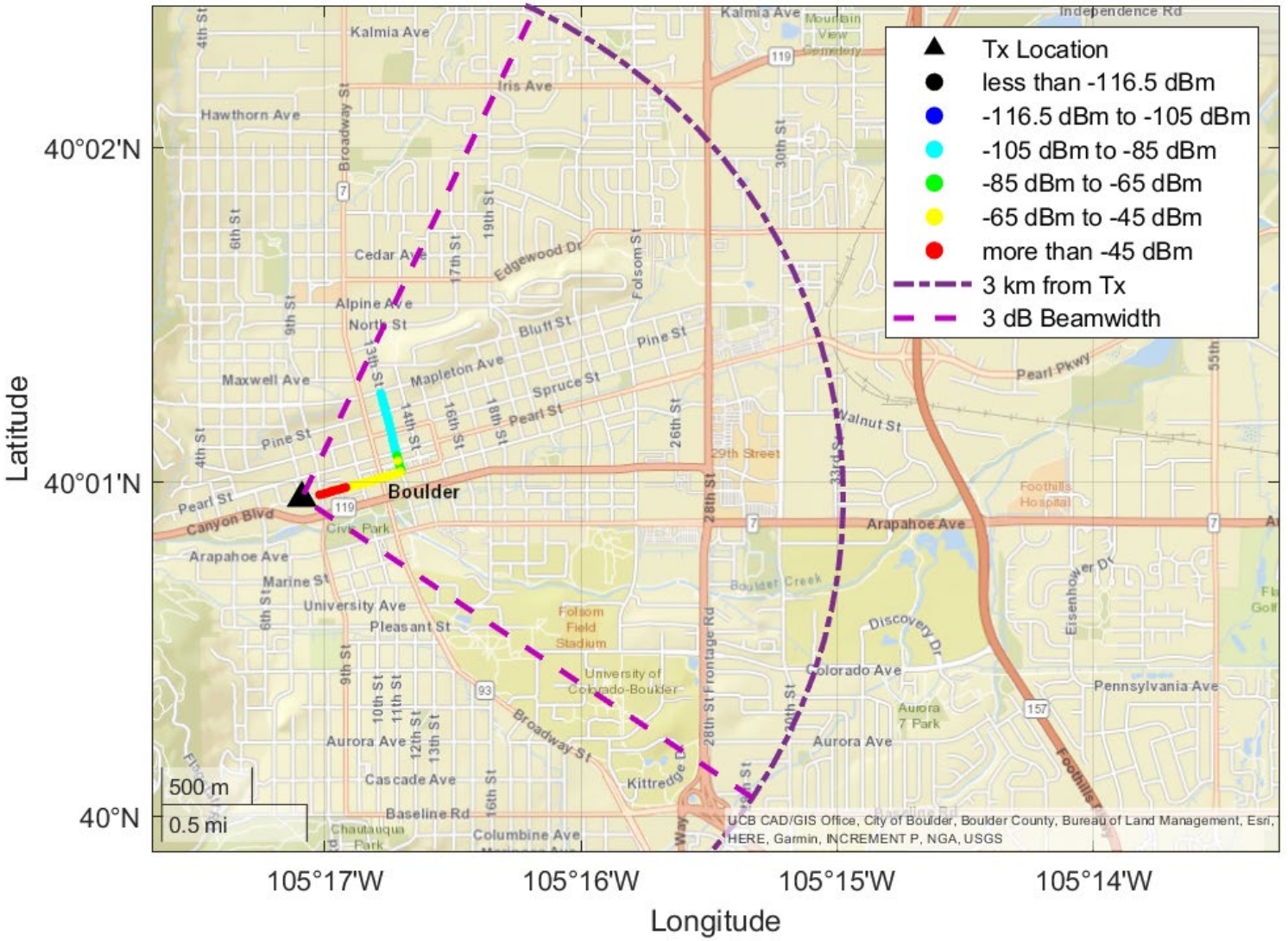

Figure A-15. Mean received signal power as a function of receiver location for the NLOS N2 Path in downtown Boulder (mean receiver noise power = -126.5 dBm).

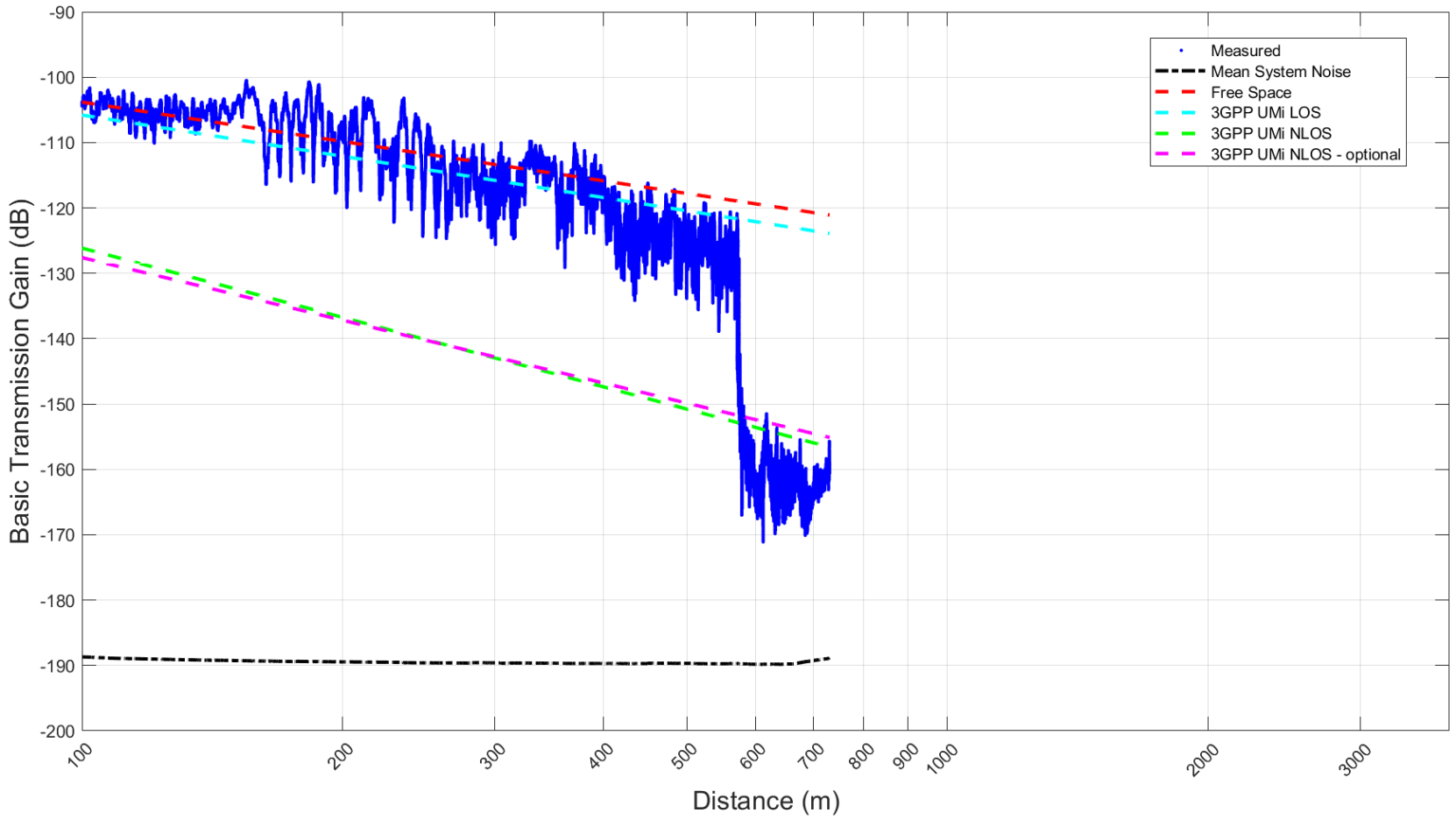

Figure A-16. G_b as a function of distance between the transmitter and receiver for the NLOS N2 Path in downtown Boulder.

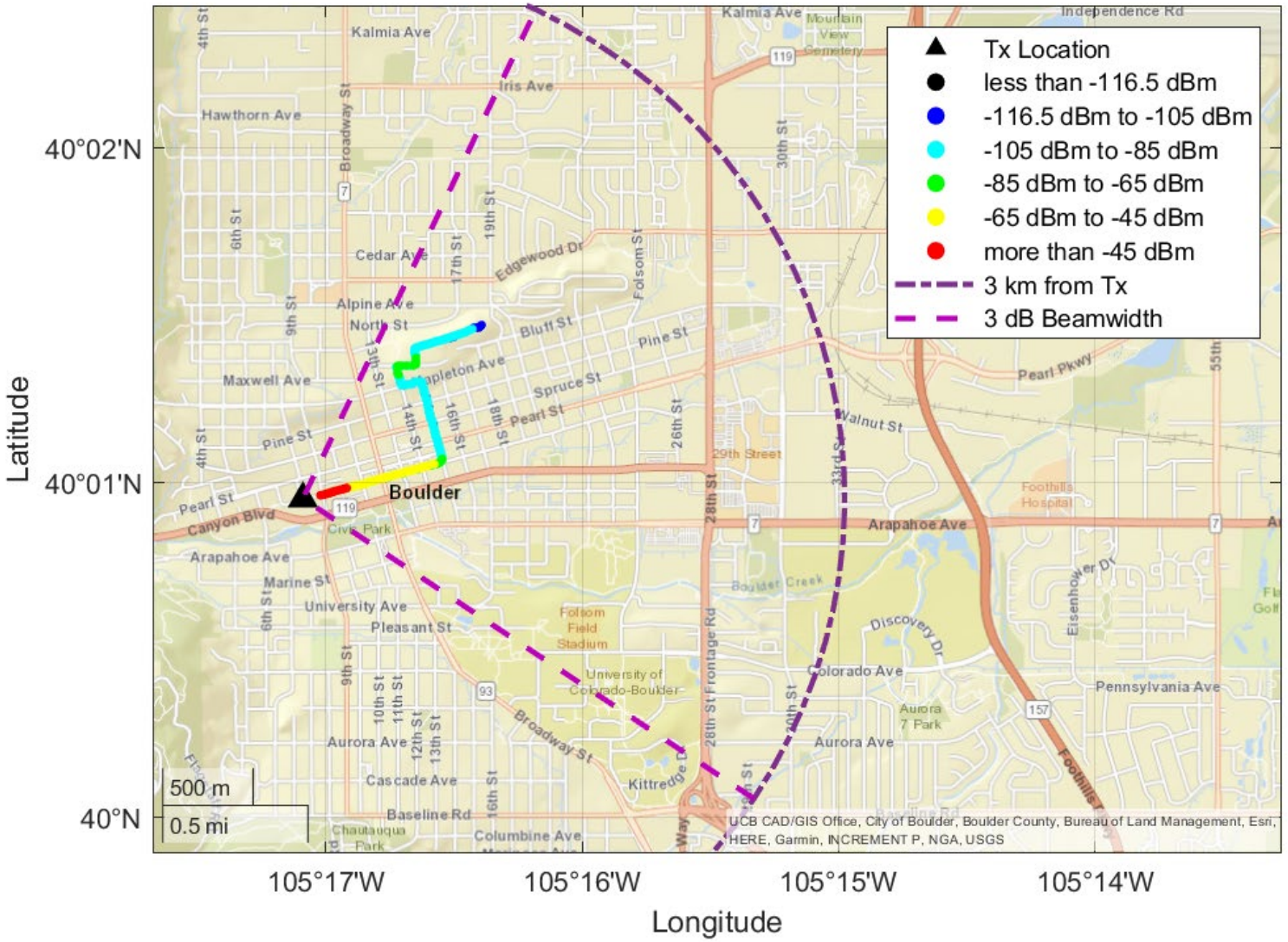

Figure A-17. Mean received signal power as a function of receiver location for the NLOS N3 Path in downtown Boulder (mean receiver noise power = -126.5 dBm).

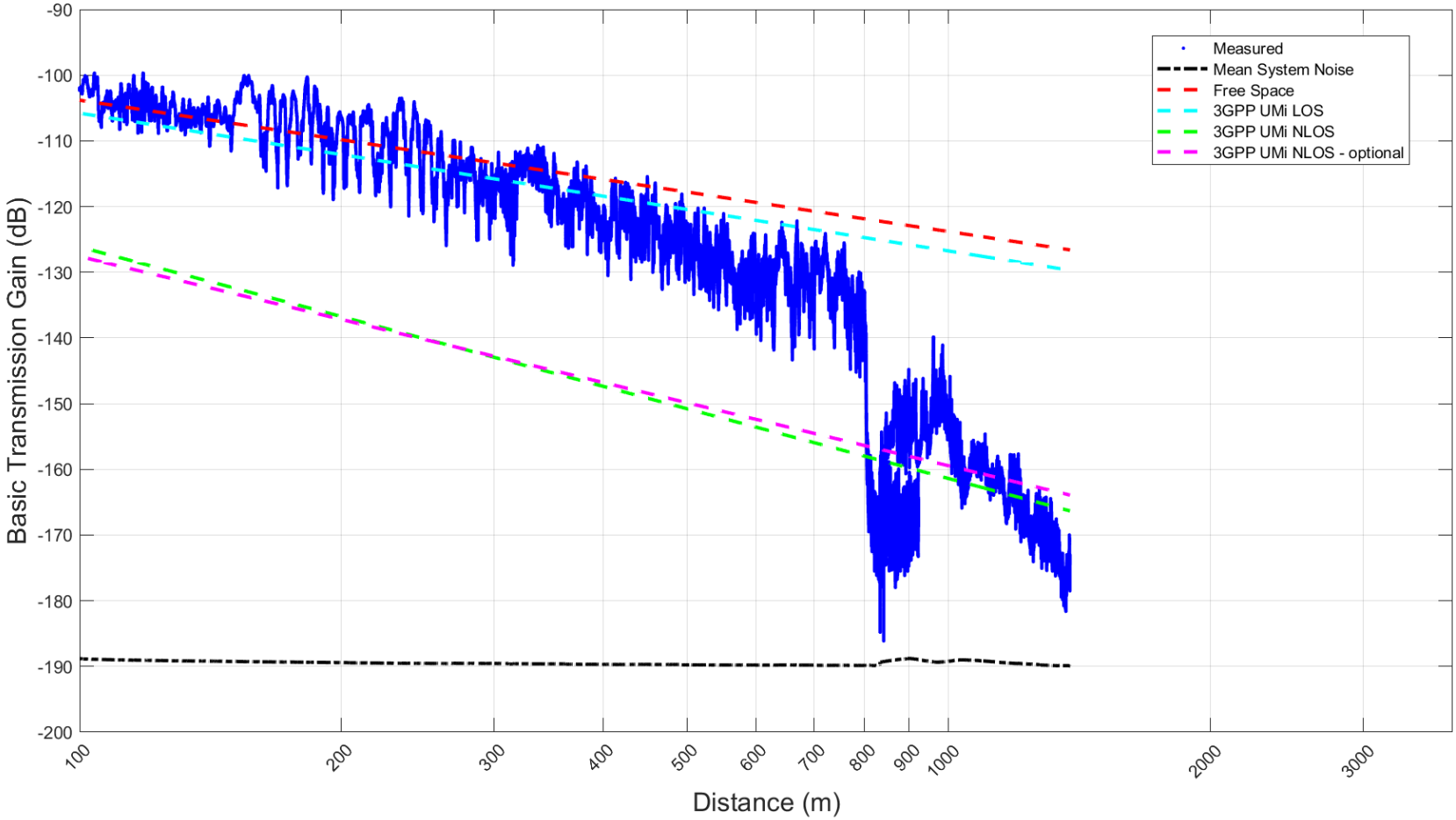

Figure A-18. G_b as a function of distance between the transmitter and receiver for the NLOS N3 Path in downtown Boulder.

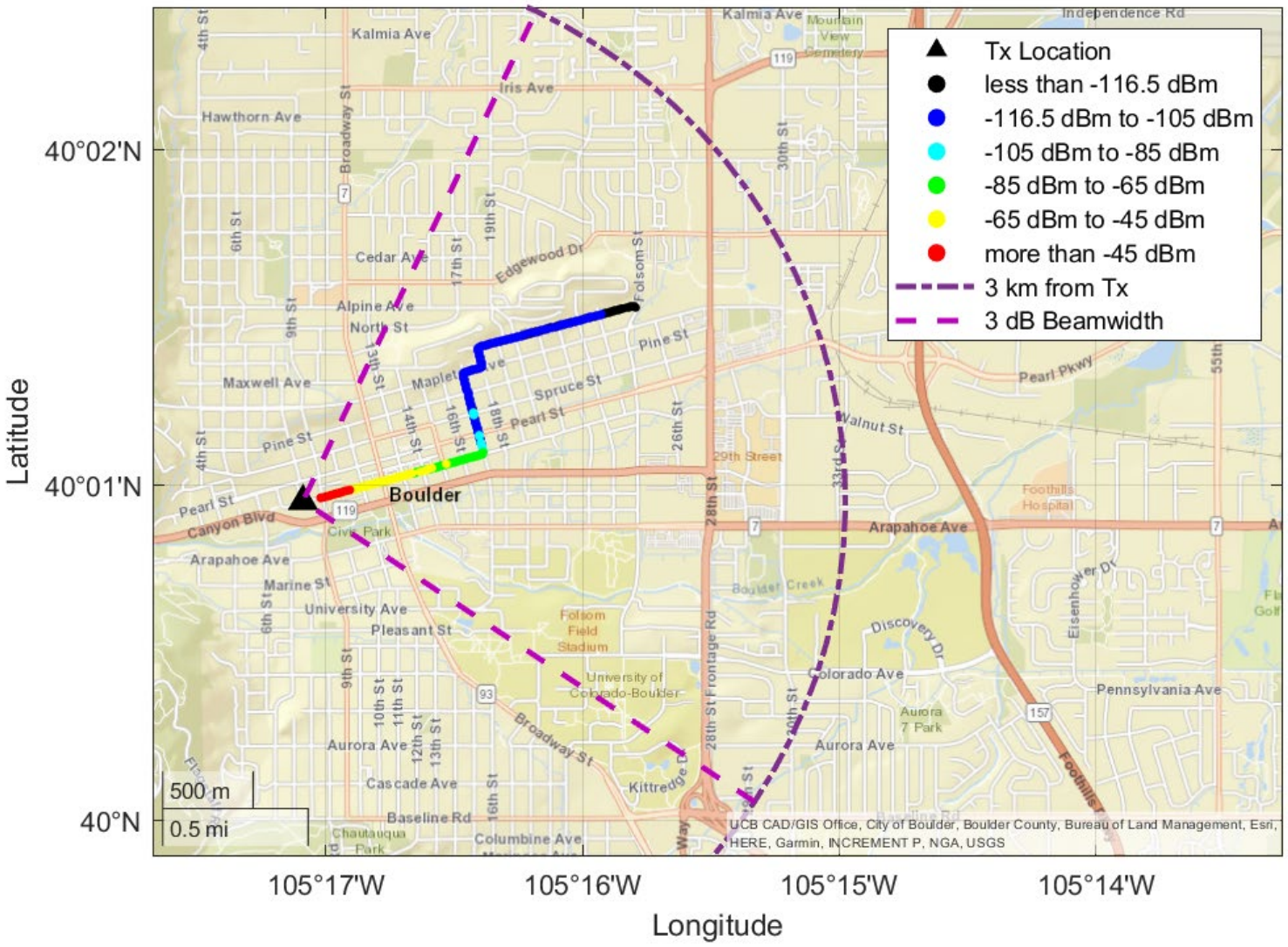

Figure A-19. Mean received signal power as a function of receiver location for the NLOS N4 Path in downtown Boulder (mean receiver noise power = -126.5 dBm).

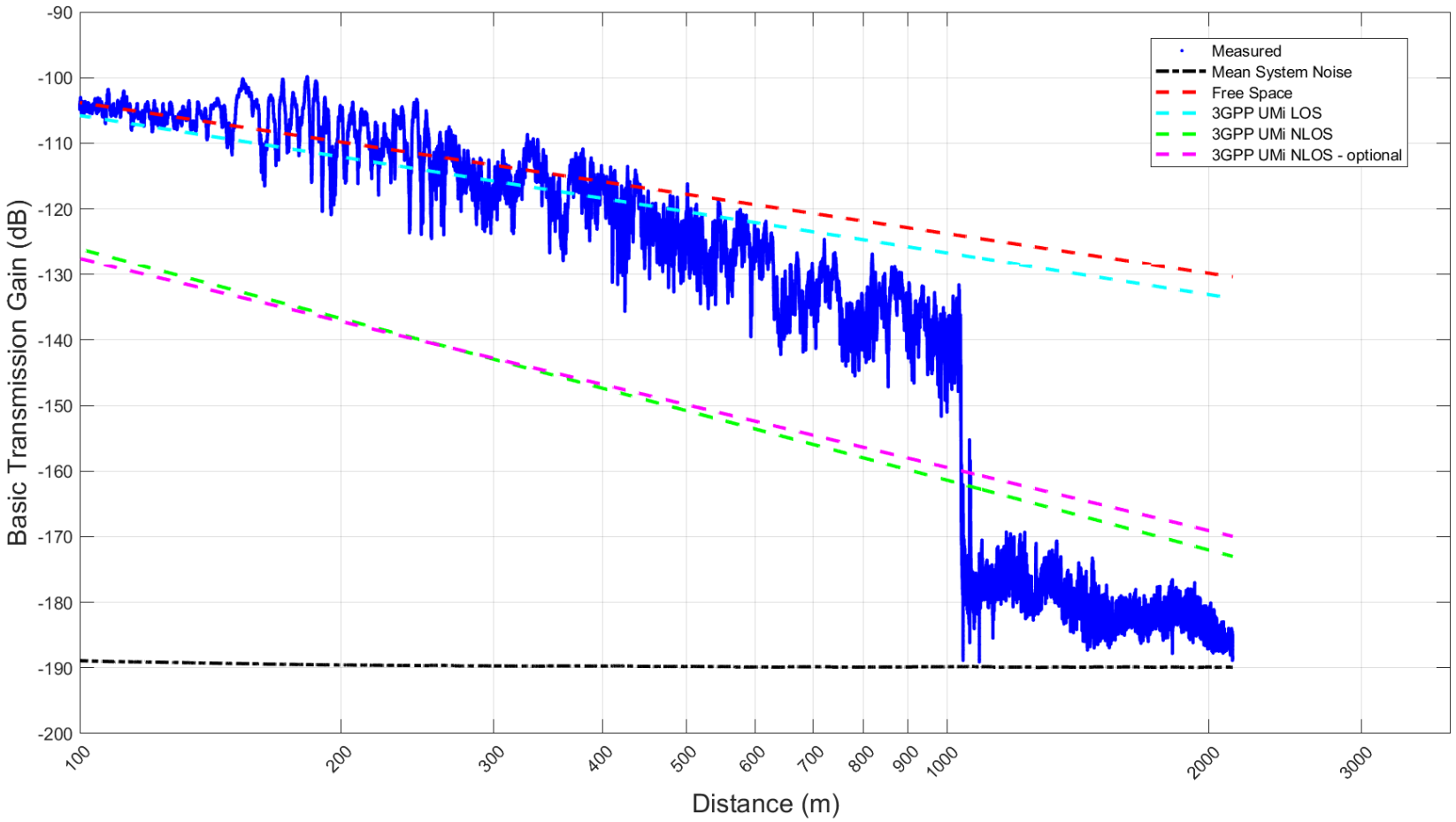

Figure A-20. G_b as a function of distance between the transmitter and receiver for the NLOS N4 Path in downtown Boulder.

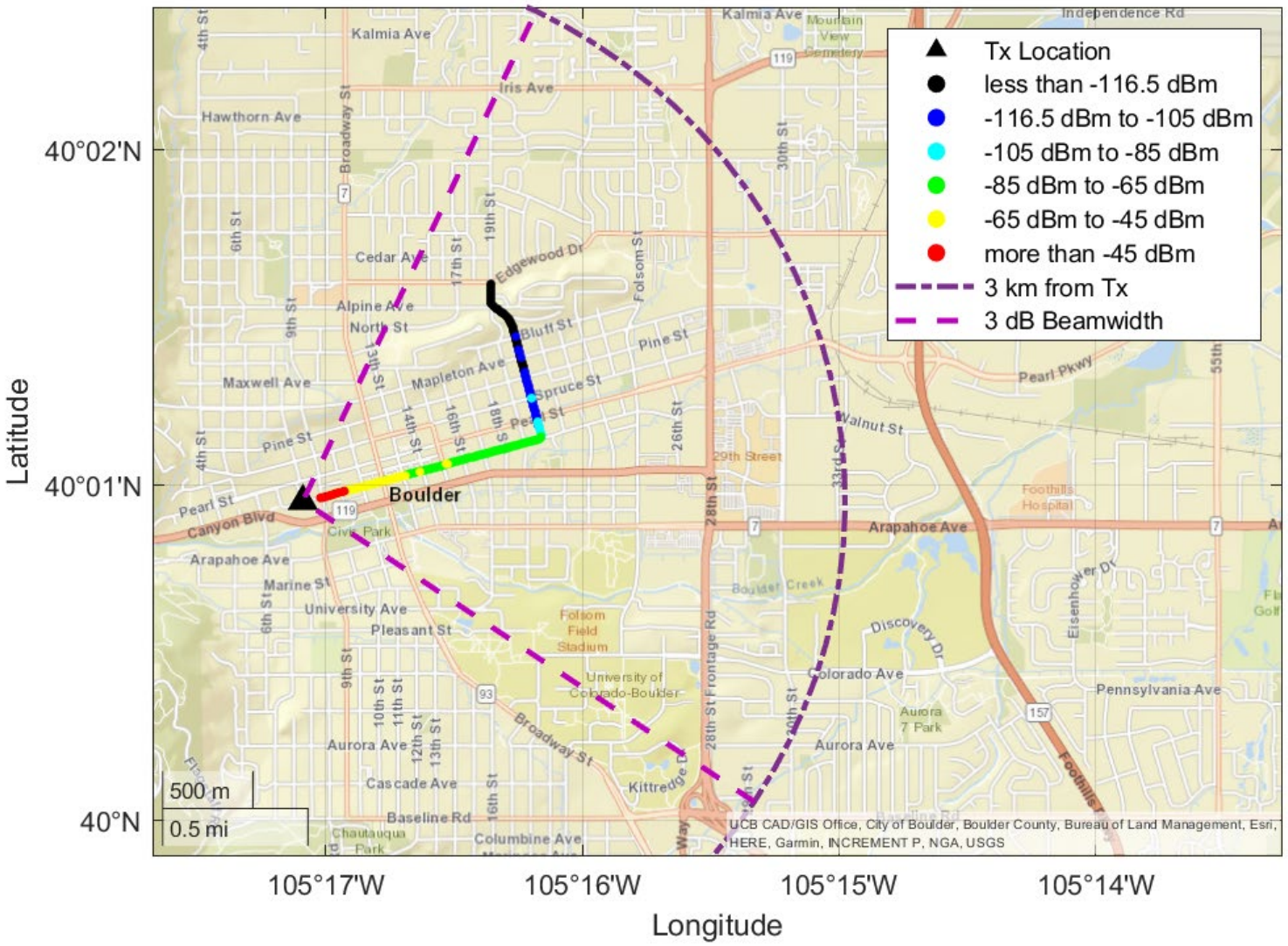

Figure A-21. Mean received signal power as a function of receiver location for the NLOS N5 Path in downtown Boulder (mean receiver noise power = -126.5 dBm).

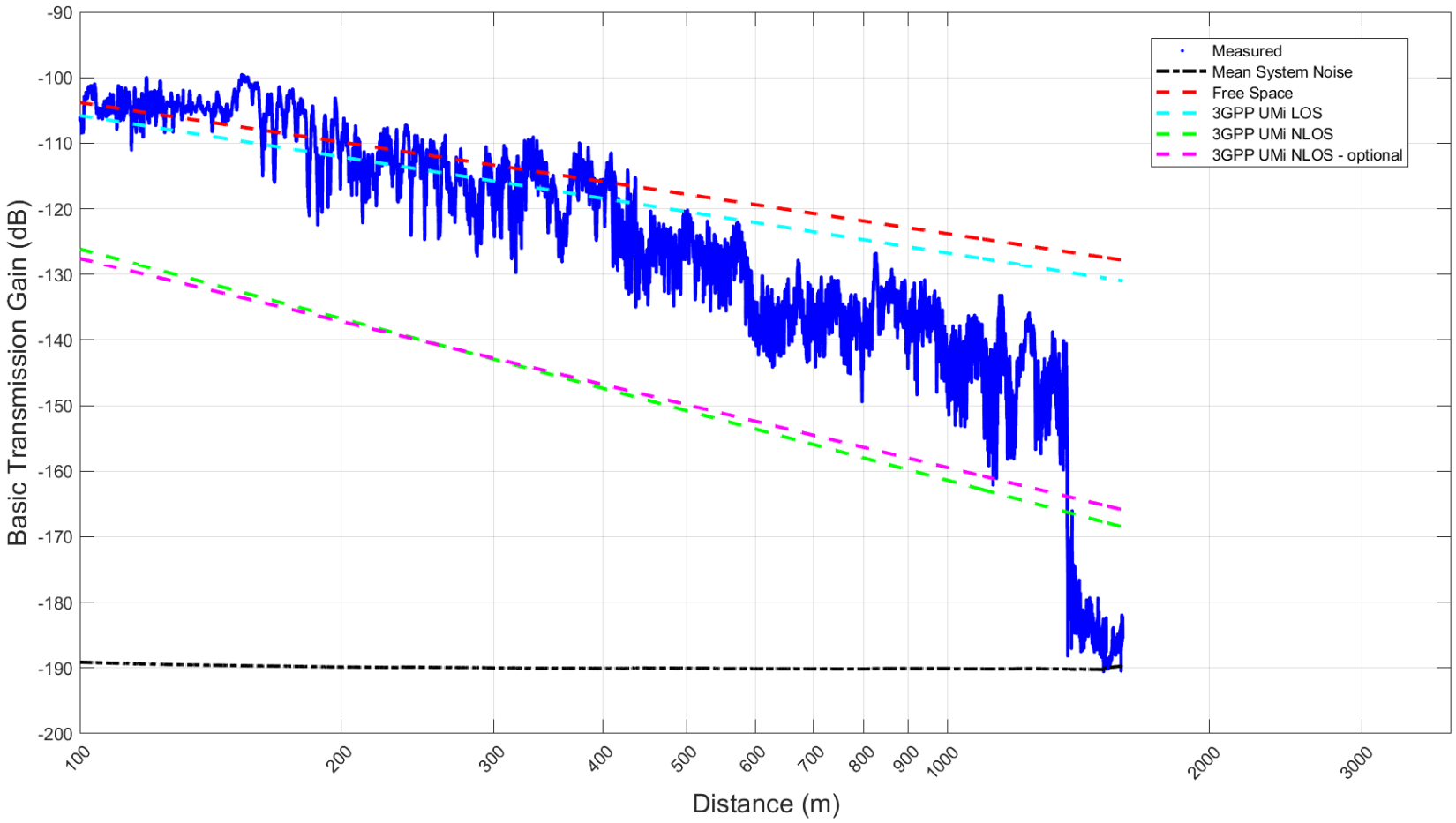

Figure A-22. G_b as a function of distance between the transmitter and receiver for the NLOS N5 Path in downtown Boulder.

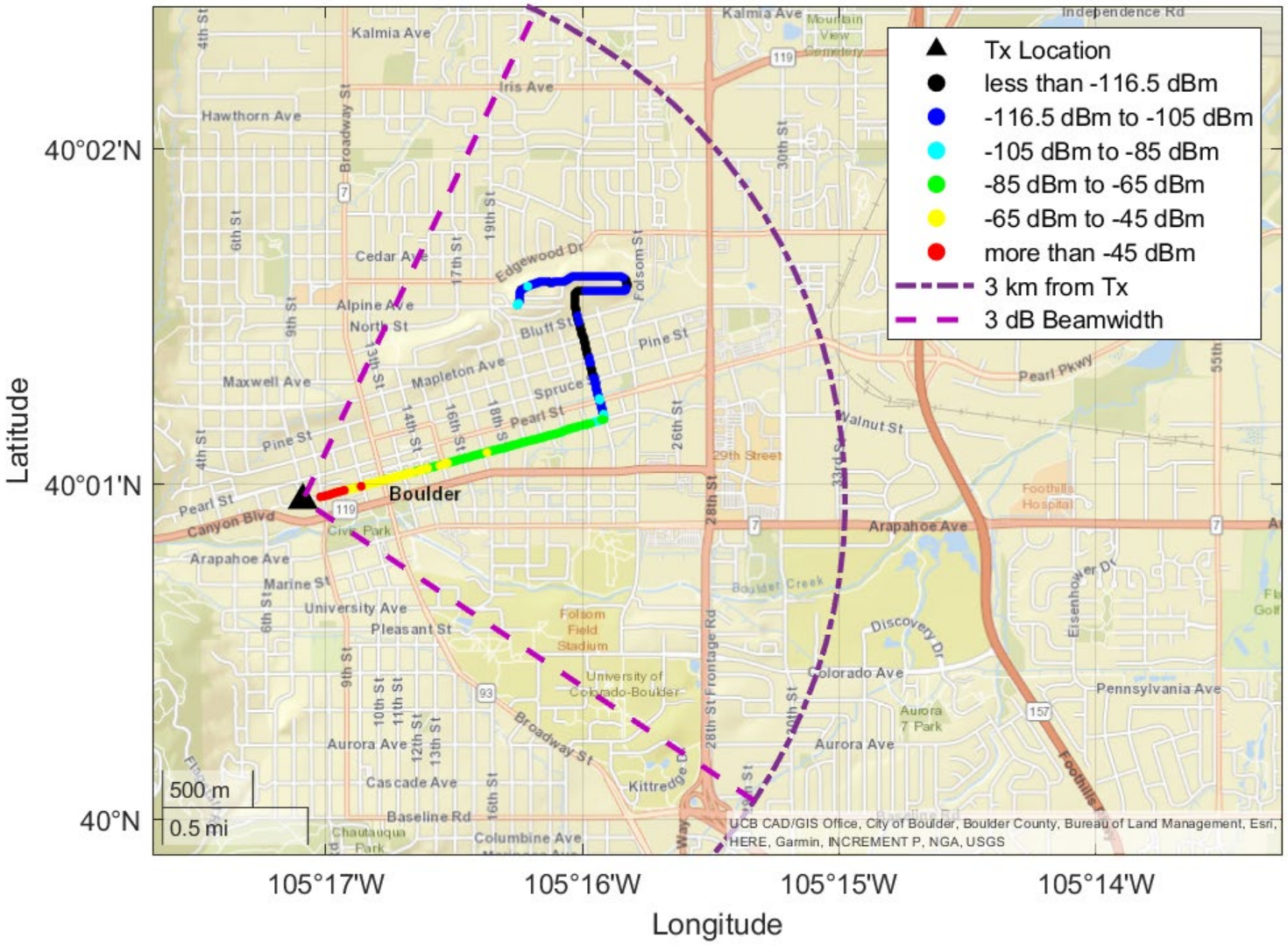

Figure A-23. Mean received signal power as a function of receiver location for the NLOS N6 Path in downtown Boulder (mean receiver noise power = -126.5 dBm).

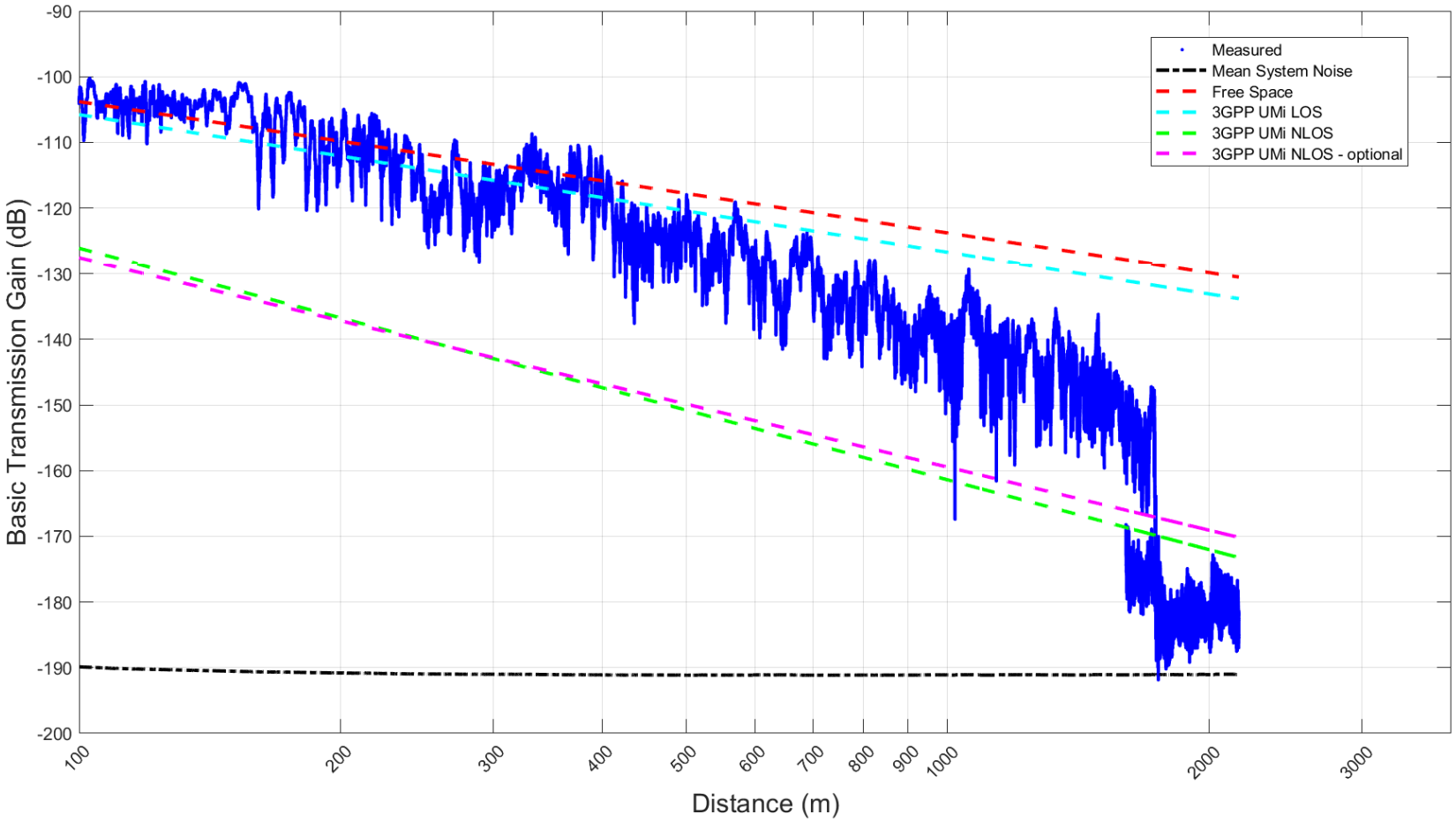

Figure A-24. G_b as a function of distance between the transmitter and receiver for the NLOS N6 Path in downtown Boulder.

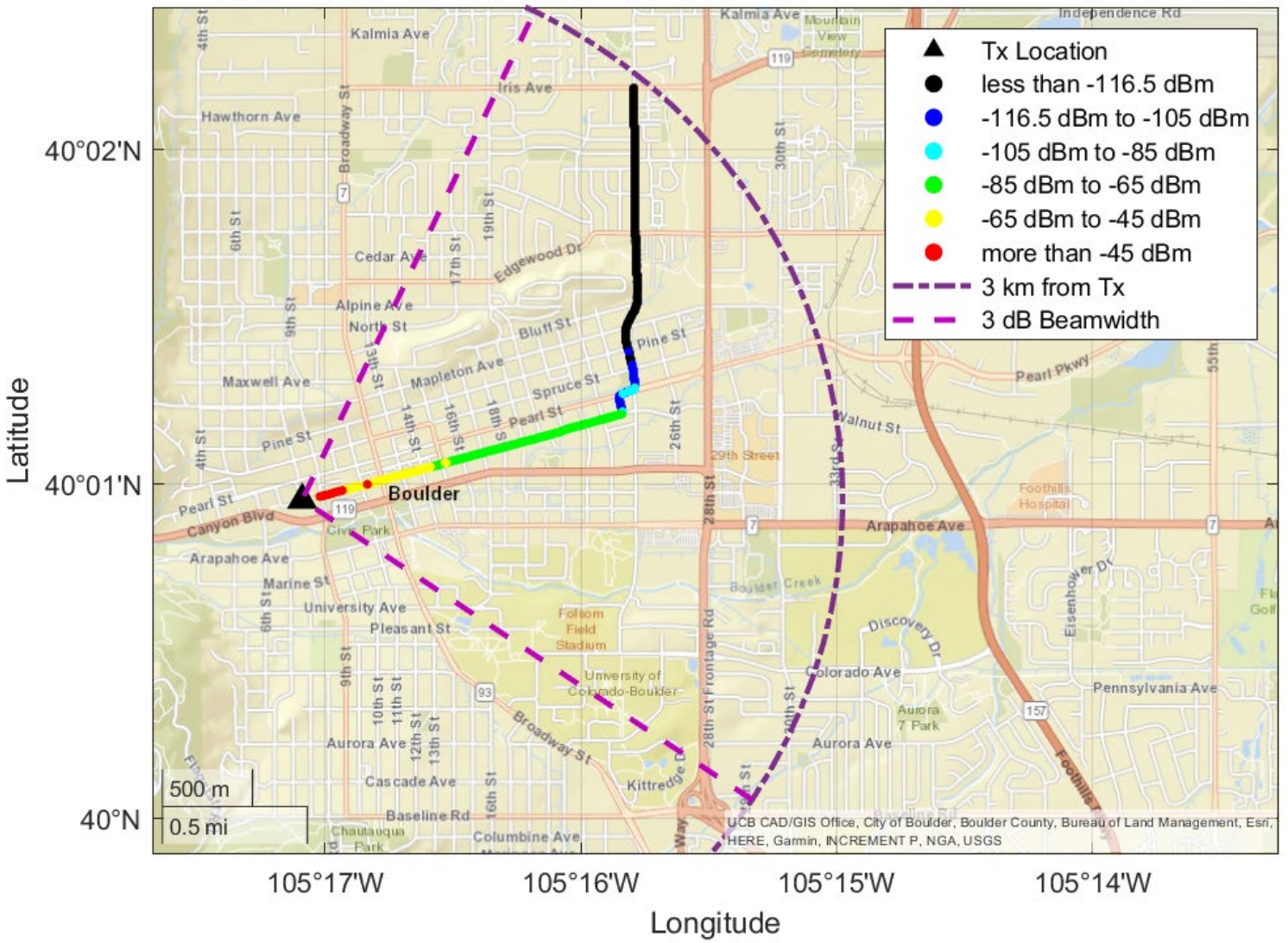

Figure A-25. Mean received signal power as a function of receiver location for the NLOS N7 Path in downtown Boulder (mean receiver noise power = -126.5 dBm).

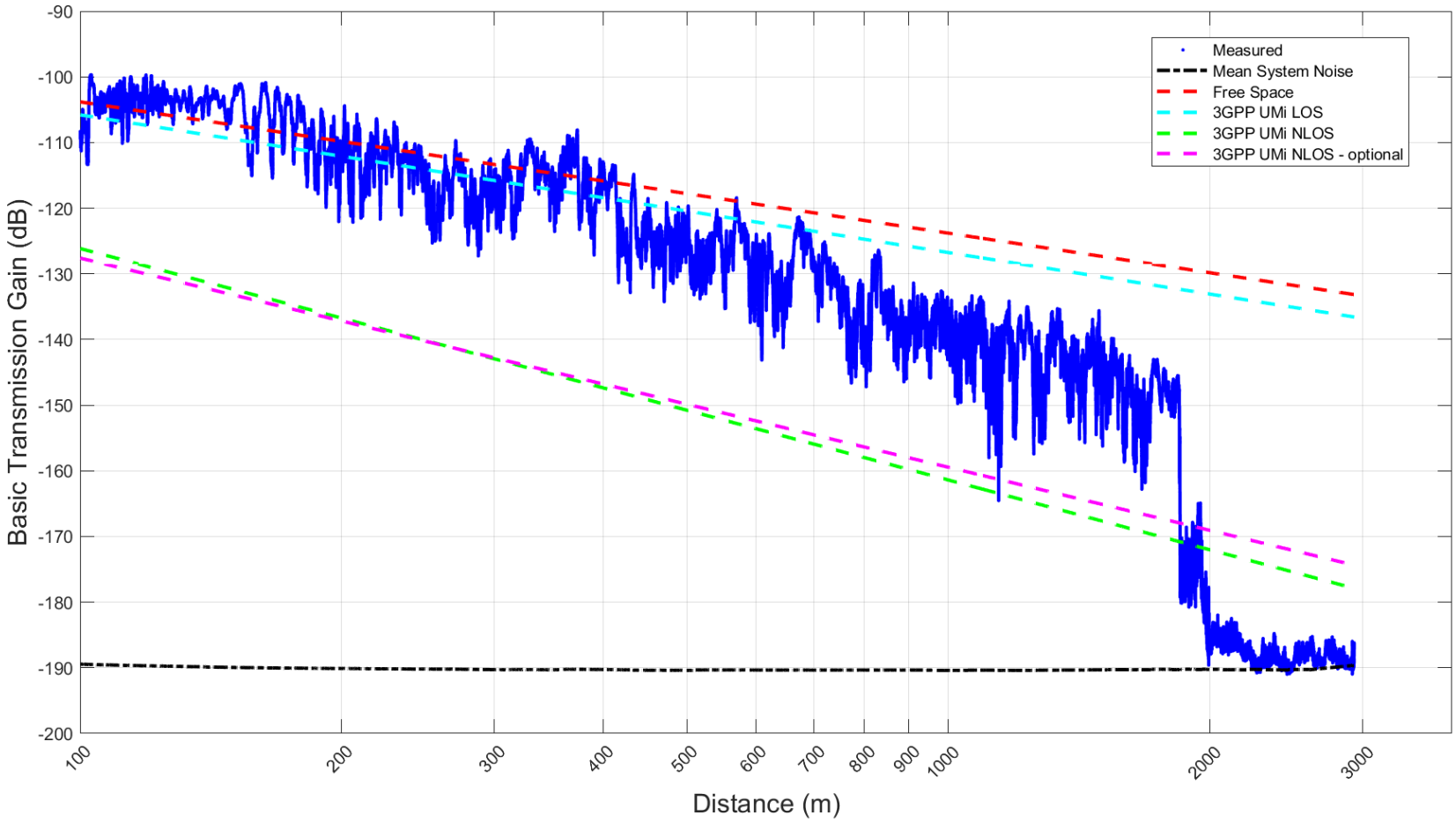

Figure A-26. G_b as a function of distance between the transmitter and receiver for the NLOS N7 Path in downtown Boulder.

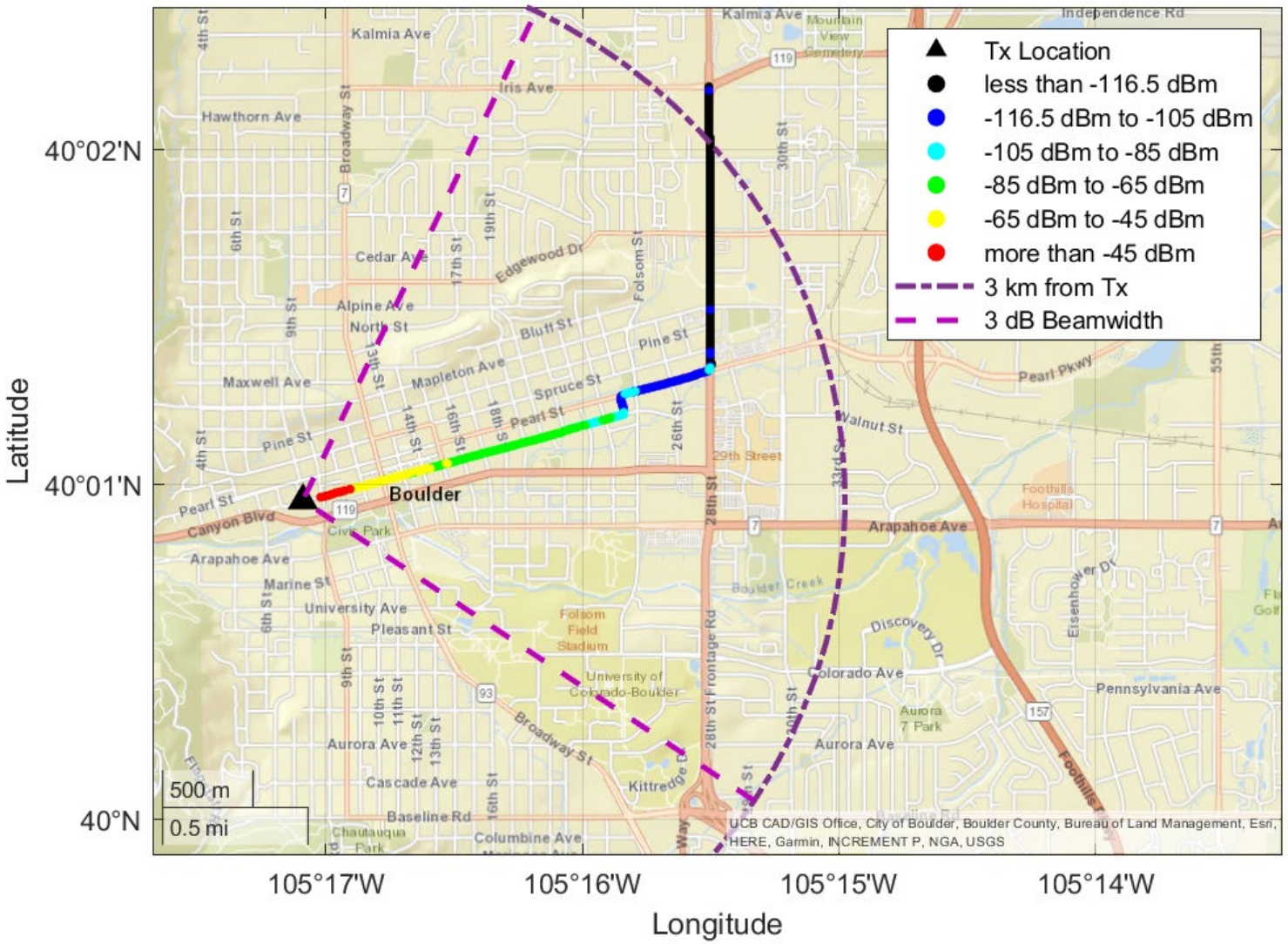

Figure A-27. Mean received signal power as a function of receiver location for the NLOS N8 Path in downtown Boulder (mean receiver noise power = -126.5 dBm).

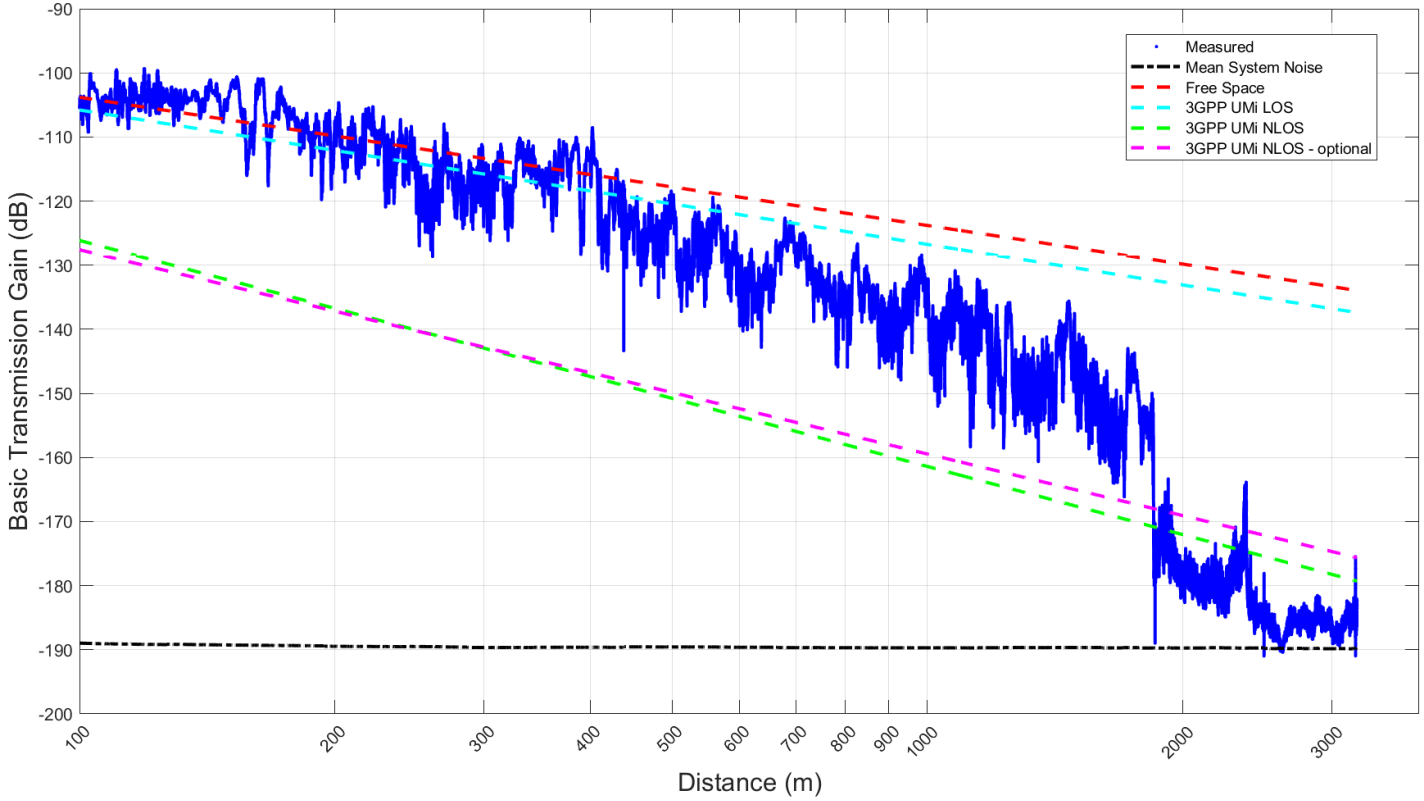

Figure A-28. G_b as a function of distance between the transmitter and receiver for the NLOS N8 Path in downtown Boulder.

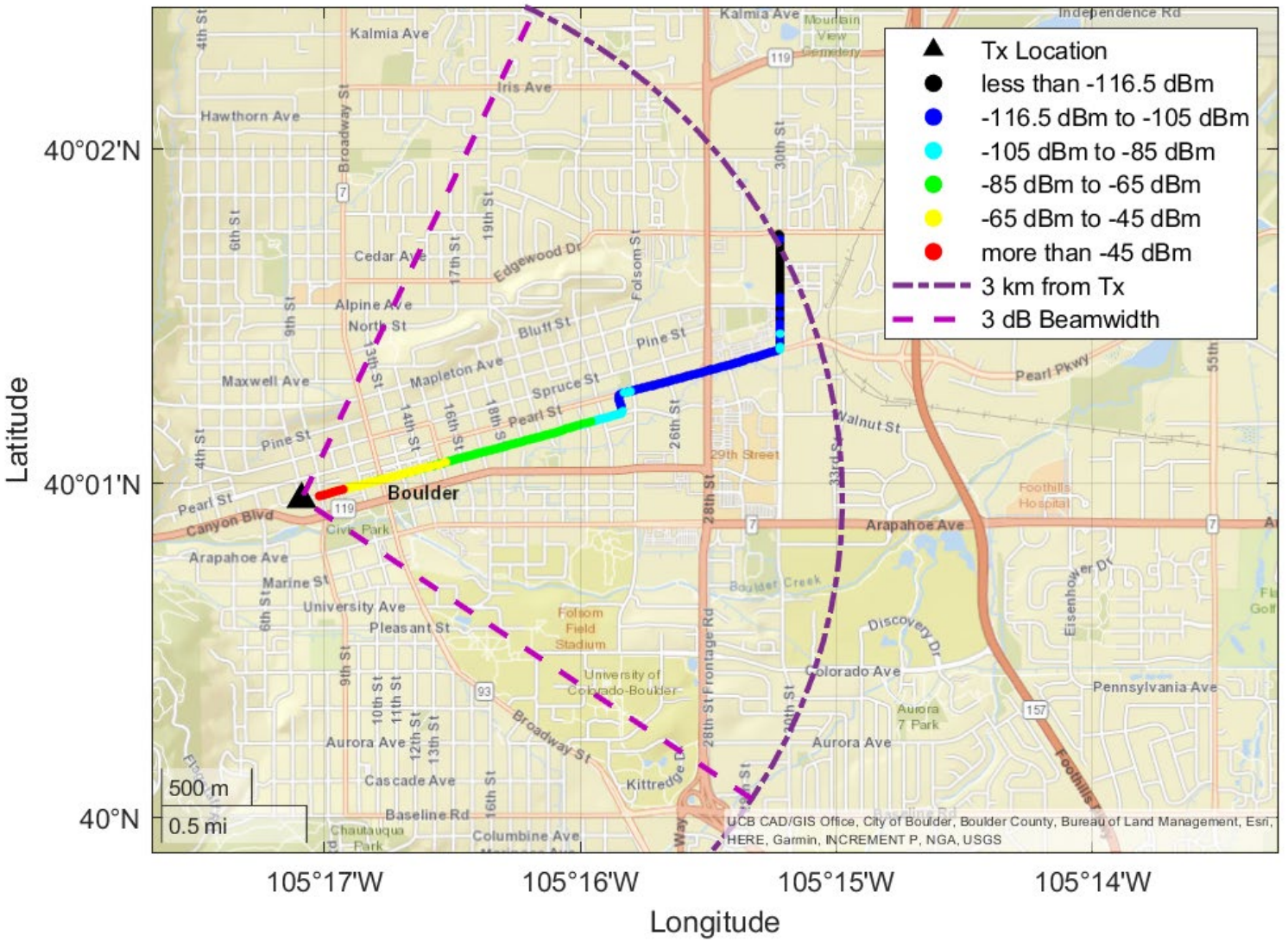

Figure A-29. Mean received signal power as a function of receiver location for the NLOS N9 Path in downtown Boulder (mean receiver noise power = -126.5 dBm).

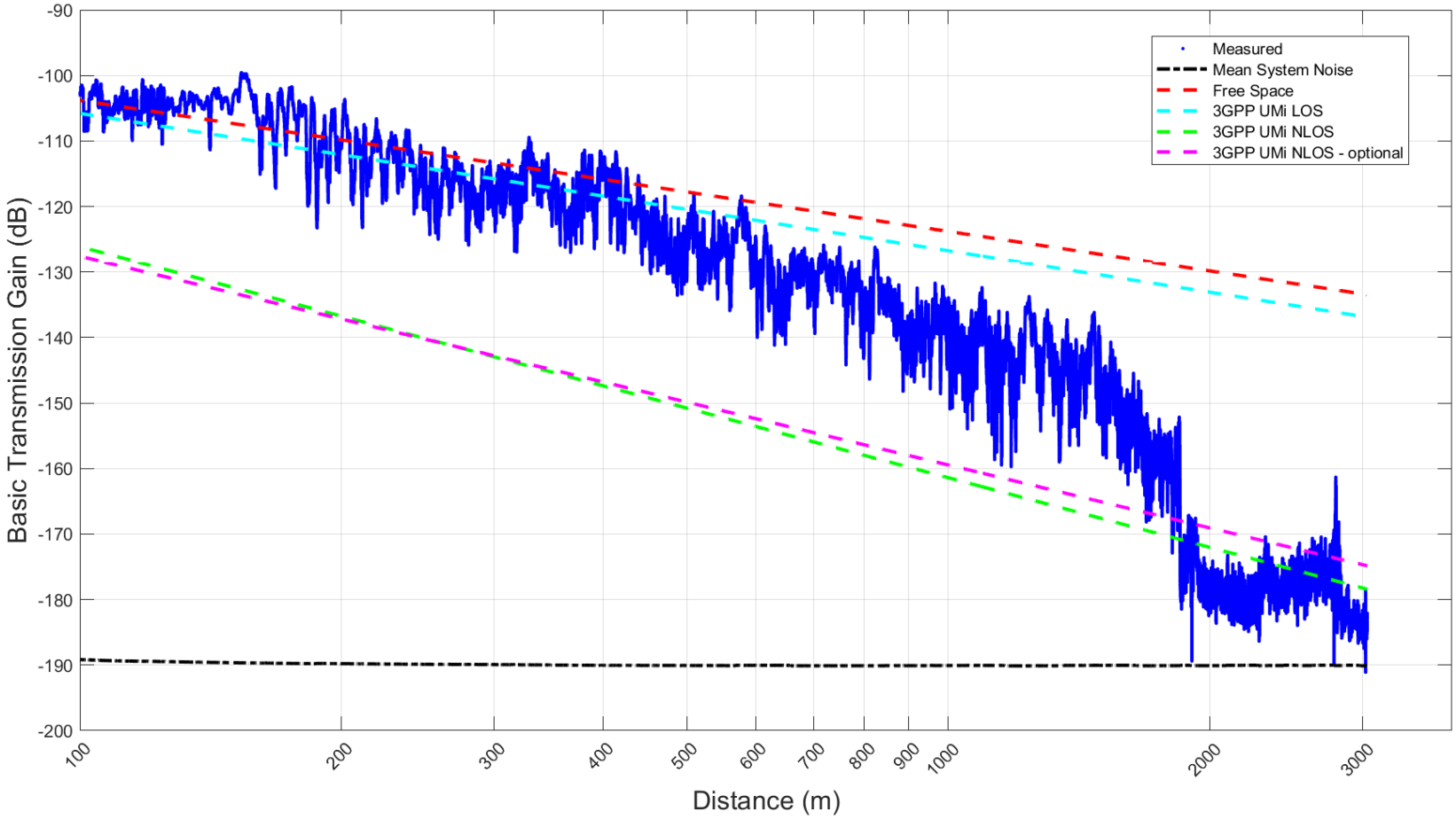

Figure A-30. G_b as a function of distance between the transmitter and receiver for the NLOS N9 Path in downtown Boulder.

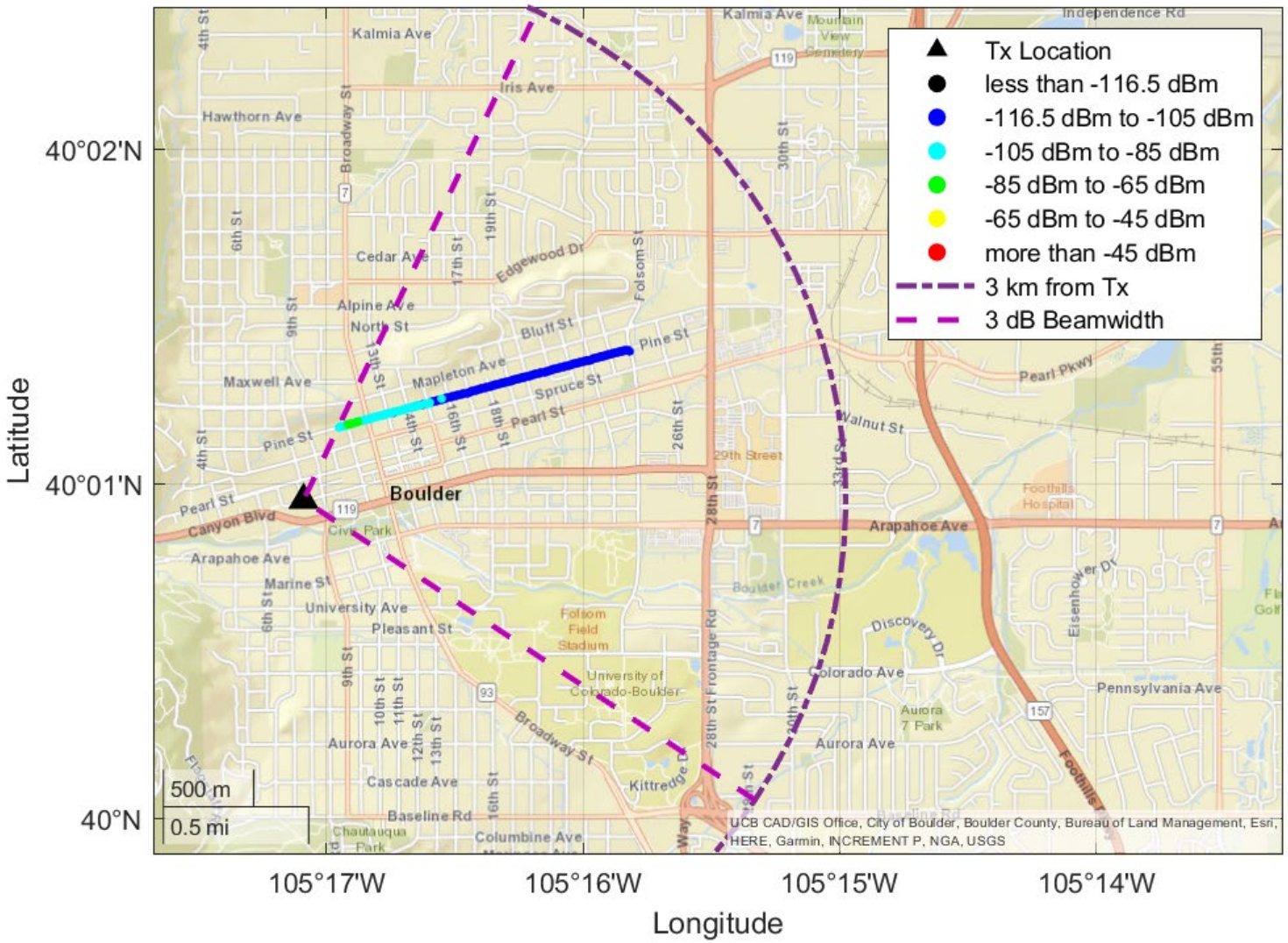

Figure A-31. Mean received signal power as a function of receiver location for the NLOS E1 Path in downtown Boulder (mean receiver noise power = -126.5 dBm).

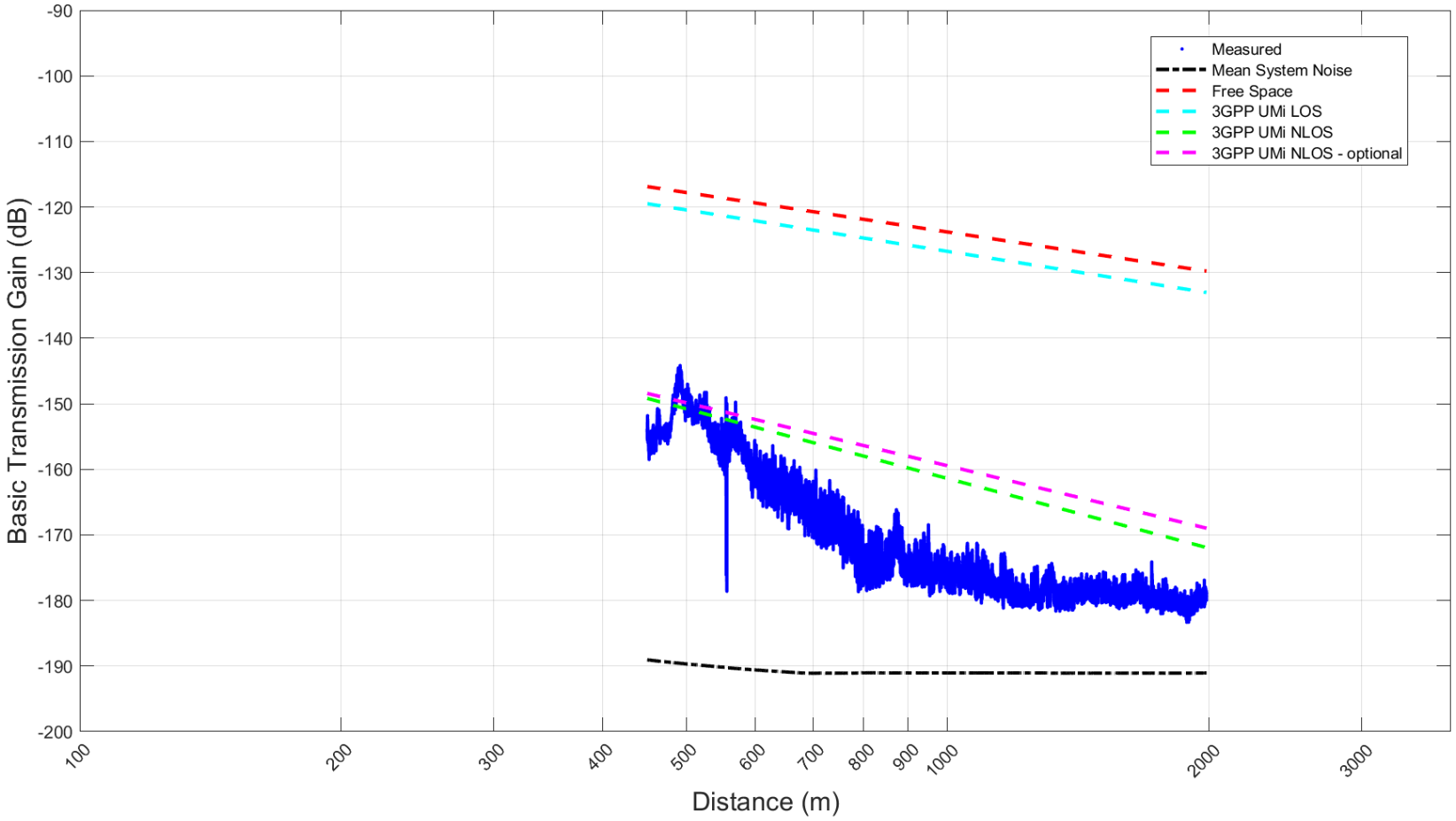

Figure A-32. G_b as a function of distance between the transmitter and receiver for the NLOS E1 Path in downtown Boulder.

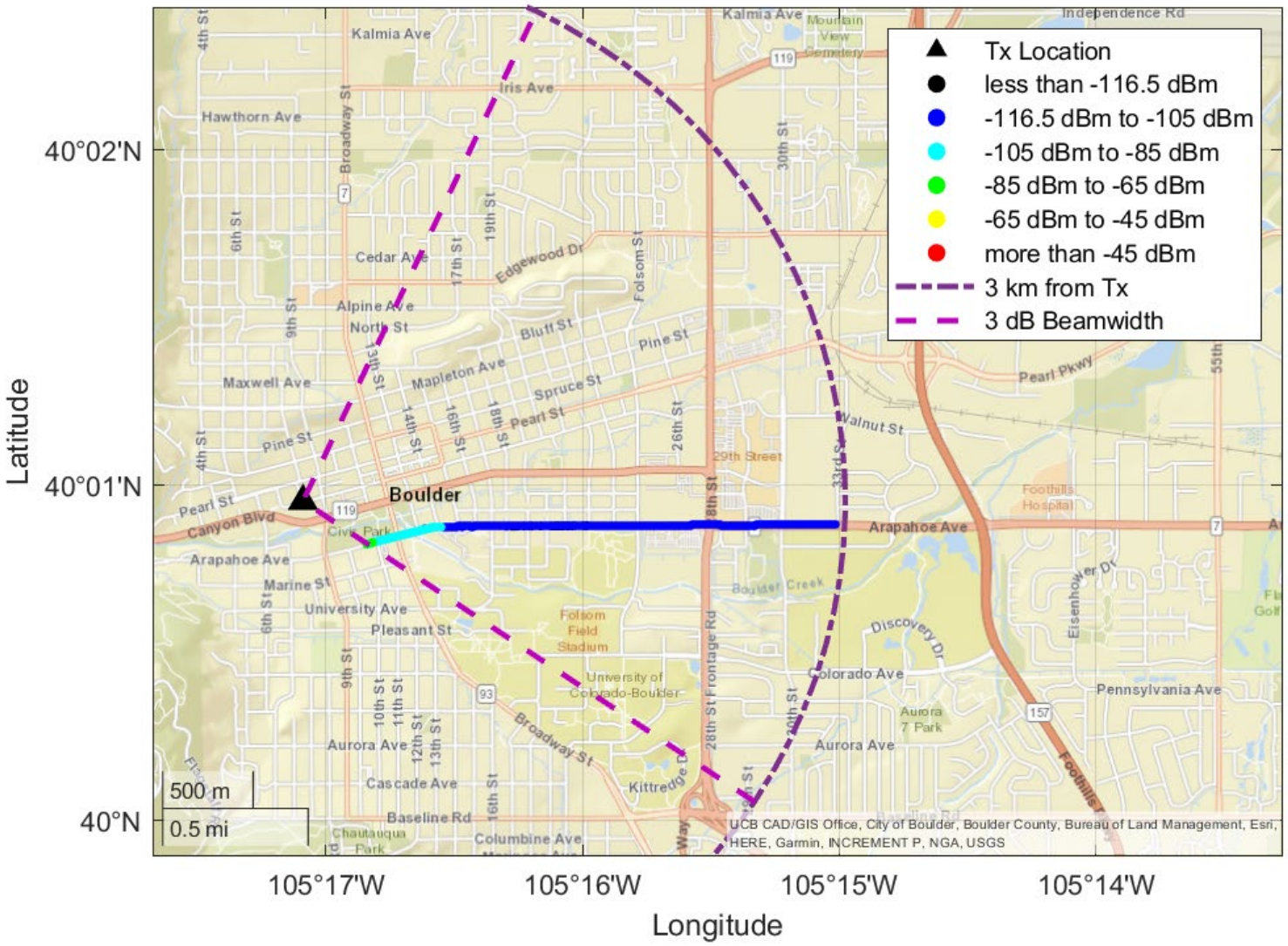

Figure A-33. Mean received signal power as a function of receiver location for the second section of the NLOS E2 Path in downtown Boulder (mean receiver noise power = -126.5 dBm).

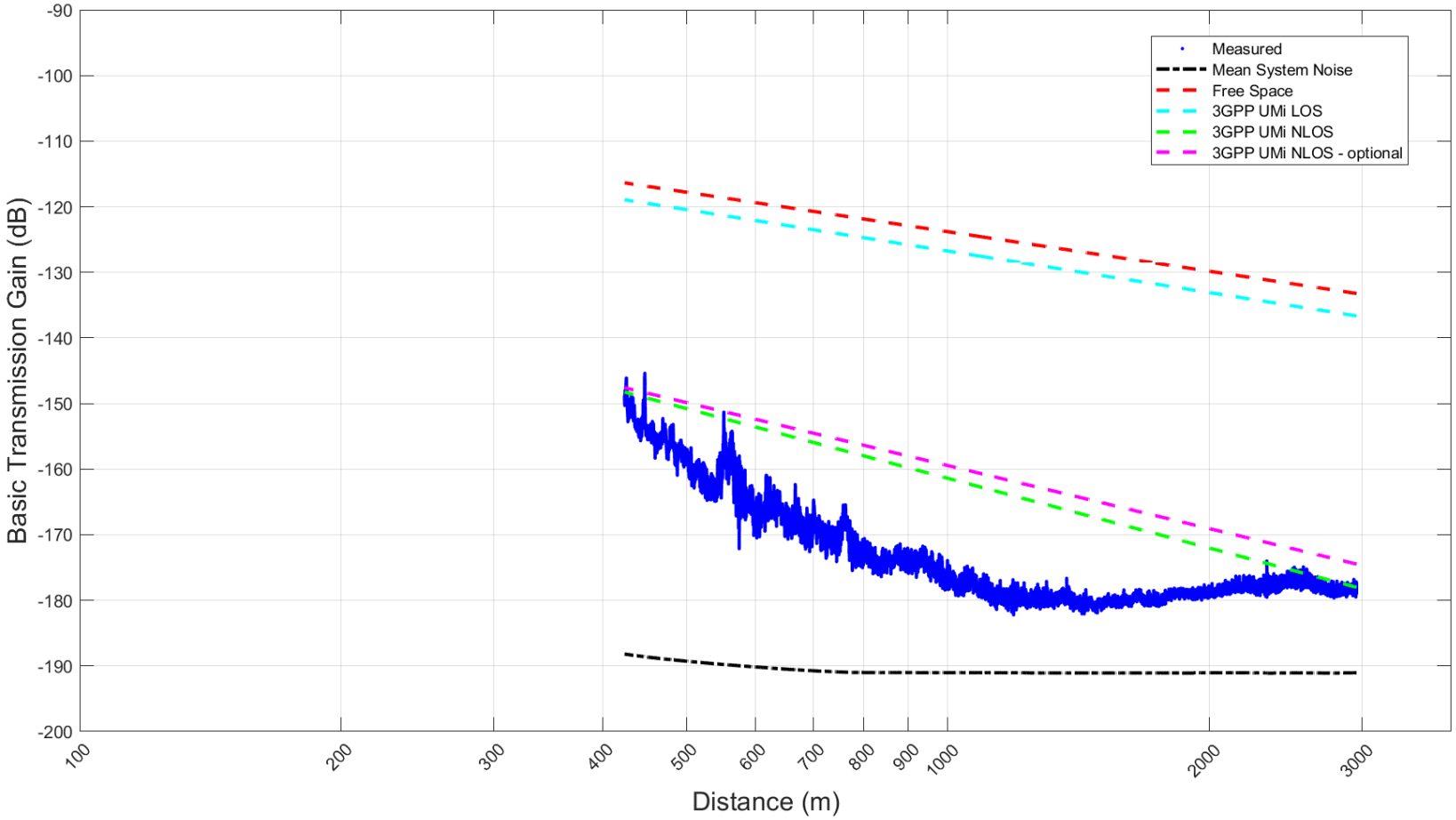

Figure A-34. G_b as a function of distance between the transmitter and receiver for the second section of the NLOS E2 Path in downtown Boulder.

NTIA FORM 29
(4-80)

U.S. DEPARTMENT OF COMMERCE
NATIONAL TELECOMMUNICATIONS AND INFORMATION ADMINISTRATION

BIBLIOGRAPHIC DATA SHEET

1. PUBLICATION NO.	2. Government Accession No.	3. Recipient's Accession No.
TR-22-561		

4. TITLE AND SUBTITLE	5. Publication Date
Outdoor Propagation Measurements in the 37–40 GHz Band in Boulder, Colorado	August 5, 2022
	6. Performing Organization Code NTIA/ITS.T
7. AUTHOR(S) Jeffery A. Wepman, Linh P. Vu, Edward F. Drocella, John D. Ewan, Kenneth J. Brewster, and Paul M. McKenna	9. Project/Task/Work Unit No. 3111012-300
8. PERFORMING ORGANIZATION NAME AND ADDRESS Institute for Telecommunication Sciences National Telecommunications & Information Administration U.S. Department of Commerce 325 Broadway Boulder, CO 80305	10. Contract/Grant Number.
11. Sponsoring Organization Name and Address National Telecommunications & Information Administration Herbert C. Hoover Building 14th & Constitution Ave., NW Washington, DC 20230	12. Type of Report and Period Covered

14. SUPPLEMENTARY NOTES

15. ABSTRACT (A 200-word or less factual summary of most significant information. If document includes a significant bibliography or literature survey, mention it here.)

Line-of-sight (LOS) and non-line-of-sight (NLOS), continuous-wave (CW), mobile outdoor propagation measurements were performed in the 37–40 GHz band in a small city downtown environment (Boulder, Colorado). The measurement system was optimized to provide measurements over the maximum practicable distance (about 3 km) between the transmitter and receiver. The transmitter was placed at a fixed location and time domain samples of in-phase and quadrature (IQ) data along with position data were collected by the mobile receiver along LOS and NLOS paths. The data were processed to provide received signal power as a function of position and basic transmission gain G_b vs. distance between the transmitter and receiver. Measured G_b as a function of distance was compared to that predicted by free space and the 3rd Generation Partnership Project (3GPP) LOS and NLOS path loss models for the urban microcell (UMi) case. In general, the measured G_b did not agree well with that predicted by the free space and 3GPP models.

16. Key Words (Alphabetical order, separated by semicolons)

Radio propagation measurements, millimeter-wave, 5G, path loss, basic transmission gain, propagation models, continuous-wave measurements, narrowband measurements, 3GPP

17. AVAILABILITY STATEMENT	18. Security Class. (This report)	20. Number of pages
☒ UNLIMITED.	Unclassified	100
☐ FOR OFFICIAL DISTRIBUTION.	19. Security Class. (This page)	21. Price:
	Unclassified	N/A

NTIA FORMAL PUBLICATION SERIES

NTIA MONOGRAPH (MG)

A scholarly, professionally oriented publication dealing with state-of-the-art research or an authoritative treatment of a broad area. Expected to have long-lasting value.

NTIA SPECIAL PUBLICATION (SP)

Conference proceedings, bibliographies, selected speeches, course and instructional materials, directories, and major studies mandated by Congress.

NTIA REPORT (TR)

Important contributions to existing knowledge of less breadth than a monograph, such as results of completed projects and major activities.

JOINT NTIA/OTHER-AGENCY REPORT (JR)

This report receives both local NTIA and other agency review. Both agencies' logos and report series numbering appear on the cover.

NTIA SOFTWARE & DATA PRODUCTS (SD)

Software such as programs, test data, and sound/video files. This series can be used to transfer technology to U.S. industry.

NTIA HANDBOOK (HB)

Information pertaining to technical procedures, reference and data guides, and formal user's manuals that are expected to be pertinent for a long time.

NTIA TECHNICAL MEMORANDUM (TM)

Technical information typically of less breadth than an NTIA Report. The series includes data, preliminary project results, and information for a specific, limited audience.

For information about NTIA publications, contact the NTIA/ITS Technical Publications Office at 325 Broadway, Boulder, CO, 80305 Tel. (303) 497-3572 or e-mail ITSinfo@ntia.gov.